Quantifying Relative Contributions of Salt Mobilization and Transport from Rangeland Ecological Sites in the Intermountain West

Mark. A. Weltz, USDA, Agricultural Research Service, Great Basin Rangelands Research, Reno, Nevada 89512

S. Kossi Nouwakpo and Awadis Arslan, University of Nevada Reno, Reno, Nevada, 89512

Kenneth McGwire, Desert Research Institute, Division of Earth and Ecosystem Sciences, Reno, Nevada, 89512

Final Report for Bureau of Land Management agreement number: 60-5370-4-001, March 2020

Executive Summary

The purpose of the salinity project is to improve the understanding of sources and transport mechanisms in rangeland catchments that deliver dissolved solids (salts) to streams within the Upper Colorado River Basin (UCRB). Changes in the land and water management that enhance vegetation density and canopy cover can be designed to reduce dissolved-solids yields, enhance the health and sustainability of rangeland plant communities and improve water quality in the UCRB. This study investigated upland hillslope scale rangeland erosion and salt transport processes on the highly erosive, saline-alkaline soils of the Mancos Shale formation. Rainfall simulations were performed at nine sites using a Walnut Gulch rainfall simulator on a variety of slope angles, canopy cover and rainfall intensities. The Rangeland Hydrology and Erosion Model (RHEM) was calibrated to provide unbiased estimates of discharge and sediment load in runoff at each site. New parameter-estimation equations for soil erodibility and hydraulic conductivity were developed for RHEM to improve runoff and soil loss prediction on saline soils. The calibrated surface erosion parameters in RHEM (K_{ss} and K_e) were substantially greater than any published in prior studies from non-saline environments. These new saline equations have been implemented in the online RHEM tool and available for land managers and stakeholders to accurately predict soil erosion and salt load on saline rangelands. The spatial distribution of vegetation canopy cover was quantified using photogrammetric modeling and landscape pattern metrics. These high-resolution spatial data will be instrumental in clarifying the link between vegetation spatial distribution and surface processes on saline rangelands. Measured total dissolved solids (TDS) in runoff water were highly correlated to measured sediment loads. Predictive equations were developed to estimate TDS in runoff water as a function of sediment load that were highly significant and simple to implement. Salt balance was partitioned between that on the soil exchange sites and the soluble fraction in the saturated extract of surface soils. Salts were also quantified in the dissolved fraction in the runoff to calculate a total salt balance for the site. Canopy cover, slope and other experimental conditions influenced the salt partitioning processes via hydrology, erosion and soil property interactions. Results from this study will improve predicting the possible deterioration of surface water quality as a result of rainfall on saline soils and suggest management practices of such soils in order to reduce their negative effect on surface water quality.

Understanding the complex partitioning of solutes between surface and subsurface processes is key to understanding the effect of rangeland management practices on salt delivery to surface waters. In this context, soil erosion/water quality models are valuable tools to assess the role of rangeland management practices on salt transport to surface waters. Since the dynamic interaction of management practices, precipitation, salt pickup and transport are synthetically handled in the RHEM model, it is possible to predict the effect of a given practice on net salt transfer from saline uplands to surface waters. This research did identify new methods to predict salt loading in the UCRB based on soil surface properties, such as Electrical Conductivity (EC), Exchangeable Sodium Percentage (ESP) and Sodium Absorption Ratios (SAR) that are available from the Natural Resources Conservation Service Web Soil Survey. Regional hot spot analysis can identify areas with highest probability of transporting salts to the Upper Colorado River Basin (UCRB). This information can then be used to match management practices with salt source areas to predict potential reduction in salt loading from rangelands in the UCRB. Finally, long term watershed continuous monitoring projects are needed to validate the effectiveness of rangeland management practices at reducing salt delivery to the Colorado River and its tributaries.

Keywords: Saline Soils; Salt Transport, Soil Erosion, Sediment Yield, Mancos Shale, Rangeland Hydrology and Erosion Model (RHEM); and Upper Colorado River Basin.

Acknowledgements

We thank Dr. Colleen Green, BLM for insights and assistance in designing this project and in assisting in conducting the field research and the analysis reported in this document. We thank the salinity field team composed of University Nevada Reno, ARS, and DRI staff for their diligence and commitment to conducting this research: Sandra Li, Todd Adams, Jacob Phillips, Ceasar Medina, Tim Jones, Erik Cadaret, Mariel Boldis, and Jason Nesbit. We would like to thank summer interns Jean Charles Gilbert, Charlène Gaultier, Alexis Normand, Pierre Landreau, Alice Boizet, Melissa Zill, Yann-Loris Yalebanda, Alexis Fourny, Sophie Duquesne, Aurore Rezette, Florian Delaporte, Thibault Pinson, Robin Pautis, Warren Teixeira, and Alexandre Sagniez for their assistance in field and lab work. We would like to thank Dr. Bob Blank and his staff Tye Morgan and Fay Allen for providing support and guidance in analyses of the soil and water quality samples associated with this project. Finally, we thank the Bureau of Land Management Colorado River Salinity Forum and the Bureau of Reclamation for the financial support for this and associated projects.

A database of the field collected data and directly measured attributes of runoff water quality has been provided with meta data.

Copies of peer reviewed and published technical papers have been provided that were developed as part of this project documenting salt transport process and ability to predict total dissolved solids in surface runoff during rainfall storm events.

Table of contents:

Quantifying Relative Contributions of Salt Mobilization and Transport from Rangeland Ecological Sites in the Intermountain West

1. Problem Statement and Background

The Colorado River and its tributaries provide water to about 36 million people and irrigation water to nearly 6 million acres of land in the United States and Mexico (Bureau of Reclamation 2013). Damages within the United States from dissolved solids in the Colorado River have been estimated to be $385 million per year (Bureau of Reclamation 2013). Salinity control efforts have largely focused on reducing anthropogenic sources of dissolved solids, especially irrigation of agricultural lands while nearly half of the salinity concentration in the river system comes from natural sources (saline springs, erosion of saline geologic formations and runoff) (Kenney et al. 2009). This suggests a significant potential to further reduce loading of dissolved solids to the Colorado River through land- and water-management activities on rangelands.

The most vulnerable rangeland areas for soil movement are where annual precipitation is between 100 and 400 mm yr^{-1} (Figure 1) which limits the soil moisture available to sustain plant growth. With low plant density and minimal plant and ground cover, arid and semi-arid areas are prone to both wind and water erosion. Arid and semi-arid regions have low plant density which often results in open and connected bare interspaces where aerodynamic roughness is low and fetch length is sufficient to allow for wind and water erosion (Okin et al. 2009). In addition, there is insufficient vegetative canopy and ground cover to prevent soil movement from raindrop splash, sheetflow, and rill erosion in the bare connected interspaces (Puigdefabregas 2005). The relatively low vegetation cover combined with high intensity convective rainfall events makes the Upper Colorado River Basin one of the most erosive areas of the United States. Average sediment yield frequently exceeds three mt ha^{-1} yr^{-1} on the Colorado Plateau (Langbein and Schumm 1958). As water erosion is exponentially related to rainfall intensity, most of the soil erosion occurs during rare convective storm events that have high rainfall intensities. Consequently, rilling and arroyo formation is very pronounced in the Colorado Plateau where convective storms annually occur (West 1983). Interaction between wind erosion/deposition and water erosion, transport, and deposition is poorly understood but linkages do exist, and total erosion may be maximized in arid and semi-arid regions because of limited cover and the steep highly dissected slopes of poorly weathered marine shales that are highly erosive in the Upper Colorado River Basin.

Salts in the Upper Colorado River Basin (UCRB) are mostly contained in soils of marine sedimentary origins (Jones et al., 2017; Tuttle et al., 2014). Halophytic plants, such as Atriplex L. (saltbush), Salsola vermiculata (Mediterranean saltwort), Halogeton glomeratus (saltlover), and Tamarix spp. (saltcedar) (Gharaibeh et al., 2011; Rodrigues et al., 2010). can uptake salts and either retain salt within the leaf or exude the salt through specific glands. This can result in the plant leaf canopy being a significant source of salts deposited on the soil surface through leaf fall or salts being flushed from the surface of the leaf during rainfall events and are an additional sources of salts contributing to surface water quality deterioration of the Colorado River. Rainfall may enter the soil directly and react with the soil's solid components (salts), some of which dissolve readily and others slowly. Therefore, to assess salt mobility and transport processes the concentration of major cations and anions in rainfall, runoff water, and the soil must be determined.

Up to fifteen percent of rangelands in Utah are classified as being in severely eroding condition (Rasely et al., 1991). Recently USDA-NRCS NRI (2011-2015) reported that on non-Federal rangeland, moderate to extreme rangeland condition departures from historic reference conditions were 12.3% (soil and surface stability), 16.1%

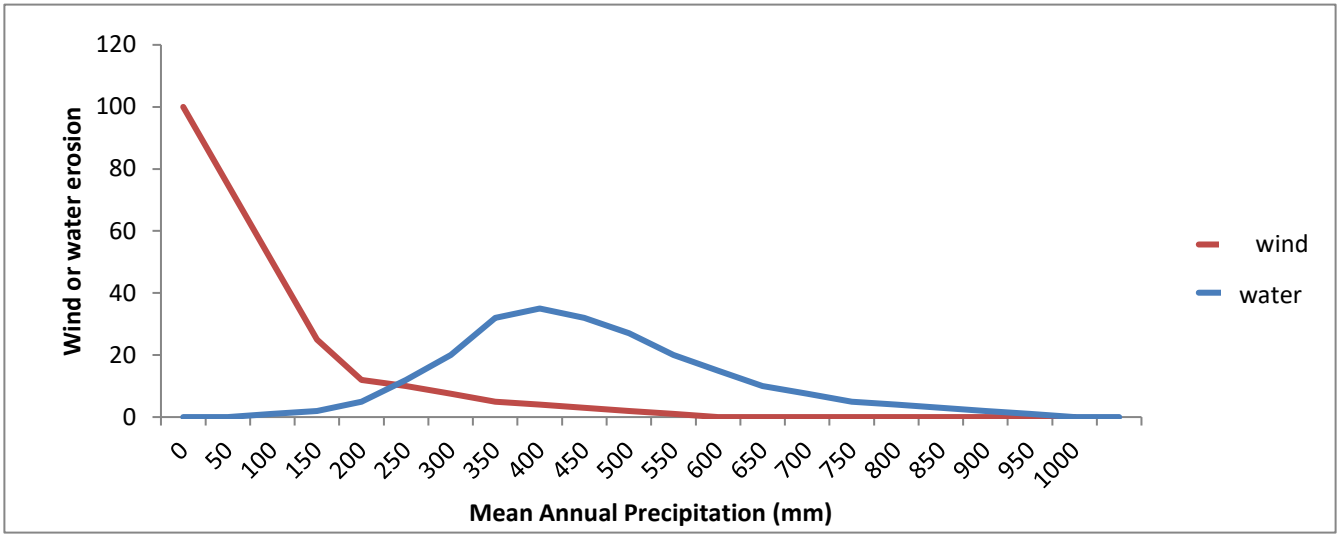

Figure 1 Conceptual diagram of wind and water erosion with mean annual precipitation for naturally vegetated arid and semi-arid range lands (Modified from Marshall (1973).

(hydrologic function), and 25.1% (biotic integrity) of Utah's total non-Federal rangeland acres (6.67 million acres) (USDA-NRCS. 2018). Some of these degraded lands are located on saline soils of the Mancos Shale formation, resulting in a disproportionate contribution of sediment, salinity, and selenium to the Colorado River (BoR, 2013; Spahr et al., 2000). Land management agencies in the U.S. are considering mitigation activities to reduce erosion on these saline rangelands, and an initial question is how to prioritize different locations for action. Outcrops of the Mancos Shale extend discontinuously through Wyoming, Utah, Colorado, New Mexico, and Arizona, with most of their area draining to the Colorado River. The various geologic units of the Mancos Shale were laid down during the Mid-Late Cretaceous in near-shore environments of the Western Interior Seaway. As such, the bedrock and soils of the Mancos Shale are saline, and sometimes sodic depending on the depositional environment. Iorns et al. (1965) attributed 60% to of salts entering the Upper Colorado River Basin (UCRB) to natural sources and 40% to agriculture. Kenney et al. (2009) using the SPARROW model found a very similar proportion and quantified the great importance of "high-yield" saline sedimentary formations from the Mesozoic like the Mancos Shale. A variety of surface and subsurface processes move salts from the rangelands of the Mancos Shale to the Colorado River. Prior studies estimate that as much as 55% of the salinity in the Colorado River is from groundwater and subsurface reemergence (Kenney et al., 2009; Warner et al., 1985; Shirnian-Orlando & Uchrin, 2000). Miller et al. (2017) revisited prior work by Kenney (2009) with the SPARROW model and found salinity from rangelands in the entire UCRB to be on the order of 30 tons per square mile. It is likely that the magnitude and significance of the contribution would be larger for rangeland soils derived from saline geological parent material, and the outline of the Mancos Shale is quite visible as the areas of highest rangeland salt yields in Figure 5 of that report. Nauman et al (2019) using new high-resolution soil datasets applied random forest regression to predict salinity sources in the upper (UCRB) with a 30-meter grid resolution. One of the most consistent predictors of salinity in that effort was an index of bare ground, particularly in mountainous terrain. Tillman et al. (2018) assessed the degree to which different reaches in the UCRB might be candidates for mitigating salinity by reducing or capturing soil erosion. While no simple relationship provided a uniform result across the UCRB, stream gauge locations that were predicted to be good candidates coincided with many drainages where the Mancos Shale is present. Since that effort focused on the stream network, hillslope scale erosion and salt transport models would be required to identify the best locations for actual mitigation activities. The dominant salt affected soil ions are calcium, magnesium, sodium, potassium, chloride, nitrate, sulfate, and bicarbonate (Ca^{2+}, Mg^{2+}, Na^{+}, K^{+}, Cl^{-}, NO_3^{-}, SO_4^{2-}, and HCO_3^{-}, respectively). The amounts of each constituent depend on the kinds and amounts of the minerals and organic matter in the soil solid phase, the kind and activity

of the vegetation, and the source of applied rain or simulation water.
The runoff water quantity and quality; soil erosion and deposition; solute movement within the soil as a result of rainfall and simulation; the changes of vadose zone moisture content; and ground water recharge quality and quantity are some parameters that need determination to describe salt mobilization and transport from rangeland ecological sites within the basin. The parameters produced from such rangelands must be incorporated in the existing models (built for non-saline non-alkaline rangelands) for better prediction under salt-affected rangelands. To assess the state-of-knowledge on rainfall/runoff-driven salt pickup and transport processes, a bibliographic search (Gagnon et al. 2014) and synthesis (Weltz et al. 2014) was first conducted as a collaborative effort between the Bureau of Land Management (BLM) and United States Department of Agriculture - Agricultural Research Service (USDA-ARS). Bibliographic references covering salt transport processes revealed a strong emphasis on water erosion and subsurface hydrology processes as the main driving mechanisms of salt delivery to surface waters. This state-of-knowledge exploration identified experimental understanding of salt pickup and transport processes as a key knowledge gap that needs to be addressed. Work on this project has documented a significant linear relationship between salinity and sediment in the runoff from experimental rainfall simulator plots on the saline Mancos Shale formation (Cadaret et al., 2016ab; Nouwakpo et al., 2018),. This work demonstrates the potential for using erosion models to predict salinity loads from these rangelands under different conditions. .

2. Project Objective

The specific objectives in this research were to: (1) experimentally understand how biotic and abiotic characteristics in these saline rangelands control the response to erosive processes, (2) understand salt mobility and transport processes, and (3) parameterize this experimental knowledge into a predictive framework with the Rangeland Hydrology and Erosion Model (RHEM). This work was conducted as a collaborative effort between BLM, BOR, USDA-ARS, University of Nevada Reno (UNR), and the Desert Research Institute (DRI).

3. Methodology

Study area

Nine sites in the Upper Colorado River Basin (UCRB) were selected to conduct the rainfall simulation experiments and cover a large area of the basin (Figure 2). The sites have wide ranges of slope, soil intrinsic properties, ground cover, canopy cover, vegetation, annual precipitation, geographic location and altitude where runoff rate and water quality (sediment concentration and total dissolved solids) were measured (Figures 3, 4, 5, and 6) to understand salt transport processes. Average cover components and slope (Table 1) show high %CV of the average site's parameters and allow for deriving suitable functions relating runoff and sediment quality and quantity as dependent variables with these parameters as independent variables.

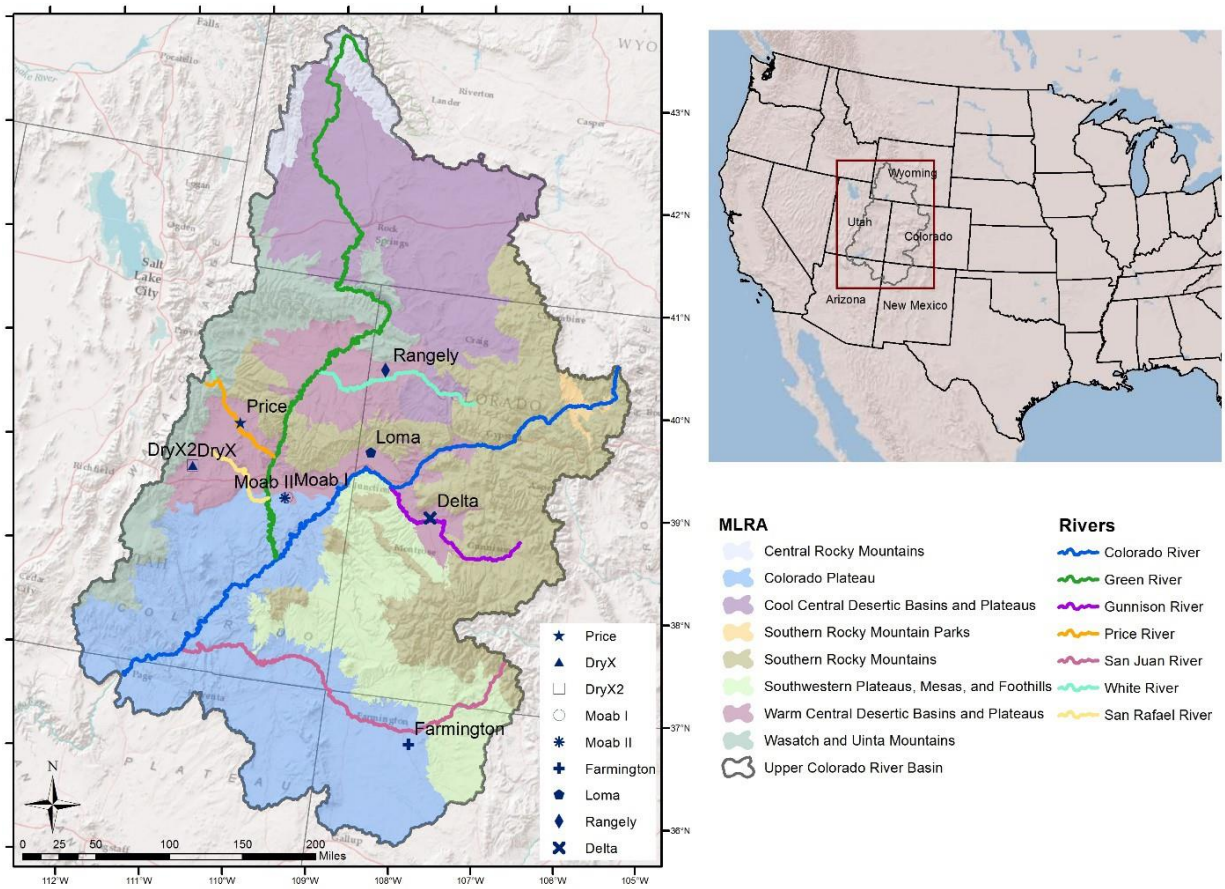

Figure 2. Map of the field sites relative to rivers in the Upper Colorado River Basin.

Figure 3. Photos from Moab, Utah (left) and Dry X, Utah (Right) showing variation in soil surface cover. At Moab, Utah soil surface dominated by biological soil crust in the interspace. At Dry X, Utah soil surface dominated by various levels of physical crusts (i.e., salt crusts) in the interspaces.

Figure 4. Experimental sites in Utah used to quantify salt loading in surface runoff and Walnut Gulch rainfall simulator.

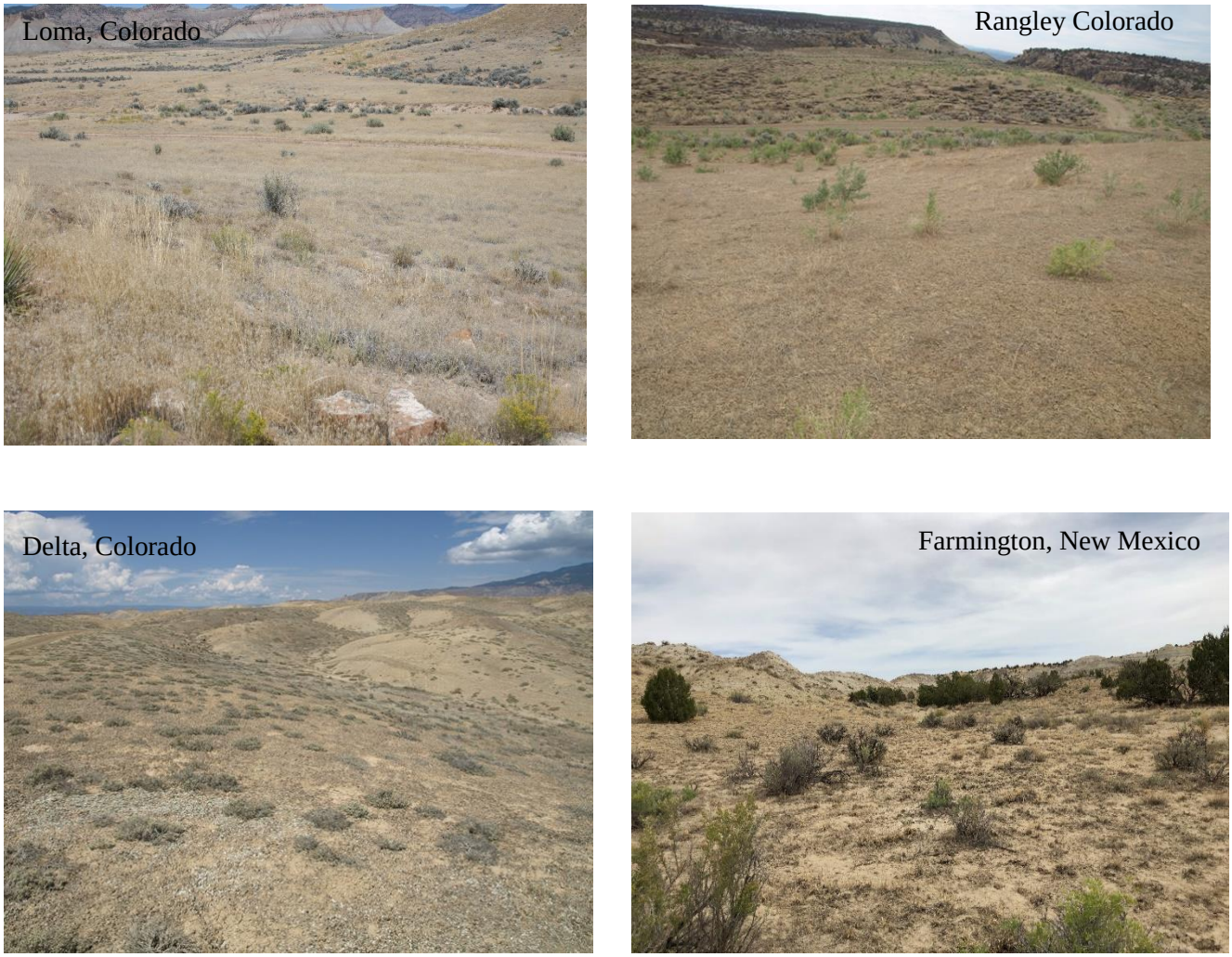

Figure 5. Experimental sites in Colorado and New Mexico used to quantify salt loading in surface runoff.

Figure 6. Measuring timed-sampling of concentration to steady state runoff rate (left) and runoff water. quality (right).

Table 1. Cover (%) components of the 9 research sites in Upper Colorado River Basin.

Site	Plant Basal	Rock	Litter	Bare	Biological Soil crust	Shrub	Forb	Bunchgrass
Price	0.86	0.09	2.20	89.27	0.00	8.43	0.00	0.00
DryX	3.98	0.24	3.33	74.70	0.00	21.75	0.00	0.00
DryX-II	0.00	0.08	3.14	85.48	0.00	11.30	0.00	0.00
Moab	18.94	31.44	17.11	50.68	8.41	18.24	0.00	0.00
MoabII	0.00	64.09	1.36	32.61	0.00	4.81	0.00	0.00
Loma	0.00	9.24	77.01	2.20	11.55	10.04	0.00	0.00
Farmington	3.61	0.00	8.07	88.32	0.00	1.86	0.00	18.36
Rangely	0.00	0.21	43.30	56.21	1.39	0.21	0.14	0.00
Delta	0.04	0.00	3.33	43.74	47.00	10.19	0.00	0.00
Average	3.05	11.71	17.65	58.13	7.59	9.65	0.02	2.04
Max	18.94	64.09	77.01	89.27	47.00	21.75	0.14	18.36
Min	0.00	0.00	1.36	2.20	0.00	0.21	0.00	0.00
%CV	202.56	189.70	147.18	50.70	202.71	73.12	300.00	300.00

The ECe range from 0.19 dS/m to 37.77 dS/m covering the five salinity classes adopted by NRCS (Table 2), and the values of soil ESP range from 0.12 to 49.63 covering the 2 classes of the National Soil Survey Handbook NSSH Part 618 (2017). Figure 7 shows the distribution of average sites electrical conductivity (ECe) and exchangeable sodium (ESP). The soil texture ranged from silty loam to loamy sand classes covering 3 of the 12 classes. All soils show a degree of $CaCO_3$ effervescent level. The gypsum content is the highest at Price producing the smallest SAR and ESP values 0.12 and 0.19 respectively associated with and ECe of 2.77 dS/m which resulted from the solubility of gypsum. The determination coefficient for the relation between the sodium ratio (SAR) and ESP values is high which allows estimating one from the other.

Table 2. Selected soil properties of the 9 research sites in upper Colorado River Basin.

Site	Sand	Silt	Clay	ECe	ESP	SAR	% Gypsum	CaCO3 Effervescent	Soil texture
Price	11.18	72.05	16.77	2.77	0.19	0.12	4.8	Violently	silt loam
DryX	11.52	66.68	21.8	26.13	27.67	41.74	4.36	Violently	silt loam
DryX-II	11.52	66.68	21.8	8.9	18.84	24.78	3.5	Violently	silt loam
Moab	58.72	37.23	4.05	3.43	1.73	2.18	0.66	Strongly	sandy loam
MoabII	74.99	18.74	6.27	16.35	37.77	43.75	0.27	Strongly	sandy loam
Loma	52.57	38.96	8.47	0.46	0.21	0.15	0.002	Violently	sandy loam
Farmington	81.42	17.38	1.2	1.41	2.16	2.47	Trace	Very Slightly	Loamy Sand
Rangely	15.35	65.21	19.44	5.01	1.45	2.73	1.87	Very Slightly	silt loam
Delta	7.34	77.42	15.23	21.25	16.5	49.63	2.67	Violently	silt loam
Average	36.07	51.15	12.78	9.52	11.84	18.62	2.27		
Max	81.42	77.42	21.80	26.13	37.77	49.63	4.80	Violently	Loamy Sand
Min	7.34	17.38	1.20	0.46	0.19	0.12	0.00	Very Slightly	silt loam
%CV	84.53	45.54	61.87	99.02	118.31	114.46	82.27		

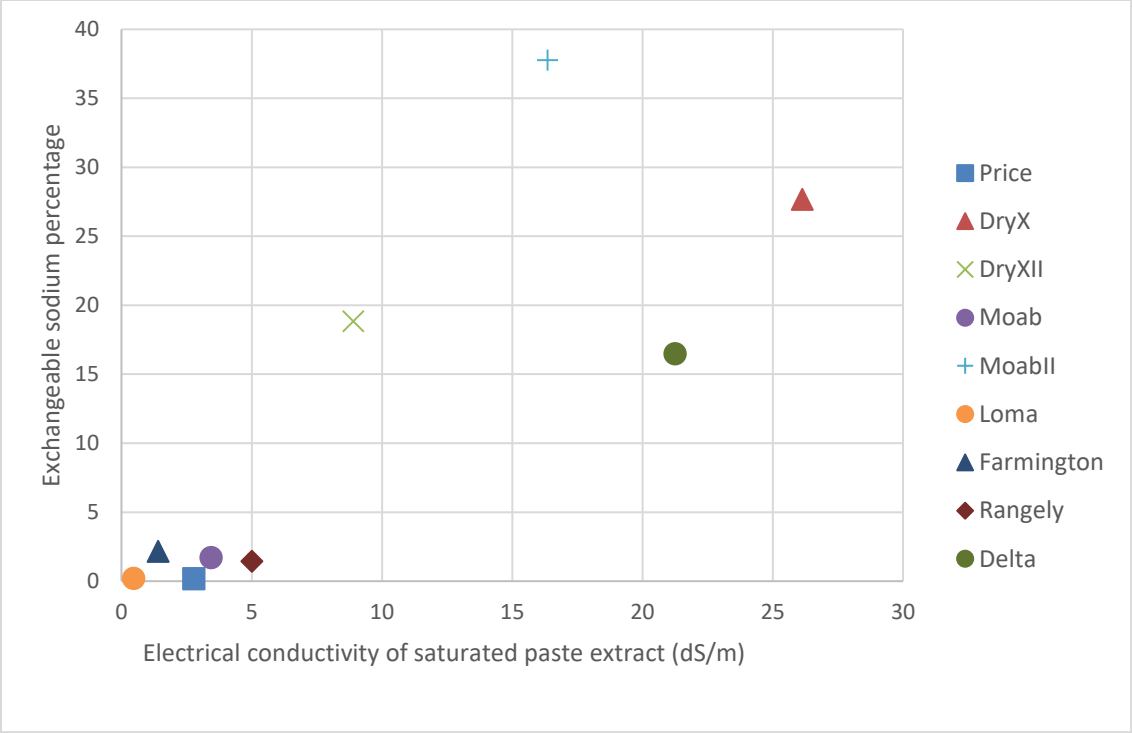

Figure 7. The ECe and ESP of the selected sites.

3.2 Experimental Site

On all experimental sites, a series of rainfall simulations were conducted on 6 m x 2 m erosion plots to quantify sediment and salt transport processes during rainfall-driven erosion processes (Figure 8). Erosion and hydrologic responses were assessed by measuring soil loss, runoff and solute transport under four rainfall

Figure 8. Walnut Gulch Rainfall Simulator operation at Dry X and DryX-II, Utah.

intensities corresponding to return periods of 2 (44.1 mm/hr), 10 (80 mm/hr), 25 (114.4 mm/hr) and 50 (135.9 mm/hr) years. Intensities were calculated based on the 15-minute depth return frequencies published in the National Oceanic and Atmospheric Administration (NOAA) Atlas 14 (Bonnin et al. 2006). On each plot, a single rainfall event was applied to ensure the capture of the process of salt efflorescence (Bowles et al. 1982) whereby a salt crust is left at the soil surface by evaporation. Each rainfall intensity on each site was replicated three times leading to a total of twelve plots per site.

In the Dry X-II experiment, three hillslopes were identified at the study site to represent low (L, canopy cover < 5%, average = 2.39%), medium (M, 5% < canopy cover < 19%, Average = 9.09%) and high (H, canopy cover > 19%, average = 22.41%) vegetation cover (Figure 9). Only the 25-year return period intensity of 114.4 mm/hr was applied to all plots. Potential hillslopes were selected by visually identifying three contrasting densities of *Atriplex corrugata* on the site. Hillslopes of similar slopes and soil characteristic were picked to minimize confounding effects of these factors on soil erosion processes. Four plots were selected on each hillslope, giving a total of twelve plots to conduct the rainfall simulation experiments. Ground and vegetation cover on each plot were assessed using a laser point frame (VanAmburg et al. 2005). This data was collected on a 0.5 m x 0.1 m grid (or 220 sample points) per plot and provided information on canopy cover (%) by lifeform (e.g., shrub, grass, forb), and ground cover (%) (e.g., plant basal area, litter, rock, biological soil crust and bare ground).

A Walnut Gulch Rainfall Simulator (WGRS) (Paige et al. 2004) was used in this study (Figure 8). The WGRS is an oscillating nozzle type simulator with four Veejet 80100 nozzles (Spraying systems, Inc., Wheaton, Ill.) mounted in-line on a central boom. The effective spray area of this simulator was 6.1 m x 2 m which determined the 6 m x 2 m plot size used in this study. Rainfall intensity is varied in the WGRS from 12 mm/hr to 200mm/hr (at 55kPa nozzle pressure) by modulating oscillation pulse length and nozzle operation timing with a computer-controlled drive circuitry. As recommended by Paige et al. (2004), a nozzle height of 2.44 m was used in this study to achieve raindrop energy within the range encountered during natural rainfall events.

At the downslope end of the plot, a runoff collection pan conveyed runoff into a supercritical flume where a Teledyne 4230 flow meter (Isco, Inc., Lincoln, NE) measured discharge at a rate of four samples per minute. This automated discharge measurement was validated with periodic manual timed-sampling of runoff rate. Runoff discharge measurements from the Teledyne 4230 were displayed in real-time on a computer screen via a serial port communication.

A rail mechanism mounted lengthwise on the frame of the simulator supported a camera which was used to take overlapping pictures before and after each rainfall event. The images were used to reconstruct soil surface microtopography at sub-millimeter resolution and vegetation canopy cover. A Canon EOS Rebel T3i (Canon Inc, Tokyo, Japan) equipped with a 20 mm lens was used for acquiring the surface reconstruction pictures. The average camera-ground distance was 2.4 m and the overlap between adjacent pictures 0.15 m. Pictures were taken along two paths 0.76 m apart on either side of the central boom of the simulator. This image network configuration resulted in 80 to 90 pictures to cover each plot. Translucent side curtains on the simulator served the dual purpose of light diffusers, reducing excessive shadowing in the pictures and limiting the effect of wind on rainfall distribution.

The surface reconstruction procedure relied on control points which were laminated paper targets marked by a checker sign and mounted on an anchor stake. Eight to ten evenly spaced targets were arranged along the perimeter of each plot. A Nikon NPR 352 Total Station (Nikon Corporation, Tokyo, Japan) was used to survey control points on each plot for scaling and registering reconstructed soil surfaces.

Soil surface microtopography was reconstructed using the structure from motion software Agisoft PhotoScan 1.0 (Agisoft LLC, 2013). Average reconstruction precisions achieved in this study were 3.1 mm and 1.6 mm

respectively for the horizontal and vertical directions. Reconstruction precisions were largely limited by the achieved precision in the survey of control points with the total station. For each plot, PhotoScan produced pre-rain and post-rain point clouds which were manually edited to remove vegetation points using the software Cloud Compare (General Public Licence, 2014). Vegetation-free point clouds were then converted in Digital Elevation Models (DEMs) (Figures 11 and 12) and analyzed within ArcGIS (ESRI, 2011).

3.3 Experimental protocol

Once a plot was prepared and the simulator set up, a series of pictures was taken before any rainfall to reconstruct soil surface microtopography prior to the event. Rainfall was started immediately after the pre-rain pictures were taken. At the onset of runoff, i.e., when runoff reached the collection pan, the time-to-runoff was recorded. At Price, rainfall was stopped after 15 minutes of runoff had occurred while at the remaining 8 sites rainfall continued until a trendless real-time hydrograph was observed for ten minutes, marking steady state conditions.

Pre-rainfall soil samples were collected on control plots using a standard hand shovel due to the lack of soil adhesion. The control plots provided information on pre-simulation soil characteristics, since sampling in the rainfall plots would affect the flow and erosion processes.

During each rainfall simulation, time-stamped runoff samples were also collected for sediment concentration and water quality analysis (TDS) in addition to the concentration of cations and anions. Sampling was done at a frequency of one sample / minute for the first three minutes and every three minutes there on. Sediment concentration samples were collected in 1L bottles which were immediately weighed to get water and sediment weights and oven-dried to get sediment mass used for concentration calculation. Water quality samples were collected in 50 mL centrifuge tubes immediately acidified with a hydrochloric acid solution and refrigerated to maintain the integrity of the liquid phase chemical speciation. At the end of each rainfall simulation, a delay of 30 minutes was observed before taking post- rain pictures for surface microtopography reconstruction. This delay allowed for ponding water to infiltrate in the soil, for accurate modeling of the soil surface.

In the plots where rainfall was applied, post-rainfall soils were collected using a split soil core sampler (AMS, Inc., American Falls, Idaho) which is 25 cm long with a 5cm inside diameter. At each plot, soils were collected at three locations under the vegetation canopy and three interspace locations. Soil sample locations were subjectively chosen in an area towards the middle portion of the plot to minimize the lateral flow effects that may occur near the plot borders. Cores were then separated by depth increments into the surface crust (0-1 cm) (Figure 6), depth increment 1 (1-6 cm), and depth increment 2 (6-11 cm) (Figure 10). The number of depth increments and the total depth of the core was determined by the depth of the wetting front from the first soil core collected at each plot. Depth increments are included in the sampling protocol because of the possible salt changes with depth that may be mobilized by greater rainfall intensities and vegetation. Finally, each soil sample was made into a composite soil sample with respect to vegetation versus interspace and by depth increment, resulting in 6 composite samples per plot. The soil samples were stored in Ziploc bags and placed in a cooler without refrigeration. At the end of our field work, we collected a total of 810 composite soil samples (90 from each site).

Soil samples were then placed in a beaker with distilled water to perform saturated water extract using the immiscible displacement method (Mubarak and Olsen 1976). The anions Cl^-, NO_2^-, NO_3^-, and SO_4^- were extracted and analyzed using the Dionex Ion Chromatography (IC) System (Thermo Fisher Scientific, Inc., Waltham, Mass.). The cations Ca^{2+}, Mg^{2+}, Na^+, and K^+ were extracted and analyzed using Atomic Absorption spectroscopy Perkin Elmer Inc., Waltham, Mass.) and 4200 MP-AES (Agilent Technologies, Inc., Santa Clara, Cal.) Ammonium acetate exchangeable cations (Ca^{2+}, Mg^{2+}, Na^+, K^+) also were analyzed using Atomic Absorption Spectroscopy. Ammonium (NH_4^+) for Cation Exchange Capacity (CEC) and the KCl extractable solutions (NH_4^+/NO_3^-) were analyzed using Lachat Quikchem Flow Injection Analyzer System (Hach Company, Loveland, Col.) and Astoria micro-Segmented Flow Analysis (Astoria Pacific, Clackamas, Ore.) . The pH of 1:2 ratio of soil

: ½ M $CaCl_2$ solution was determined using a ph/mV/˚C meter (Oakton Instruments, Vernon Hills, IL) and the EC was quantified using a Model 2052 Portable EC Meter (VWR International, Radnor, PA).

Runoff water was collected and analyzed from the simulation plots (12 m^2). The concentrations of major cations and anions in the simulation water and runoff water were determined by Atomic Absorption Spectroscopy and Dionex IC.

Figure 9. Surface cap at Dry XII, Utah illustrating the cracked surface in irregular polygons with minimal aggregate stability and no surface foliar or ground cover to protect it from erosion processes.

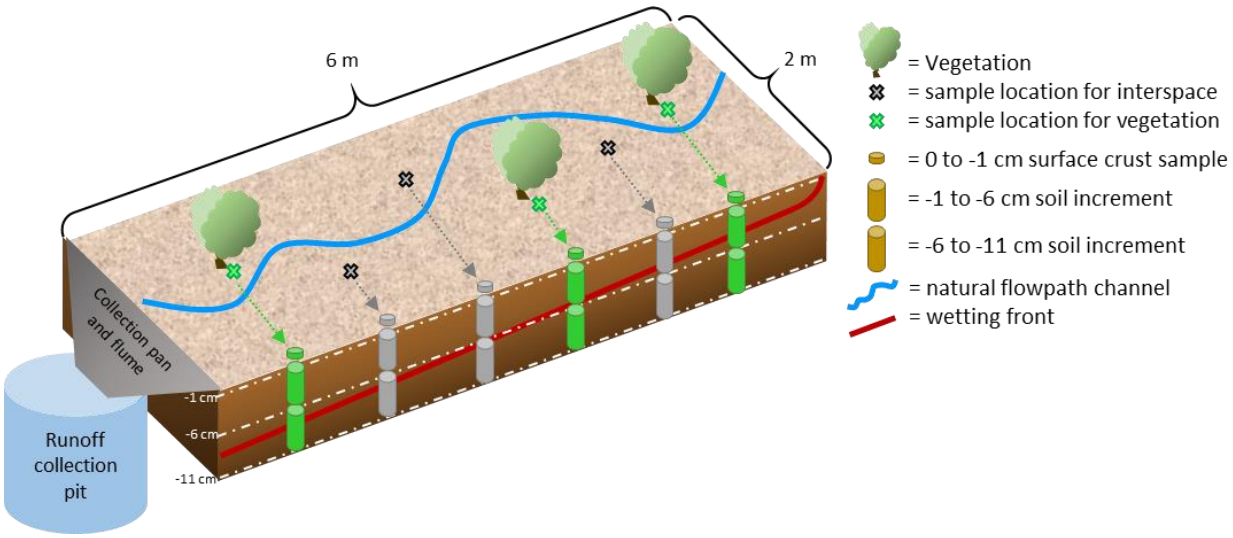

Figure 10. Conceptual drawing of the plot setup and sampling locations for runoff and soil.

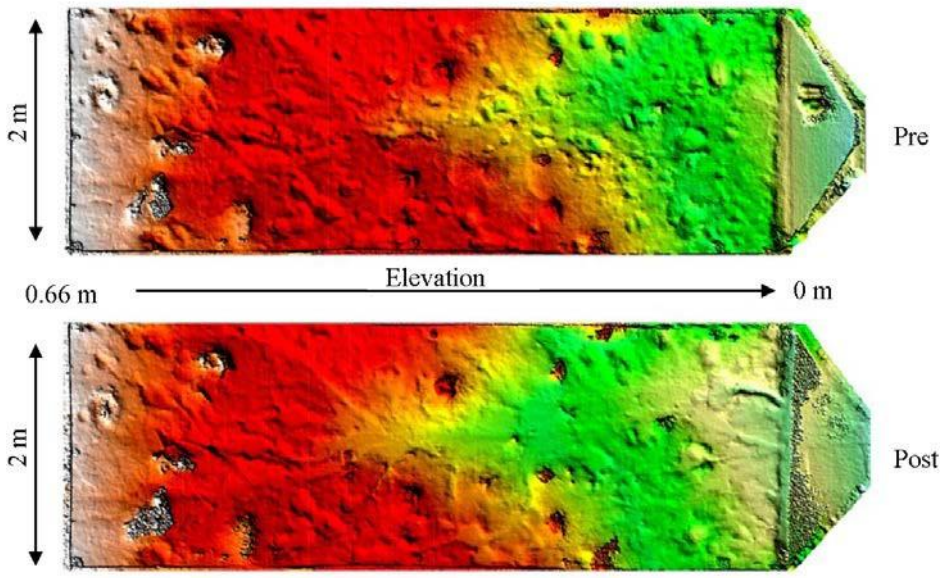

Figure 11. Example of 5 mm resolution DEMs representing soil microtopography reconstructed pre and post rainfall.

3.4 Quality Assurance (QA) and Quality Control (QC)

To ensure data integrity and minimize measurement errors throughout the site selection, site characterization, rainfall simulation process, and soil and water analysis, quality assurance and quality control measures were applied from planning objectives to data collection, to data analysis and interpretation. The group of researchers and technicians at USDA- ARS and UNR adopted protocols for simulation, soil and water sampling, vegetation and soil cover determination at the field and applied them on the nine selected sites. Data are collected at the field using computers and software to save data.

Quality assurance took place daily to clean data and correct techniques applied in the field at nearly every step of the project: planning, calibrating the equipment and the testing the software, data collection in the field and laboratory, data compilation, and data review. Errors detected during QA were corrected immediately or later in the office after comparing the obtained data using different techniques such as the determination of runoff with time using different methods. Everyone involved in the simulation processes, laboratory analysis, and data entry, data analysis and reporting were responsible for QA. After each simulation day, researchers and technicians reviewed data sheets for completeness and correctness, checked the soil and water collected samples numbering, backed up the collected data, recalibrated the equipment used in the field, and recharged the equipment for the simulation next day. QA was applied in lab work by:

1. Ensuring use of protocols to organize the samples collected from the field
2. mixing the soil subsamples taken from the same depth and the same micro-zones together according the protocols
3. selecting the appropriate analysis methods on the available equipment
4. calibrating the analysis equipment and running known samples before to ensure proper performance
5. using Excel to file analysis results
6. reviewing data sheets for completeness and correctness
7. backing up the collected data
8. Quality control processes were performed

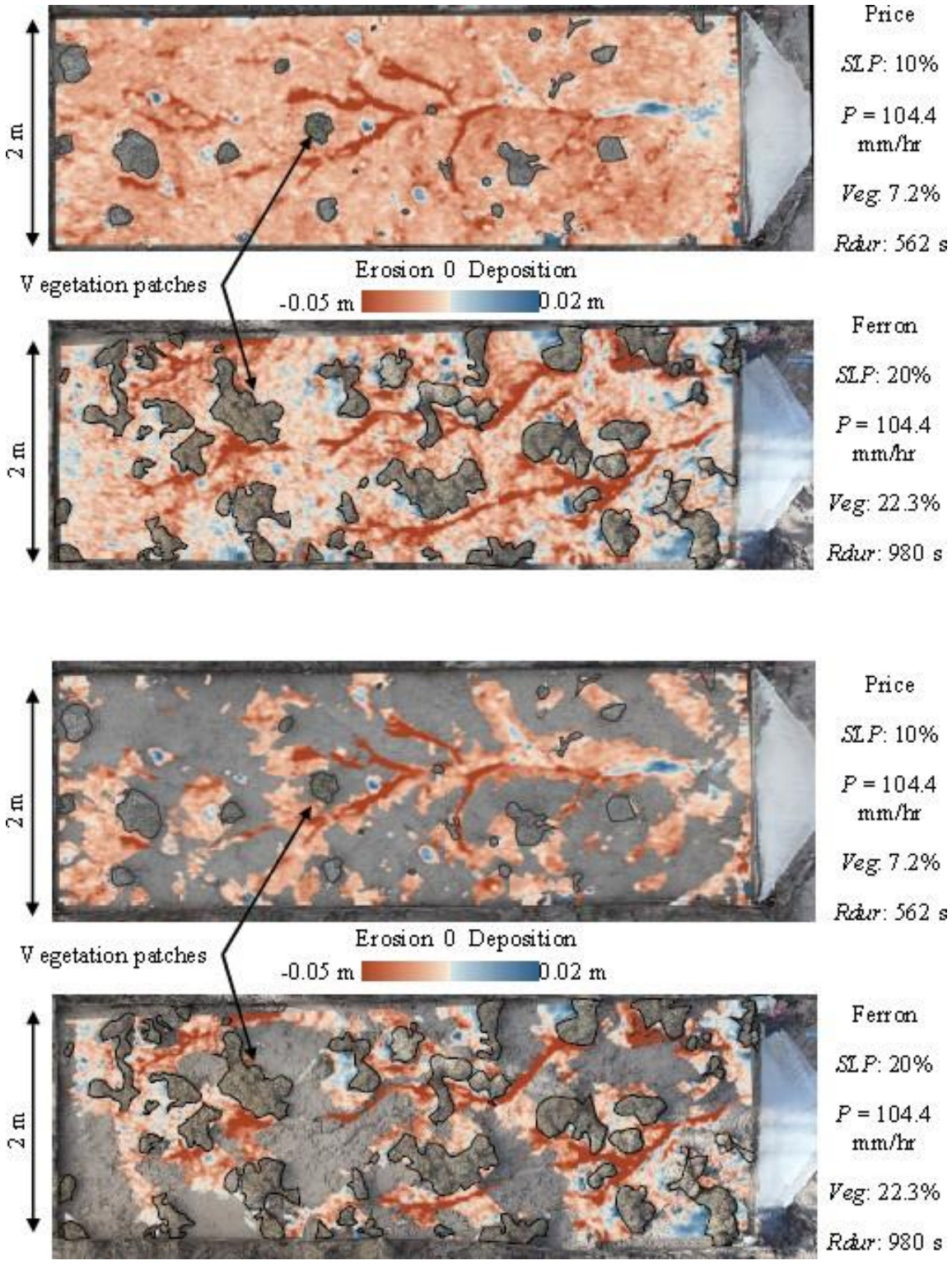

Figure 12. Example of elevation change maps used for the analysis of channel processes.

Quality control processes were performed in the office after collecting all field and laboratory analysis. Error corrections during QC were limited because simulation plots cannot be rerun with the exact conditions that occurred during the simulations and data collection in the field. Concerning lab analysis, we rerun some samples when errors were expected in the results. The researchers who know the limits and the parameters of the data performed the QC.

Cross-Checking Chemical Analyses for Consistency and Reliability was performed according to Brown et al. (1954) through considerable number of interrelations that exist among the values obtained for various determinations such as:

- The EC of soil saturation extracts when expressed in millimhos per centimeter at 25 °C and multiplied by 10 is approximately equal to the total soluble-cation concentration in mmolc/l.
- The total soluble anion concentration or content and the total soluble cation concentration or content, expressed on mmolc/l basis, are nearly equal.
- As a general rule, soils with saturation extracts that have a calcium concentration of more than 20 meq./l. should be checked for the presence of gypsum.
- The pH reading of gypsiferous soils at the saturation percentage is seldom in excess of 8.2 regardless of the ESP.
- In general, ESP increases with SAR. There are occasional deviations, but generally low SAR values of the saturation extract are associated with low ESP values in the soil, and high SAR values denote high ESP values.

Some parameters were measured using more than one method to ensure data integrity and minimize measurement errors such as soil moisture (gravimetric method and using sensors), runoff (automated discharge measurement was validated with periodic manual timed-sampling of runoff rate). Composite soil samples were obtained by mixing subsamples to reduce the coefficient of variation and better represent soil properties. In addition to the set of soil analysis according the protocol, % gypsum and $CaCO_3$ effervescence was performed on the pre-simulation samples for better explanation of the analytical results and better description of the sites.

4. Key Findings

4.1. Relationship between runoff TDS and sediment concentration

Regression analysis for sediment concentration (kg/L) versus Total Dissolved Solids (TDS, mg/L) in runoff was done in order to investigate the relationship between sediment and salt loading (Figure 13) using data from Price and Dry X. Average sediment concentration significantly predicted average TDS concentration ($b = 5548$, $p < 0.001$, $R^2 = 0.82$) and the linear model did not over-fit the data ($R^2_{pred} = 0.76$). Except for one outlier (Dry X, plot 6), the residuals (Figure 14a) are well behaved. The normal probability plot (Figure 14b) does not reveal any departure from normality as indicated by visual inspection and the Anderson-Darling normality test ($AD = 0.509$, $p = 0.179$).

This strong linear relationship is consistent with findings from other studies on salinity transport processes (Ponce 1975; Evangelou 1981; Laronne and Shen 1982). Ponce (1975) studied soil erosion and salinity transport processes on the Mancos Shale formation near our study area in the Price River watershed. Ponce conducted rainfall simulations with variable rainfall intensity (25 – 75 mm/hr) over time (60 and 100 min). Ponce found statistically significant correlations between suspended sediment and TDS in runoff for several plots located on the undivided Mancos ($R^2 = 0.28 – 0.81$) and the Upper Blue Gate Member ($R^2 = 0.00 – 0.46$) of the Mancos Shale formation. Ponce attributed the variability in the linear correlations to be representative of the variability in dissolution rates of suspended sediment particles.

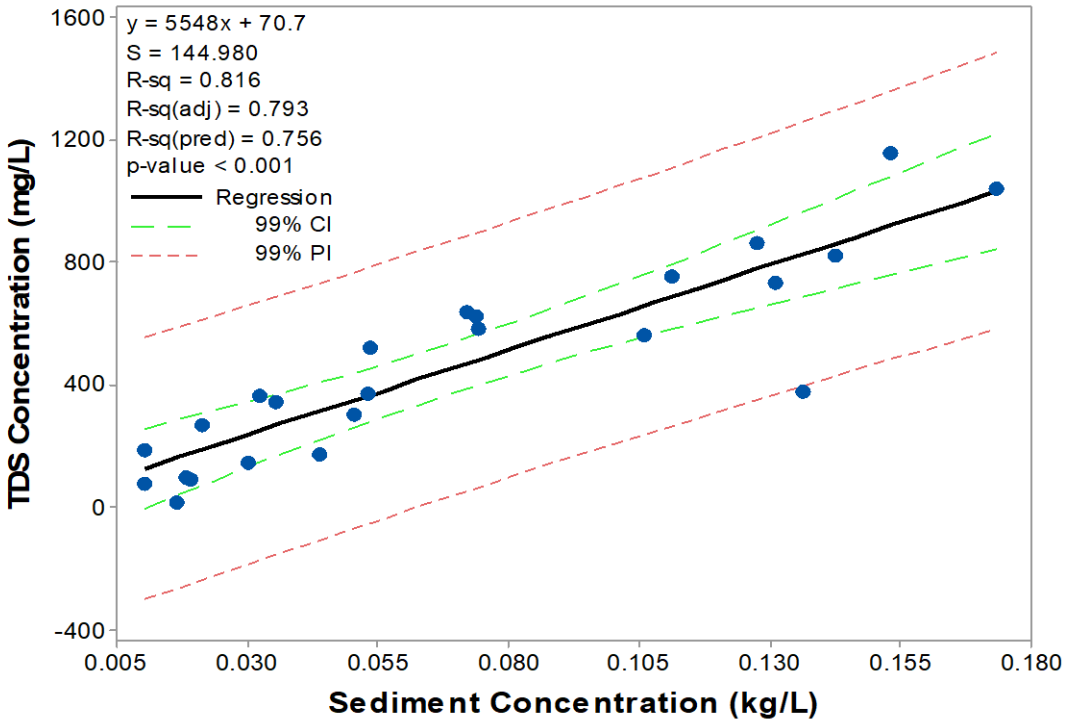

Figure 13. Regression of plot average sediment concentration vs. plot average run off TDS.

Laronne and Shen (1982) directed a runoff study on the Mancos Shale formation which investigated several mechanisms to explain the variability in TDS in runoff and to also verify the findings by Ponce (1975). Evangelou (1981) conducted a chemical and mineralogical study to investigate the diffuse source of salts from the Mancos Shale formation and concluded that CEC is the mechanism that drives a substantial increase in salinity loading on Mancos Shale soils. This suggests the primary process related to salinity transport is a combination of (1) a dissolution of free (not included in CEC) soil salts and (2) a release of CEC-bound salts into soil solution during the erosion process.

4.2. Biotic and abiotic factors controlling sediment transport at the sites studied

A series of studies were conducted using the select sites in the entire dataset to improve understanding on the land surface characteristics that best control soil erosion, sediment transport and soil and water chemistry in these arid ecosystems. These studies are part of published (Nouwakpo et al. 2018) and upcoming peer-reviewed papers. Fine-scale vegetative heterogeneity of a hydrologically stable grassland facilitated run on processes. Coarseness or increased spatial distance between shrubs in degraded rangelands amplifies runoff with increasing slope length (Figure 15) (Abrahams et al. 1995; Parsons et al. 1996). On disturbed rangelands, increased connectedness of bare soil patches allows the formation of concentrated flow paths, which initiates gully formation, increased runoff, and soil loss (Wilcox et al. 2003a; 2003b; 2003c; Pierson et al. 2009; Urgeghe et al. 2010). Once the ecosystem's flow paths have been altered, subsequent storms reinforce gully formation, further accelerating soil loss and decreasing water infiltration rates (Appendix II).

In arid and semiarid rangelands, where vegetation is typically sparse, a synergistic relationship has traditionally been observed between spatial distribution of vegetation and runoff structuring. The VDSH system stems from differential soil development and evolution processes between areas under canopies and bare ground (De Ploey 1984; Nulsen et al. 1986; Caldwell et al. 2012) resulting in feedback mechanisms perpetuating or further accentuating the bare ground – under canopy soil dichotomy. Observations in semiarid rangelands suggest that deposition mounds form upstream of plant clumps as a result of energy losses and changes in transport capacity

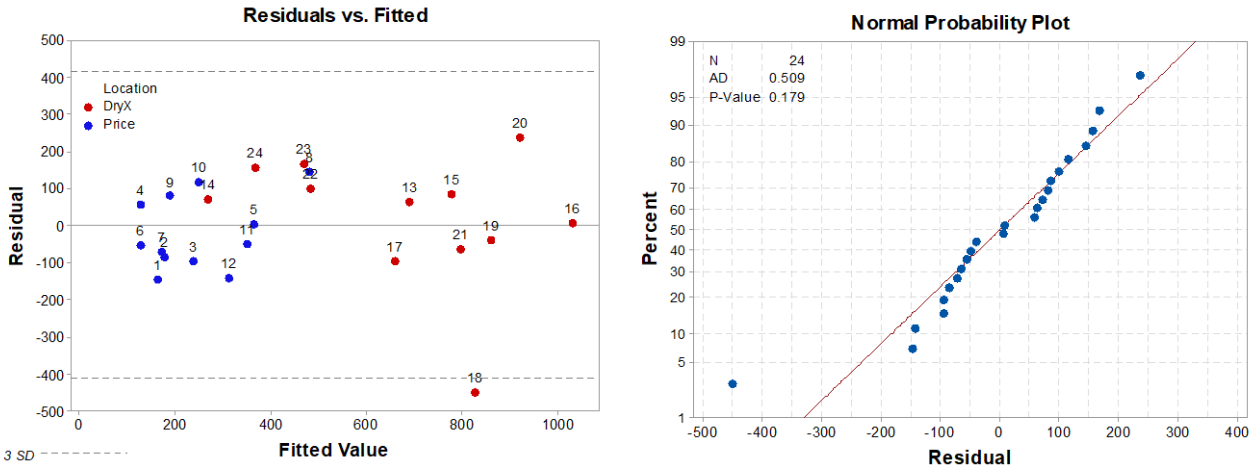

Figure 14. Residual and Normal Probability Plots for average sediment vs. average TDS. (a) Residual plot of regression. (b) Normal Probability plot of regression.

Figure 15. Sparse vegetation at Dry X illustrating concentrated flow and formation of gullies due to limited vegetation and inter-connected interspaces (left) and measuring tapes for determine vegetation gap, rill density and canopy and ground cover (right).

that accompany overland flow diversion by plant stems (Rominger and Nepf 2011; Meire et al. 2014). Entrapment of nutrients along with sediments in these mounds creates areas of nutrient concentration where plants thrive, spatially alternated by bare or poorly vegetated zones of water and nutrient depletion, forming the premise of the "resource islands" or "vegetation island" concept (Li et al. 2007; Ridolfi et al. 2008). From a hydraulic standpoint, these "vegetation islands" can further exacerbate the concentrated flow process.

Examples of this negative feedback loop are seen most often in shrub-dominated landscapes in the United States, which have formed coppice dunes such as sagebrush (*Artemisia* spp.), saltbush (*Atriplex* spp.), creasotebush (*Larrea tridentata*, DC. Coville), mesquite (*Prosopis glandulosa* Torr.), greasewood (*Sarcobatus vermiculatus*, Hook. Torr.) and in pinyon (*Pinus* spp.) and juniper (*Juniperus* spp.) woodland dominated areas in arid and semi-arid rangelands (Pierson et al. 1994a; Pierson et al. 1994b; Spaeth et al. 1994; Davenport et al. 1998; Eldridge and Rosentreter 2004; Li et al. 2013). These studies illustrate that a coarsely arranged source-sink structure, as observed on degraded sites, potentially generates and releases more surface runoff than a finely structured source-sink community (Schlesinger et al. 1990; Abrahams et al. 1995; Parsons et al. 1996; Wilcox et al. 1996; Davenport et al. 1998; Bhark and Small 2003). Numerous studies have been conducted that provide comparative examples of these relationships for fine (grassland) versus coarsely arranged (shrubland) rangeland communities in southern Arizona (Parsons et al. 1996; Wainwright et al. 2000; Turnbull et al. 2010; Turnbull et al. 2012), (2010). Pierson et al. (2013) and Williams et al. (2014a) present examples of similar relationships following pinyon and juniper encroachment into Great Basin shrub steppe.

Litter and slash from fallen woody plants can result in formation of debris dams (Figure 16). Debris dams form when concentrated flow pushes loose unconsolidated organic material down slope. When the material contacts restrictions like rocks or the basal area of a plant the material can bridge the gap forming a dam. As more litter is pushed down slope the dam can build to several centimeters high. This results in a temporary detention pond being formed, downslope water velocity is retarded, and sediment is deposited behind the dam. These dams are not stable and can be breached if the velocity and/ or volume of the incoming water increases (increase in rainfall intensity). This breach can result in a sudden release of water and the formation of an incised rill with accelerated soil erosion.

Figure 16. Debris dam formed from loose pinyon and juniper slash, litter and duff .

Soil fauna activity is enhanced by the microclimate, moisture regimes, and nutrient availability underneath canopies. The associated biological activity further improves soil aggregation, macroporosity, and infiltration (Cammeraat and Imeson 1998; Puigdefabregas et al. 1999; Dunkerley 2002; Belnap et al. 2005; Ludwig et al. 2005). Stemflow concentrates water input at plant bases, allowing rapid vertical recharge of the soil profile via preferential flow along root channels (Thurow et al. 1987; Navar and Bryan 1990; Martinez-Meza and Whitford 1996; Devitt and Smith 2002; Bhark and Small 2003; Lebron et al. 2007). Plant growth form also influences infiltration processes. Infiltration rates are generally higher for bunchgrasses than sod-forming grasses (Wood and Blackburn 1981; Knight et al. 1984; Thurow et al. 1986; Thurow et al. 1988; Blackburn et al. 1992; Pierson et al. 2002). Greater vegetative biomass and organic matter accumulation on bunchgrasses than sodgrasses result in greater rainfall and runoff interception (Knight et al. 1984; Thurow et al. 1986; Thurow et al. 1988). Additionally, biomass and organic matter accumulations under bunch-grasses most likely favor infiltration-increasing microbial activity (Blackburn et al. 1992). Infiltration under shrub canopies is usually greater than under grass canopies (Wood and Blackburn 1981; Schlesinger et al. 1999), but the relationship may be reversed depending on grass biomass (Wilcox et al. 1988). The overall greater infiltration in canopy patches on shrublands and grasslands increases water availability beneath canopies, which in turn stimulates biological activity, plant growth, and

organic matter and nutrient recruitment. This creates a continuous positive feedback (Schlesinger et al. 1990; Belnap et al. 2005; D'Odorico et al. 2007).

Interspace areas on rangelands, particularly shrublands, are often associated with surface and subsurface characteristics that inhibit infiltration and soil water storage and promote rapid ponding and runoff initiation. Interspaces occur with various amounts of herbaceous cover, or exist as contiguous bare patches (Blackburn et al. 1992; Pierson et al. 1994a; Pierson et al. 1994b; Wilcox and Breshears 1994; Abrahams et al. 1995; Parsons et al. 1996). Well-vegetated interspaces may exhibit similar surface characteristics as canopy areas to some degree, but usually generate more surface runoff (Reid et al. 1999; Bhark and Small 2003; Wilcox et al. 2003b). On more water-limited or degraded sites, interspaces have low plant biomass and organic matter and thin surface soil horizons (Blackburn and Skau 1974; Abrahams and Parsons 1991; Parsons et al. 1996; Wilcox et al. 1996; Pierson et al. 2010). These characteristics result in poor aggregate stability and soil structure, and high bulk densities relative to coppices. They also facilitate low infiltration rates (Blackburn and Skau 1974; Roundy et al. 1978; Johnson and Gordon 1988; Wilcox and Wood 1988; Blackburn et al. 1992). In general, surface characteristics of interspace areas are consistently different from coppices throughout the year, but the magnitude of the differences and respective influences on infiltration exhibit some seasonality. The spatial differences in vegetation cover and surface characteristics exert a greater influence than do seasonal differences on infiltration and runoff generation from sparsely covered shrublands; whereas seasonal differences in spatially arranged plant biomass might be of greater influence on infiltration patterns on well-vegetated grass-dominated sites (Blackburn et al. 1992).

Rock cover on the soil surface has a complex relationship with infiltration and soil erosion processes (Figure 17). The effects of rock cover (> 2 mm) depend on the size, amount, and embeddedness of the rocks (Wilcox and Wood 1988; Poesen et al. 1990; Poesen and Ingelmo-Sanchez 1992). Infiltration is generally positively correlated with rocks lying on top of the soil matrix due to increased surface roughness and greater porosity and aggregation around rocks; surface rock extends time to ponding and runoff, increasing time for infiltration (Poesen et al. 1994; Valentin 1994; Cerdà 2001) .

Figure 17. Accelerated upland rill erosion showing exposed rock fragments in interspace following intense thunderstorm.

Infiltration is negatively correlated with embedded rock cover due to a decrease in nonabsorbing area. Numerous authors reported negative correlations between rock cover and infiltration in interspace areas, but did not explicitly evaluate embeddedness (Wilcox and Wood 1988; Abrahams and Parsons 1991, 1994; Pierson et al. 2010; Pierson et al. 2013). The studies by Wilcox et al. (1988) and Abrahams and Parsons (1991) indicate interspace areas occurred in swales and were more compacted and crusted than coppice areas. These authors suggested that the negative correlations were not exclusively associated with rock cover; instead, the relationship was due to co-occurring low infiltration rates of the bare interspace areas and extensive rock cover. Wilcox et al. (1988) further indicated infiltration was negatively correlated with smaller size rock cover (2 to 12 mm) and positively correlated with rock cover of intermediate sizes (26 to 150 mm). Tromble et al. (1974) also reported a negative relationship in infiltration and small-size rock cover (less than 10 mm). These studies suggest rock cover can facilitate infiltration and that negative effects of rock cover on infiltration most likely occur when smaller rocks dominate and the rock cover is embedded rather than freely lying atop the soil surface (Brakensiek and Rawls 1994). Rock fragments may provide protection from raindrop impact but do not substantially reduce hydraulic shear stress or rilling in semi-arid shrub dominated landscapes. For large rainfall events, the depth and shear stress of flow in the rills exceeds the resistance offered by the rock fragments and substantial rilling does occur between the shrub dominated coppice dunes in the desert southwest (Tiscareno-Lopez et al. 1993).

Infiltration in interspace locations is strongly influenced by the expanse of bare ground, rock cover, or vesicular crusts (Blackburn and Skau 1974; Wood et al. 1978; Johnson and Gordon 1988; Pierson et al. 1994a; Parsons et al. 1996; Reid et al. 1999; Pierson et al. 2010). Exposure of bare ground to raindrop impact increases the potential for surface sealing or development of infiltration-inhibiting surface crusts (Branson et al. 1981; Puigdefabregas et al. 1999). Decreasing infiltration and increasing runoff with increasing expanse of bare or vesicular surfaces are well documented in literature (Blackburn et al. 1992; 1994a; Schlesinger et al. 1999; Schlesinger and Andrews 2000; 2002; Pierson et al. 2007a; 2010; 2014; Williams et al. 2014a; 2014b). Of interest in rangelands are biological soil crusts (cryptogams) which have significant soil erosion resistance-conferring properties and have extreme susceptibility to disturbance (Figure 18). Biological soil crust is a term used to define a collection of nonvascular plants: mosses, algae, lichens, liverworts, and cyanobacteria.

Figure 18. Biological soil crust near Moab Utah.

The impact of biological soil crusts on infiltration rates and soil erosion is poorly understood and often contradictory. Biological soil crusts can reduce infiltration rates and increase soil erosion by blocking flow through macropores or they may enhance porosity and infiltration rates by increasing water-stable aggregates and surface roughness (Loope and Gifford 1972; West 1991; Eldridge 1993). Disturbance of the soil surface can disrupt biological soil crusts and result in enhanced wind erosion and may or may not affect water erosion processes (Belnap and Gillette 1998; Eldridge and Koen 1998; Barger et al. 2006; Li et al. 2008; Belnap et al. 2009). Li et al. (2008) evaluated the interactions between biological soil crusts and runoff on a hillslope with patchy shrub vegetation and reported that in undisturbed areas 53% of the simulated rainfall became runoff from the crust patches and 55% of this was redistributed and absorbed by the shrub patches. In addition, approximately 75% of the sediments, 63% soil carbon, 74% nitrogen, and 45% to 73% of the dissolved nutrients transported in runoff from the crust patches were delivered to shrub patches. The disturbance of crust patches tended to result in the uniform distribution of water over the whole slope with a corresponding reduction in the transport of runoff and nutrients from the crust patches to the shrub patches.

The exact response on runoff and soil erosion is a function of site disturbance and level of development of the biological soil crusts (Belnap et al. 2013). When studies are evaluated based on biological crust type and utilizing naturally occurring differences among crust types, results indicate that biological crusts in hyper-arid regions reduce infiltration and increase runoff, biological soil crusts have mixed effects in arid regions, and increase infiltration and reduce runoff in semi-arid cool regions. Most research has shown that intact biological soil crusts are effective at reducing soil erosion and transport of soils and associated contaminants (Belnap 2006). Additional research is required before the role that biological soil crusts play in altering transport of salts (dissolution of salt crusts by efflorescence) is fully understood. Also, while mechanisms of concentrated flow detachment are well understood, prediction of sediment delivery is often complicated by the less studied deposition processes.

Numerous attempts have been made to establish cover guidelines required for site protection from soil erosion. There are various cover types (i.e., rock, cryptogams, litter, and vegetation), each offering varying degrees of soil protection. The amount and effectiveness of cover necessary for site protection depends upon other factors such as slope, soil type, time of year, and rainfall intensity and duration. Wilcox (1994) found that within the bare interspace areas of pinyon-juniper woodland, most erosion was produced by large convective summer thunderstorms and erosion was slight during the winter, even with high runoff rates from snow melt, due to the absence of raindrop detachment. Generally, the greater the bare soil area, the greater the erosion rate. Reported levels of cover necessary for site protection range from 20% in Kenya (Moore et al. 1979) to 100% for some

Australian conditions (Costin et al. 1959). Most studies indicate that cover of 50 to 75% is probably sufficient to minimize soil erosion (Packer 1951; Orr 1970; Gifford 1984).

The percentage of event rainfall captured by vegetation and associated ground cover generally decreases as rainfall intensity increases (Carlyle-Moses 2004; Owens et al. 2006). For low-intensity, short-duration rainfall events, most of the precipitation is captured by plant canopies, litter, and other ground cover and is lost to evaporation (Owens et al. 2006; Dunkerley 2008). Water input during high- intensity or prolonged rainfall events usually exceeds interception storage capacity, resulting in delivery of water to the ground surface via throughflow and stemflow (Martinez-Meza and Whitford 1996; Carlyle-Moses 2004; Dunkerley 2008). Interception by individual shrubs and conifers commonly averages 50–60% of water input for low-intensity rainfall events and 5–35% for high intensity or prolonged rainfall events (Hamilton and Row 1949; Skau 1964; Owens et al. 2006; Taucer et al. 2008). Water arriving at the ground surface during an event either ponds at the soil surface, is stored in the litter layer, infiltrates into the soil, or is transferred downslope as runoff. Organic matter contributions and soil fauna activity are typically greater in vegetated and litter covered areas relative to bare areas and facilitate macropore development and soil properties associated with enhanced infiltration (Blackburn 1975; Cammeraat and Imeson 1998; Imeson et al. 1998; Puigdefabregas et al. 1999; Dunkerley 2002; Belnap et al. 2005; Ludwig et al. 2005). Litter layers underneath vegetation also trap water input behind debris dams and thereby delay runoff generation. Prolonged storage at the ground surface allows water to slowly infiltrate, even in the presence of water repellent soils (Leighton-Boyce et al. 2007; Pierson et al. 2013).

Experimental research at the Walnut Gulch Experimental Watershed in southern Arizona revealed that coarsening of the spatial structure of vegetation in shrublands led to an increase in flow concentration and erosion rates (Abrahams et al. 1995; Parsons et al. 1996; Wainwright et al. 2000). VDSH influences not only runoff partitioning into sheet and concentrated flow processes but also seems to control flow characteristics in hillslope rills and channels. The same landscape with uniform disturbance may experience significantly more runoff and soil loss from a similar runoff event due to increased connectivity of bare soils and formation of well-organized concentrated flowpaths. These organized flowpaths rapidly accelerate runoff velocity and the ability of water to erode and transport sediment downslope (Wilcox et al. 1996; Davenport et al. 1998; Urgeghe et al. 2010). Tongway and Ludwig (1997) found for example that on degraded tussock grasslands, overland flow was concentrated in long straight paths between the grasses. In the good condition grassland overland flow was tortuous, uniformly distributed, and produced less soil loss. Plant community physiognomy affects concentrated flow by controlling the connectivity of runoff and sediment sources and the energy of overland flow where it does occur (Williams et al. 2014a; 2015; 2016).

On well vegetated rangelands, downslope transmission of runoff and erosion generated by raindrop splash and sheetflow in isolated bare or sparsely vegetated patches is limited by ground cover or roughness elements that promote infiltration and deposition (Pierson et al. 1994a; 1994b; Reid et al. 1999; Wilcox et al. 2003a; 2003b; 2009). Soil detachment by concentrated flow is well correlated with flow velocity and discharge (Nearing et al. 1997; 1999; Govers et al. 2007; Pierson et al. 2008a; 2009; Al-Hamdan et al. 2012a; 2012b). Flow velocity is strongly related to discharge (Nearing et al. 1997; 1999; Giménez and Govers 2001; Govers et al. 2007; Al-Hamdan et al. 2012a; 2012b). Grass clumps, plant bases, root mounds, and litter dams create topographic highs that may concentrate overland flow where runoff occurs, but the transport and erosive energy of concentrated flow are greatly reduced when flow intersects these roughness elements (Abrahams et al. 1991; Abrahams and Parsons 1994; Al-Hamdan et al. 2012b, 2013).

Reduced flow velocities and energy limit detachment and transport and allow surface runoff to disperse and sediment to fall out of suspension. Rangeland studies from the Great Basin Region, USA, have reported two-fold higher concentrated flow velocities for experiments on bare plots (80% bare ground) relative to well-vegetated plots 20–60% bare ground, (Pierson et al. 2007a; 2007b; 2009). In those studies, erosion from concentrated overland flow was four-fold to eight-fold greater for bare than well-vegetated plots. Sediment transported by concentrated flow where it does occur on well- vegetated sites often forms miniature alluvial fans adjacent to

vegetative clumps (Emmett 1970; Rominger and Nepf 2011; Meire et al. 2014). These features indicate that concentrated flow does redistribute surface soil from bare areas to vegetated zones on hydrologically stable rangelands, but hillslope soil loss from this process is minor under such conditions (Pierson et al. 2007a; 2007b; 2009). Al-Hamdan et al. (2013), infers that the existence of a channel network is dictated not by hydraulic stresses exerted by runoff on bare soil but rather by the spatial distribution and structure of vegetation to which this network is in equilibrium. Concentrated flow becomes the dominant erosion mechanism on degraded rangelands where ground cover is sparse (Pierson et al. 2008a; 2008b; 2009; 2011; 2013; Williams et al. 2014a; 2014b; 2015).

Using data from hundreds of rangeland experimental plots across the semi-arid Great Basin, Al-Hamdan et al. (2012a) proposed a predictive framework characterizing concentrated flow erosion on rangeland hillslopes. Two findings from Al-Hamdan et al. (2012a) are highly relevant to improving understanding of VDSH on flow hydraulics: (1) flow velocity increased exponentially with percentage of bare ground on rangeland hillslopes and this increasing effect was magnified by slope steepness; (2) flow width decreased with proportion of bare ground with again a noticeable reducing effect of slope steepness. In other words, runoff tends to concentrate in more narrow channels as vegetation becomes sparse. The widening of flow concentration pathways with an increase in vegetation as suggested by Al-Hamdan et al. (2012a) seems to reflect the existence of a channel network dictated not by hydraulic stresses exerted by runoff on bare soil but rather by the spatial distribution and structure of vegetation to which this network is in equilibrium.

A series of rainfall simulation experiments were conducted at the Ferron experimental site in July 2015 (DryX-II) to study the effect of changing vegetation cover on sediment transport and total dissolved soils in runoff. In this experiment, three hillslopes of similar slope steepness (14.5 – 17.7%) were identified to fit three vegetation cover classes (Low = L, <5% canopy cover; Medium = M, 5 – 19% canopy cover; and High = H, >19% canopy cover). Four erosion plots were installed on each of the L, M and H hillslopes (Figure 19) and a 25-year return storm simulated until 10 minutes of steady-state runoff discharge was attained. Runoff discharge, sediment concentration and water quality data were collected at regular intervals during each simulated rainfall event.

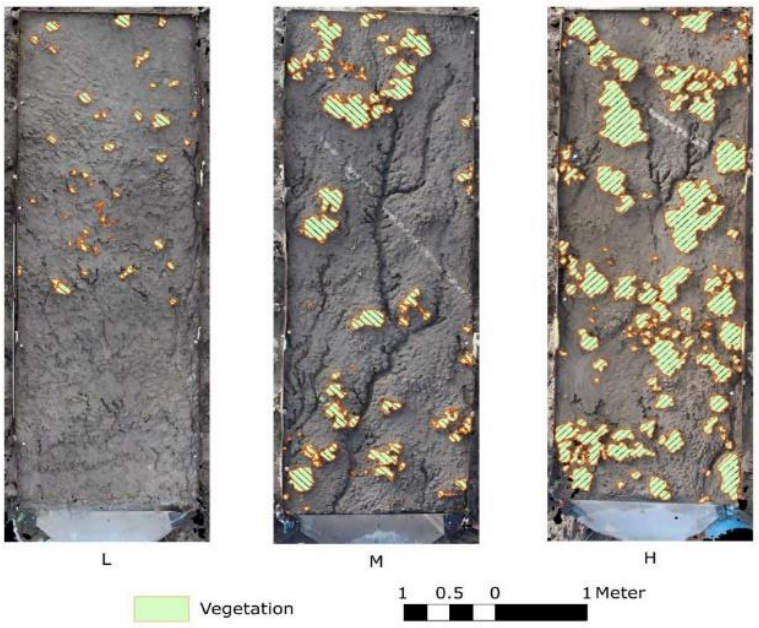

Figure 19. Example of synoptic view of post-erosion plots with low (L), medium (M) and high (H) vegetation canopy covers. Plots were classified as L if canopy cover < 5%, M if 5% < canopy cover < 19% and H if canopy cover > 19%.

The same decreasing trend perceived between runoff volumes and canopy cover can also be observed with the cumulative soil loss after 20 minutes of rainfall simulation (Figure 20). Nevertheless, due to high variability in the erosion data, this inverse relationship was not statistically significant. Runoff volumes after 20 minutes of simulation showed a strong negative correlation with canopy cover (Figure 21). Plots on the H hillslope had generated on average 8.2 mm less runoff than those on the M plots whereas the L plots were not statistically different from the M plots.

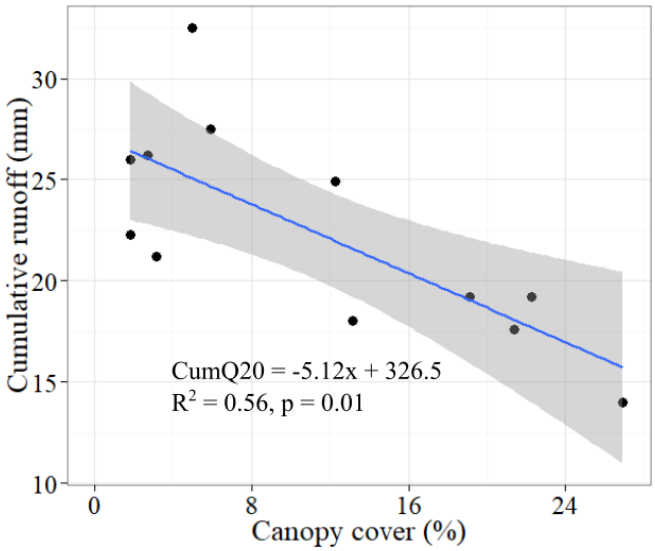

Figure 20. Cumulative runoff after 20 minutes of rainfall simulation (CumQ20) as a function of canopy cover. The grayed area represents the confidence band.

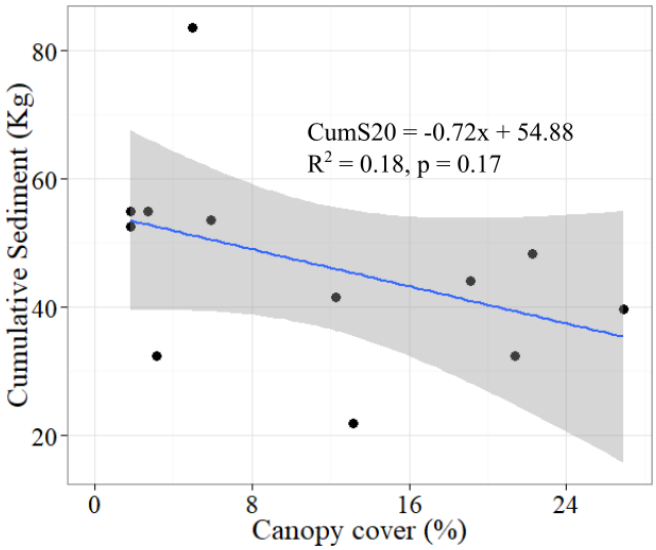

Figure 21. Cumulative soil loss after 20 minutes of rainfall simulation (CumQ20) as a function of canopy cover. The grayed area represents the confidence band.

Analyses of the 3D and GIS data from Price and DryX provided a spatially explicit insight into sediment (and potentially salt) transport as affected by vegetation and other biophysical factors (Figure 22). These findings can be summarized as:

- Erosivity which in this study is represented by runoff discharge drives detachment and transport processes

positive response of the plot-wide and within-rills net erosion volumes TVN and CVN with discharge (as defined in Figure 22).

- Factors controlling surface roughness such as vegetation oppose transport of the detached particles. Illustrated in a decreasing effect of canopy cover on TVN and on CVRN, the ratio of net volume change within rills over plot-wide net volume change.
- Topography (slope) controlled detachment and possibly transport efficiency leading to a positive effect on net volume of erosion within the channel network.

We found that cumulative runoff performed better than cumulative soil loss at predicting plot-wide 3D erosion volumes, an indication that runoff may be responsible for hydrodynamic changes to soil surface microtopography in addition to detachment and transport of soil particles. Plot-wide deposition values were poorly correlated with soil loss and discharge but were primarily controlled by vegetation with a mild influence of slope. Our results suggest that erosivity drives detachment and transport processes. Factors controlling surface roughness such as vegetation promoted deposition and these patterns were accentuated within the channel network.

Across the Price, Dry X and Dry X-II sites studied, the extent of the channel network was primarily controlled by discharge, with vegetation structuring runoff into flow paths to maintain a channel network extent in equilibrium with discharge. Concentrated flow erosion volumes and average depths were lower at Price than they were at Dry X and Dry X-II, due to the lower slopes at the former site. Deposition volume in channels was also a function of vegetation cover with average depth of deposition increased when area available for deposition was reduced by discharge. When concentrated flow detachment energy was parsed into that acting on channel walls and that acting on channel bottoms, the former was dependent on discharge alone while the latter was controlled by both discharge and slope. This finding has significant implications in concentrated flow erosion modelling.

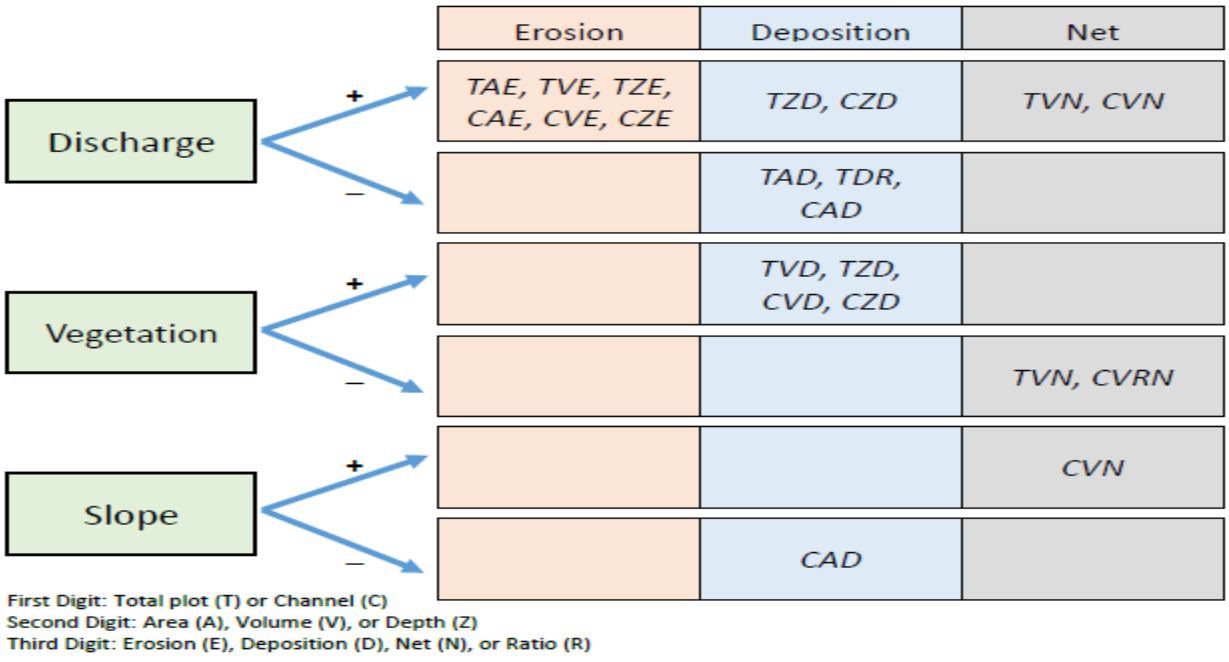

Figure 22. Summary of statistically significant relationships between discharge, vegetation, and slope and key surface change metrics. *TAE*, *TAD*, *CAE* and *CAD* are areal extents (m^2) of erosion and deposition. *TVE*, *TVD*, *CVE* and *CVD* are volumes (m^3) of erosion and deposition. *TVN* and *CVN* are the net volume (m^3) change (Erosion-Deposition); *TZE*, *TZD CZE* and *CZD* are average depths (m) of erosion and deposition; *TDR* is the ratio of deposition over erosion volumes (*TVD*/*TVE*). *CVRN* is the volume-based ratio of net volume change in channels with respect to the entire plot. The symbols (+) and (-) represent respectively positive and negative relationships.

This study showed that significant improvements to erosion and sediment transport models can be achieved by augmenting traditional soil loss and runoff measurements with 3D surface change information. It is often the case that environments where these 3D reconstruction techniques perform well are also susceptible to soil erosion and sediment transport. Knowledge gained from this improved understanding of sediment transport processes will help design effective management and mitigation strategies that target specific physical processes to achieve desired outcomes. Through this work, we have found for example that the key to runoff soil and salt load reduction likely lies in promoting deposition by creating zones of increased roughness along concentrated flow pathways. This can be achieved by increasing vegetation density across the hillslope through restoration activity.

4.2.1. Changes in runoff water quality during rainfall simulation

The reactions between simulation water, soluble and slightly soluble salts, and exchangeable ions tend towards equilibrium. In the following figures (23-25), we present one simulation run (Run 1 of DryX-II) to show detailed results of runoff water quality analysis.

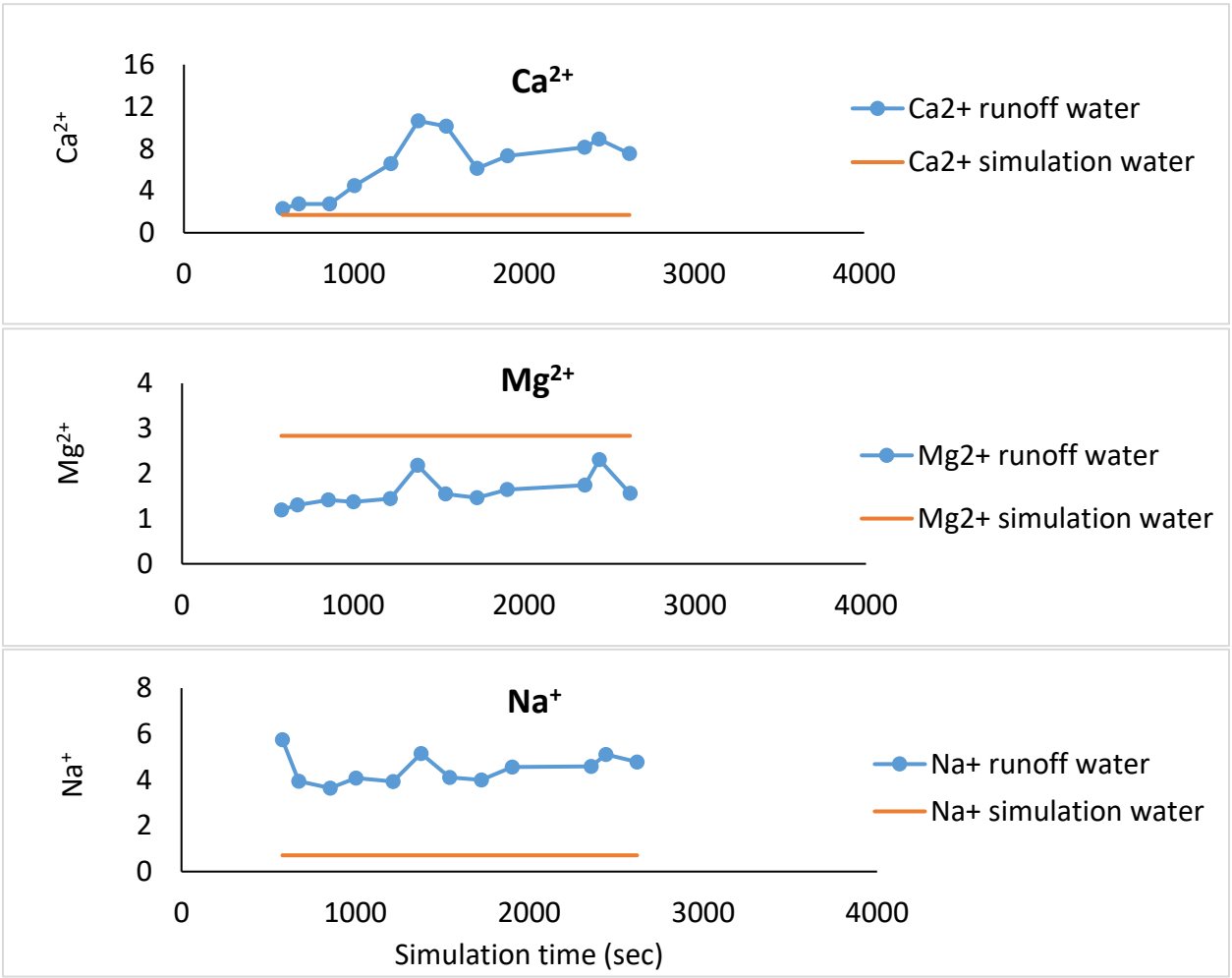

Figure 23. The concentration of three major cations in the simulation water and runoff water of Run 1 at Dry X-II, 2015.

Overall, the concentration of the ions in the runoff water was higher than in the simulation water except for Mg^{2+} which was lower than the simulation water (Figure 23). The increase in ion concentration in the runoff water is the result of fast reactions between the simulation water and the precipitated salts on the canopy, the soluble, and the exchangeable ions of the soil. The concentration of Ca^{2+} and Mg^{2+} in the runoff water starts low and increases with time, while that of Na^{+} starts high and decreases with time which can be explained by the fast solubility of Na-containing salts in the soil such as NaCl and the slower solubility of Ca^{2+}, $Mg^{2+}$and SO^{2-} containing salts such as gypsum (Bharmoria et al. 2012; Lebedev and Kosorukov 2017).

The Cl^{-} has a trend like that of Na^{+} in the previous figure, which can be explained by the higher and faster solubility of salts containing Cl^{-} compared with SO_4^{2-}. The high concentration of Ca^{2+} and SO_4^{2-} in the runoff water might be a result of the dissolution of gypsum in the soil which is limited in the water and slower than the solubility of NaCl (Bharmoria et al. 2012; Lebedev and Kosorukov 2017). A rainfall event of less than one hour is capable of extracting some plant nutrients such as NH_4^{+} and NO_3^{-} from the soil (Figure 24) which might be higher and more important from crop producing lands.

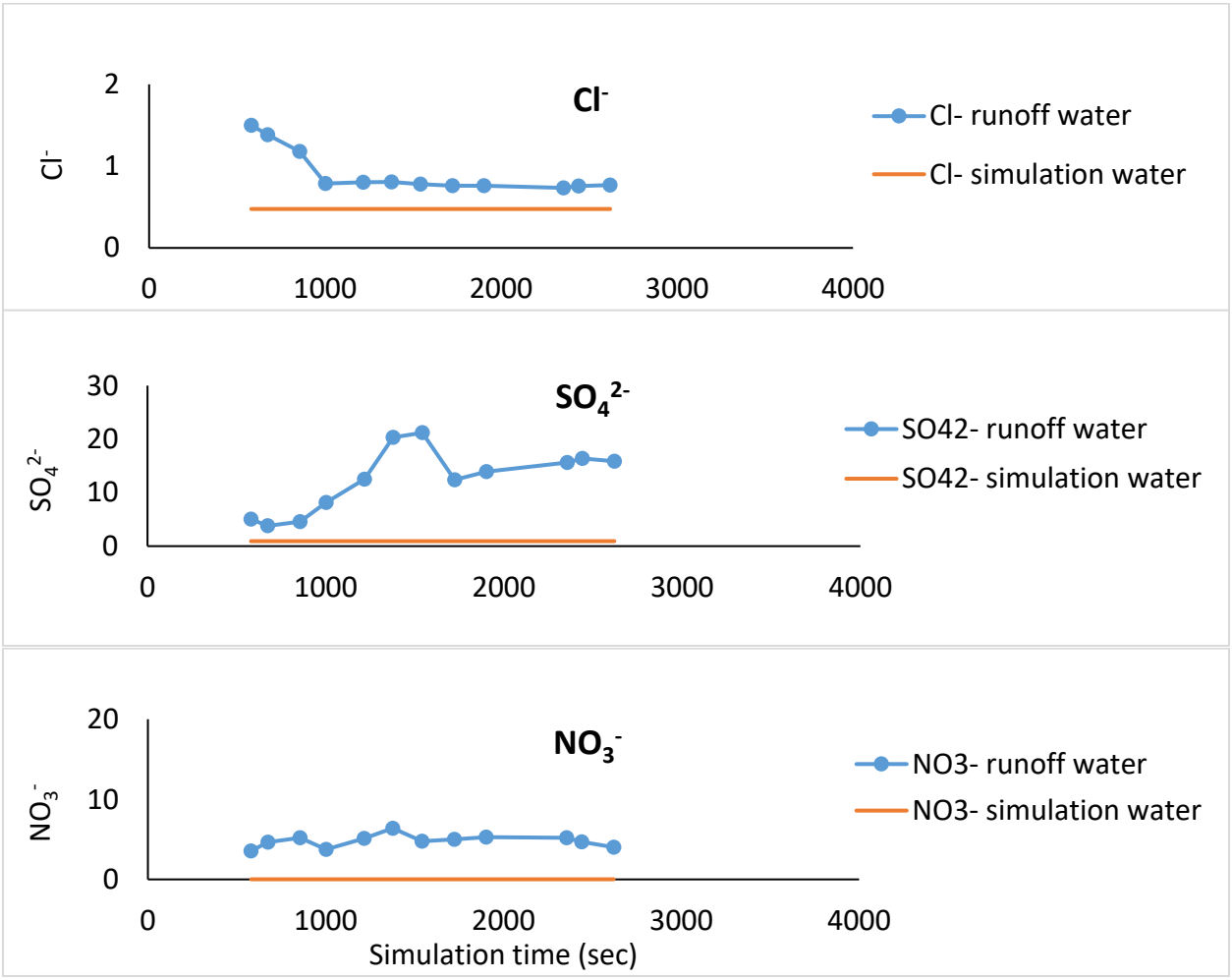

Figure 24. The concentration of three major anions in the simulation water and runoff water of Run 1 at Dry X-II, 2015.

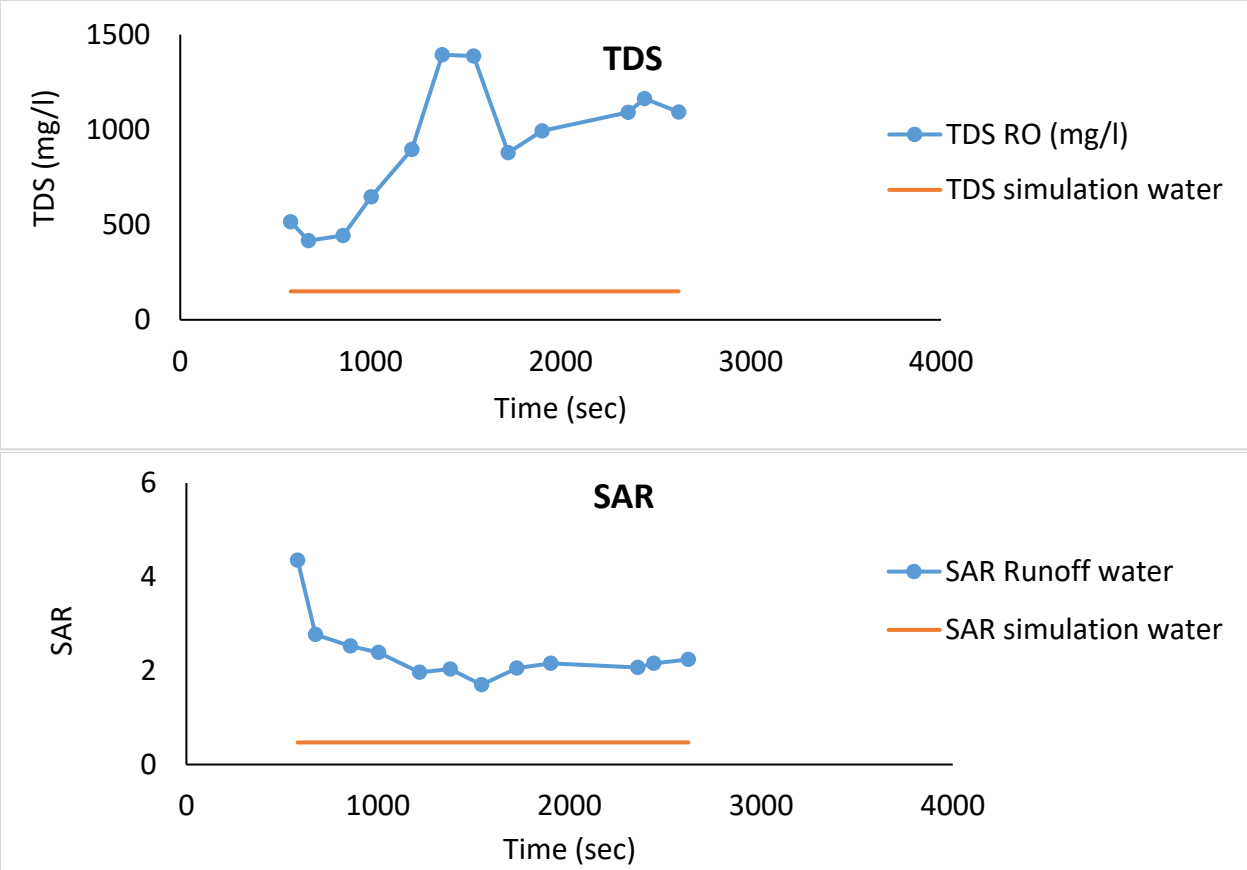

Figure 25. The TDS and SAR of the runoff water and simulation water of Run 1 in Dry X-II, 2015.

As a result of the fast reactions between simulation water and soil, runoff water quality deteriorated and its suitability for irrigation, municipal, and industrial use decreased as a result of increased TDS and N content in addition to Sodium Absorption Ration (SAR). The higher SAR values at the start of the runoff are the results of higher concentrations of Na^{+} compared with Ca^{2+} and Mg^{2+} because of speed and the limitation of salt solubility.

4.2.2. Effects of depth, rainfall intensity on salt transport

Changes to soil chemistry by depth as the result of the rainfall simulation experiment at Price and Dry X are illustrated in Figures 26 - 29. Multiple linear regressions were performed on the sums of cations and anions in the soil for each of the sites to assess the effect of various factors on solute mobility in the soil profile in Tables 3 through 6. The predictors used in these linear models were depth, rainfall intensity and microsite (vegetation vs. interspace).

Soil cations and anions generally increased in concentration with depth at both Price and Dry X before each rainfall event (values at 0 mm/hr intensity in Figures 26 - 29). At DryX, there was an effect of soil depth significant at 10% confidence level (Table 5 and 6). Concentration in positive charges (cations) increased with depth. An increasing gradient in negative charges with depth was also observed in the anion analysis at DryX but only the coefficient of the surface layer (Depth 0) was statistically different from 0. At Price, soil depth also had an increasing effect on concentration in ions with again a more pronounced effect on cations. Overall, this finding suggests that at both Price and DryX, surface layers were depleted of ions perhaps through processes of

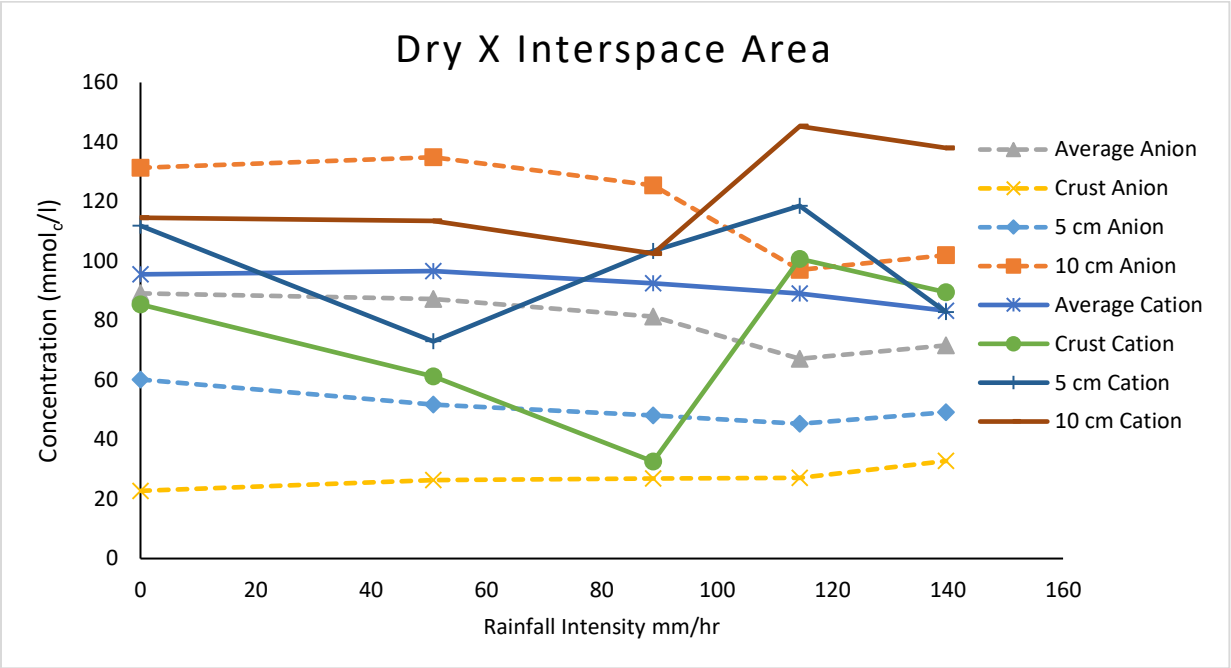

Figure 26. Mean cation and anion concentrations in saturated extract without bicarbonates in the soil interspace between shrubs at Dry X, Utah as a function of rainfall intensity and soil depth.

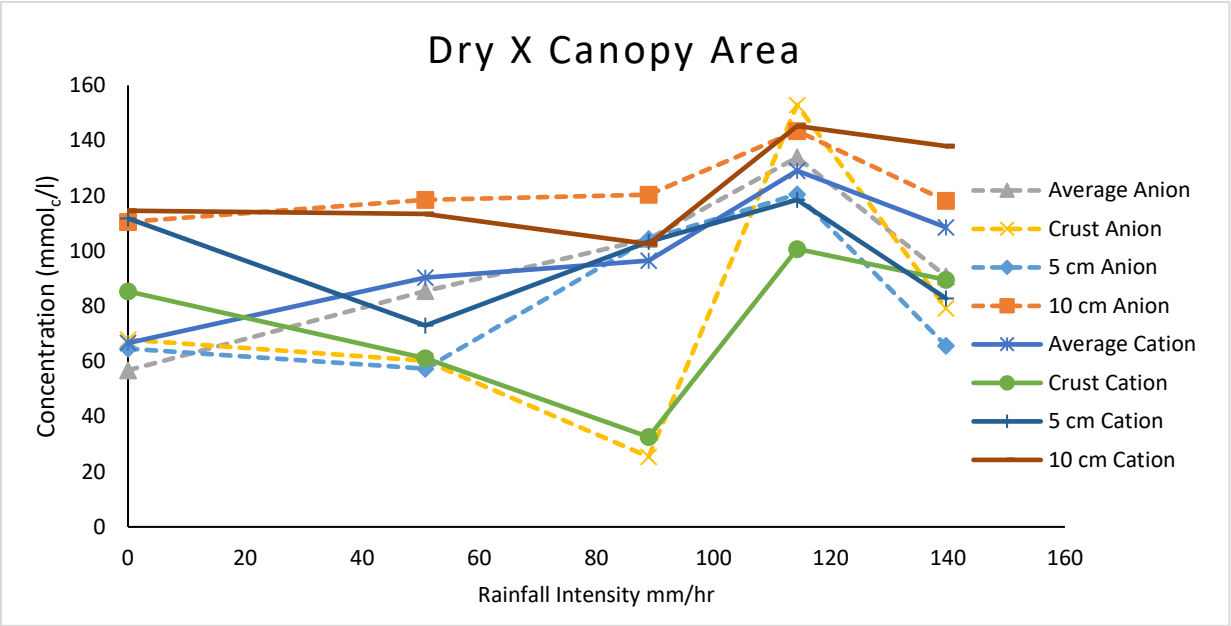

Figure 27. Mean cation and anion concentration in saturated extract without bicarbonates under the dominant shrub species at Dry X, Utah as a function of rainfall intensity and soil depth.

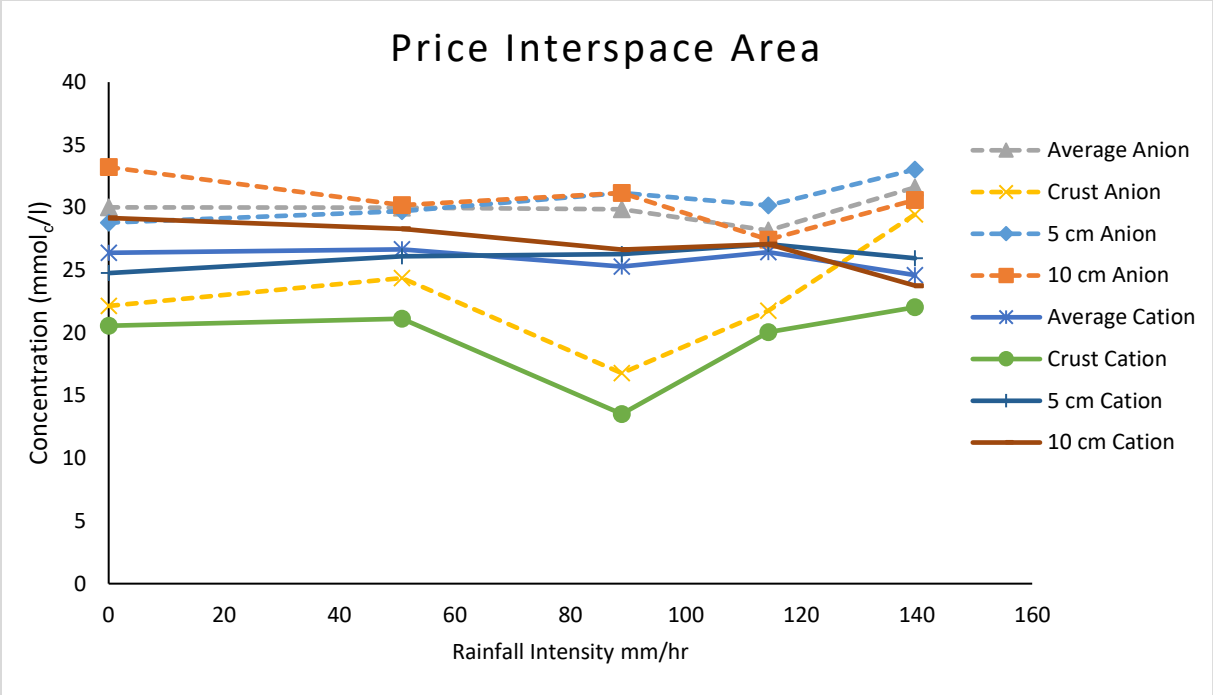

Figure 28. Mean cation and anion concentration in saturated extract without bicarbonates in the soil interspace between shrubs for the Price, Utah site as a function of rainfall intensity and soil depth.

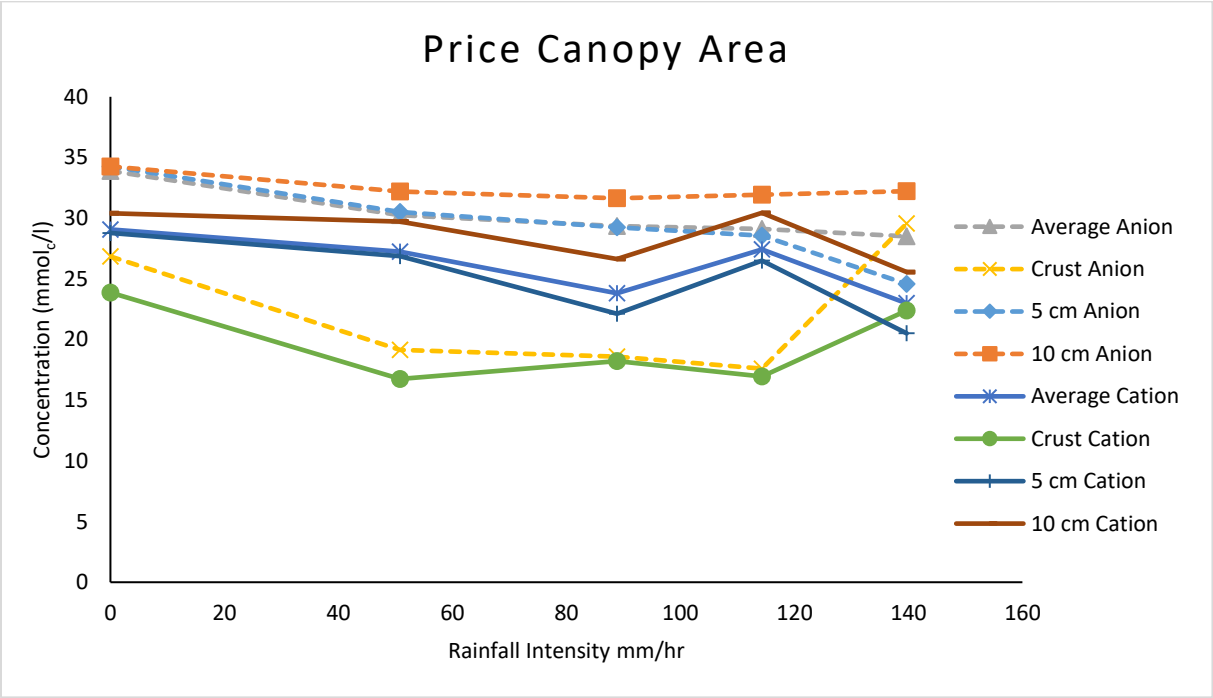

Figure 29. Mean cation and anion concentration in saturated extract without bicarbonates in the soil directly under dominant shrubs species for the Price, Utah site as a function of rainfall intensity and soil depth.

Table 3. Analysis of Variance table of concentration in soil cations with depth at the DryX site.

	Sum Sq	Mean Sq	F value	Pr(>F)
Depth	72380	36190	2.70	0.09 .
Intensity	48235	48235	3.60	0.07 .
Microsite	7917	3958	0.30	0.74

Significance codes: 0-0.001:***, 0.001-0.01:**, 0.01-0.05:*, 0.05-0.1:.

Table 4. Analysis of Variance table of concentration in soil cations with depth at the Price site.

	Sum Sq	Mean Sq	F value	Pr(>F)
Depth	331.10	165.55	25.12	0.00 ***
Intensity	29.15	29.15	4.42	0.04 *
Microsite	5.45	2.73	0.41	0.66

Significance codes: 0-0.001:***, 0.001-0.01:**, 0.01-0.05:*, 0.05-0.1:.

Table 5. Analysis of Variance table of concentration in soil anions with depth at the DryX site.

	Sum Sq	Mean Sq	F value	Pr(>F)
Depth	6123	3061.6	2.60	0.09
Intensity	1679	1679.3	1.43	0.24
Microsite	15186	7592.9	6.46	0.01 **

Significance codes: 0-0.001:***, 0.001-0.01:**, 0.01-0.05:*, 0.05-0.1:.

Table 6. Analysis of Variance table of concentration in soil anions with depth at the Dry X-II site.

	Sum Sq	Mean Sq	F value	Pr(>F)
Depth	376.41	188.21	14.05	0.00 ***
Intensity	13.18	13.18	0.98	0.33
Microsite	1.78	0.89	0.07	0.94

Significance codes: 0-0.001:***, 0.001-0.01:**, 0.01-0.05:*, 0.05-0.1:.

infiltration and leaching. Nevertheless, evidence of salt efflorescence at the DryX site indicates that surface layers might be enriched in certain ions through upward movement of soil water processes following rainfall events through the process of evaporation. Overall this redistribution was inconsequential on total ion concentration.

In the interspaces at DryX (Figure 26), the concentration of anions in the upper 11 cm decreased from 95.52 to 67.14 $mmol_c/l$ with increasing the intensity of simulation to 114.3 mm/hr, and increased a little to 71.63 mmolc/l with increasing the intensity further to 139.7 mm/hr. In general, as one increased the depth of sampling, the concentration of sum of anions increased under all simulation intensities.

Other key findings include:

- The 1 to 6 cm layer had the same trend of the average 11 cm of the soil (decreasing with increasing the intensity to 114.3 mm/l and increasing a little after that for the highest intensity 139.7 mm/hr, but with lower values and ranged between 60.19 and 45.29 mmolc/l.
- The 6 to 11 cm layer had the same trend of the average 11 cm of the soil (decreasing with increasing the intensity to 114.3 mm/l and increasing a little after that for the highest intensity 139.7 mm/hr but with higher values ranged between 131.31 and 97.01 mmolc/l.
- At Dry X, cations were modestly predicted by the explanatory variables with only 26% of the variability explained. Anions at this site responded better to the linear model ($R^2 = 0.42$).

At Price, Figure 28 indicates that the upper 11 cm of the interspace soil at Price is slightly affected by salinity (the sum of cations and anions are between 20 and 40 mmolc/l in the saturated extract.). The changes in cation and anion concentration in the different soil layers of the interspace behave similarly. The crust has the lowest salinity, and the salinity increases with deeper layers. The salinity of the saturated solution under vegetation was similar to the interspace, and increasing the intensity did not change the salinity of the saturated extract in the upper 11 cm of the soil. Soil cations and anions at Price were better predicted by the multiple regressions with 67 and 52% of the variability explained respectively.

In both interspace and under plant canopies at Price and in the interspace at DryX, rainfall intensity had a decreasing effect on soil salt concentration. This decrease affected both surface and deeper layers of the soil profile, which is consistent with a vertical downward flushing of soil cations. An increase in rainfall intensity leads to an increase in runoff depth and greater infiltration rate. In this study, increase in rainfall intensity was also positively correlated with total rainfall amount because rainfall durations did not significantly vary between intensities. Ions are mobilized in infiltrating water and rapidly mobilized downward in the soil profile. From field observations, we found the wetting front to be between 8 and 10 cm of depth, suggesting that a considerable amount of solute flux occurred under unsaturated conditions below 10 cm of depth. A decrease in soil anions with intensity likely occurred but was masked by the higher variability measured in the anion analyses. Figures 26 - 29 show a tendency of salt content within the soil profile to homogenize with increasing rainfall intensity (i.e. rainfall amount), illustrated by all anions and cations graphs seeming to converge towards similar ranges after the most intense event. The increase in salt ions with intensity observed under canopy areas at DryX may be due to a number of factors including: leaching of salts from the leaves of the mat saltbush that makes up most of the vegetation at this site or sediment and salt deposition under shrub canopies when runoff water flowing in the interspaces encounters the rougher vegetated patches.

It is important to note that the measured concentration of cations appears higher than anions because bicarbonate concentration was not estimated in the soil saturated extract used to determine soil chemistry.

4.2.3. Effect of vegetation on salt transport and spatial variability

The rainfall simulations at Dry X-II were conducted to determine the changes in salinity and the amounts of ions moved with runoff water as a function of percent canopy cover. The concentration of major cations and anions (Ca^{2+}, Mg^{2+}, Na^{+}, K^{+}, NH_4^{+}, Cl^{-}, NO_3^{-}, SO_4^{2-}, and HCO_3^{-}) in the simulation water, runoff water, CEC, soil saturated extract and on the colloidal surfaces were determined. Runoff water was collected and analyzed from the simulation plots (12 m^2). The presence of gypsum, which was confirmed by acetone test (Brown et al. 1954; Burt 2011) and the predominance of calcium and sulfates (Khechai and Daoud 2016) of the saturated soil extract required a special selection of ion determination methods and calculation procedures (Arslan and Dutt 1993; Arslan 1995; Khechai and Daoud 2016).

4.2.4. Runoff water quality

At DryX-II, average discharge after ten minutes of steady state runoff was 527.38 L, corresponding to an overall runoff ratio of 48.94%. The average eroded sediment (84.25 kg) formed 15.98% of the runoff water by weight and contained an average of 697g of total salts removed from the upper 11 cm, while average ammonium and nitrates in the runoff water were 4.18g and 3.93g respectively (Figure 30). The amounts of salts, ammonium and nitrates are the net values calculated after subtracting their concentrations in the simulating water (Table 7). Small coefficient of variation (%CV) values were obtained for runoff (4.02%) and erosion (7.13%) after grouping the results into high (H), medium (M), and low (L) percent canopy cover compared with the %CV of salts moved with runoff water (18.91%).

The sediment concentration in runoff water ranged between 15% and 17% without significant differences between the three canopy covers. The concentration of salts in the runoff water is controlled by salt concentration on the soil particles' exchange sites and a free soluble fraction. Salt loss in runoff from plots with high density cover (0.90 g/L) was much smaller than that from plots with medium (1.52 g/L) and low (1.60 g/L) canopy cover, suggesting a beneficial effect of vegetation on salt delivery to runoff during erosive events.

4.2.4.1. Vegetation and soil chemistry

During each rainfall simulation, soil moisture increases to reach values close to saturation in the upper layer of the soil and moves deeper in the soil with time, diluting soil solution and dissolving the existing salts in the studied soil layer. After rain, the soil dries up and the concentration of ions in the soil increases and salts might precipitate again. In our study we determined in saturated extract the concentration of Ca^{2+}, Mg^{2+}, Na^{+}, K^{+}, NH_4^{+} as cations; and Cl^{-}, NO_3^{-}, SO_4^{2-}, and HCO_3^{-} as anions to follow the movement up and down in the soil. The average electrical conductivity (EC_e) of the soil under shrubs before the rain (9.56 dS/m) was higher than the interspace (8.24 dS/m), which can be attributed to the precipitated salts from the *Atriplex* leaves fallen under canopy. In addition, the unsaturated movement of solute towards elevated mounds of the soil underneath shrubs (Nouwakpo et al. 2017) is also expected to move and deposit salts under the canopy. The average SAR before rain under canopy (27.62) was higher than that of the interspace (21.92) which is an indication of higher Na concentration to Ca and Mg under canopy (Lesch and Suarez, 2009). The salinity of the soil under canopy after all runs remained higher than under interspace and increased in most cases, while the salinity of the interspace decreased after simulations.

During each rainfall simulation, soil moisture increases to reach values close to saturation in the upper layer of the soil and moves deeper in the soil with time, diluting soil solution and dissolving the existing salts in the studied soil layer. After rain, the soil dries up and the concentration of ions in the soil increases and salts might precipitate again. In our study we determined in saturated extract the concentration of Ca^{2+}, Mg^{2+}, Na^{+}, K^{+}, NH_4^{+} as cations; and Cl^{-}, NO^{-}, SO_4^{2-}, and HCO_3^{-} as anions to follow the movement up and down in the soil.

The average electrical conductivity (EC_e) of the soil under shrubs before the rain (9.56 dS/m) was higher than the interspace (8.24 dS/m), which can be attributed to the precipitated salts from the *Atriplex* leaves fallen under canopy. In addition, the unsaturated movement of solute towards elevated mounds of the soil underneath shrubs (Nouwakpo et al. 2017) is also expected to move and deposit salts under the canopy.

The concentration of the saturated extract salts of the upper 11 cm of the soil increased under canopy and changed in the interspace (average high canopy cover) after rainfall which is an indication of water and salt movement from the surface down to the 6 -11 cm depth. This is associated with movement of moisture observed after the runs. One expects a downward movement through depletion at the surface and an enrichment below (Figure 31).

Table 7. Cumulative amounts of runoff water and its constituents from each simulation plot (12 m^2) at Dry X-II.

Run	*Q (l)*	*Sediment (Kg)*	*Salts (g)*	*NH_4^+ (g)*	*NO_3^- (g)*
1	799.34	122.91	645.97	5.61	2.96
2	679.40	96.70	462.33	5.46	1.62
3	439.91	86.99	379.07	3.64	1.88
4	315.55	66.46	512.41	2.59	1.16
5	518.95	94.69	722.79	4.13	3.54
6	430.68	70.98	782.39	3.52	9.76
7	414.90	52.66	592.21	3.28	1.93
8	617.78	101.93	1073.95	5.19	4.23
9	479.23	76.61	614.79	3.90	1.96
10	648.68	114.96	949.35	5.25	4.70
11	594.23	83.42	995.83	4.68	4.21
12	389.88	42.75	643.33	2.97	2.76
Average	527.38	84.26	697.87	4.18	3.39
%CV	25.69	0.03	29.73	23.58	65.30
Average H	558.55	93.26	499.94	4.32	1.90
Average M	528.00	79.44	800.82	4.20	3.41
Average L	495.58	80.07	792.84	4.03	4.86

Figure 30. Super critical flume for measuring runoff volume, flow rates runoff, sediment concentration, and water quality (left) and collecting water quality samples to determine salt transport off site (right). Detailed photos showing all steps in data collection are in appendix II.

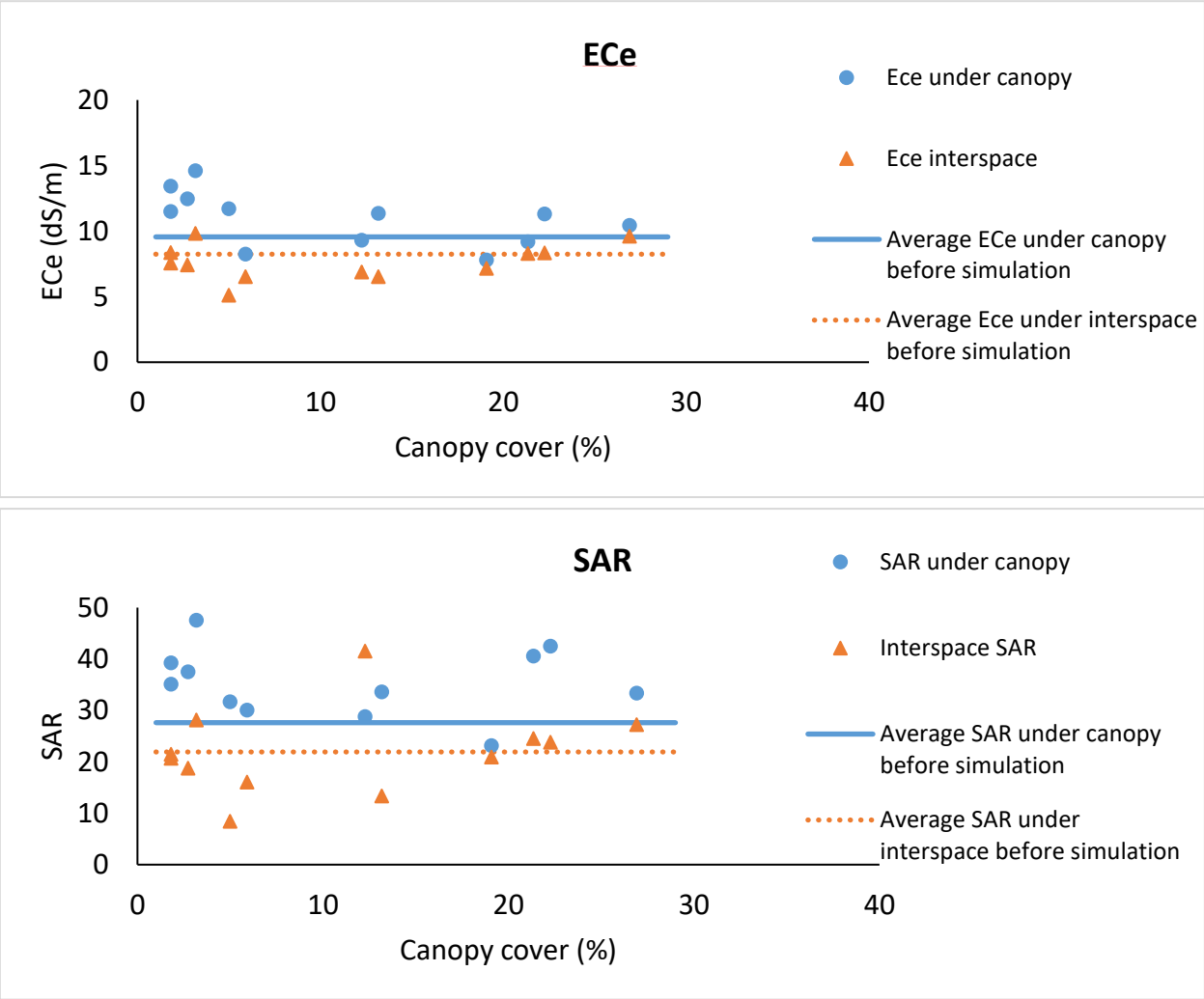

Figure 31. Average Interspace and under canopy ECe of the upper 11 cm of the soil before simulation and after simulation for different canopy covers in Dry X-II, 2015.

We found in this study that the sum of exchangeable cations (60.67 $mmol_c/kg$) was much higher than the CEC determined with NH^+ (11.10 mmolc /kg). This finding combined with the positive gypsum test and the high EC_e are evidence of the presence of slightly soluble and soluble salts of the upper layer of the soil. The presence of such salts in the soil requires special care in analysis and calculation of the studied cations and anions balance, where no method is satisfactory (Page et al. 1982). Eliminating gypsum and salts from high EC_e soil before exchangeable cations and CEC determinations is one possible method (Sumner and Miller 1996) to mitigate discrepancies between the sum exchangeable cations and CEC. Corrections for gypsum and calcite dissolution are required from SO_4^{2-} and HCO_3^- contents of the soil solution prior to extraction and the saturating and extracting solution (Amrhein and Suarez 1990; Arslan 1995).

4.2.4.2. Vegetation and spatial variability of salinity:

No statistical difference was observed in cation and anion charges between vegetation and interspace microsites at Price, but at DryX a significant effect of microsite was noted on soil anions (Table 5). The concentration of cations and anions under canopy was lower than in the interspace before rainfall

simulation. Increasing the concentration of cations and anions with increasing salinity coincides with the deposition of sediment under canopy with higher rainfall intensity and the amount of water applied and the 3D reconstructions which show the deposition of sediment (Nouwakpo et al. 2016; 2017). To calculate the overall change in salinity we quantified the saturated extract, percent canopy cover and interspace. The sum of cations under canopy increased with higher rainfall rates and peaked at 114.3 mm/hr but decreased at the 139.7 mm/hr rate where there was less accumulation of sediment and therefore a decrease in the sum of cation and anion concentrations.

Our results (Figure 32) show higher Exchangeable Sodium Percentage (ESP) on the soil exchange sites under canopy before simulation compared with interspace. The ESP increased after all runs under canopy. Th increase in ESP can be attributed to 1) the movement of sediment from the interspace to under canopy as a result of erosion from interspace and deposition under canopy which was clear from the 3D structure from motion analysis (Nouwakpo et al. 2016; 2017, 2018). 2) the dissolution of the precipitated salts from saltbush leaves by simulation water, and 3) the fast solubility of the Na containing salts in the soil.

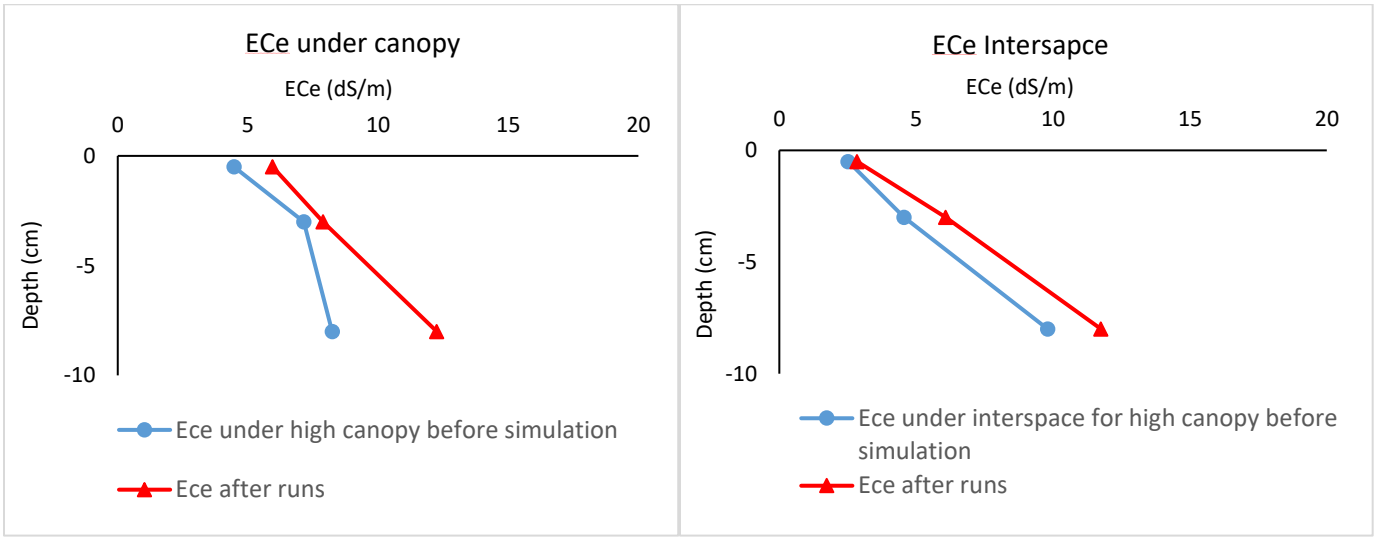

Figure 32. ECe under canopy and interspace before simulation and after runs of the H canopy densities in Dry X-II, 2015.

Although the interspace ESP was lower than that under canopy before simulation, its values decreased after some runs (Figure 33 and 34). Figure 32 shows clear increases of all under canopy ESP values after runs which might be considered evidence of the movement of sediment from the interspace to under canopy as a result of erosion and the dissolution of the precipitated salts on saltbush leaves by simulation water and the solubility of the Na containing salts in the soil.

4.2.5. Linking runoff water quality to readily available soil properties.

Figure 35 shows that the saturated soil water extract solution for the post-rainfall soil cores is a good predictor of the runoff water quality. The ratio of runoff TDS to saturated soil water extract varied between 3 and 35%, suggesting that 65 to 97% of the transported salts in runoff were still protected in the solid phase associated with soil aggregates. While our study was not designed to specifically determine factors controlling the dissolution rate and release of salts into the runoff liquid phase, we can hypothesize the proportion of salt dissolved in runoff to be controlled primarily by mechanical action (e.g., disruption by raindrop impact, frictional forces during transport) and physiochemical disintegration of aggregates

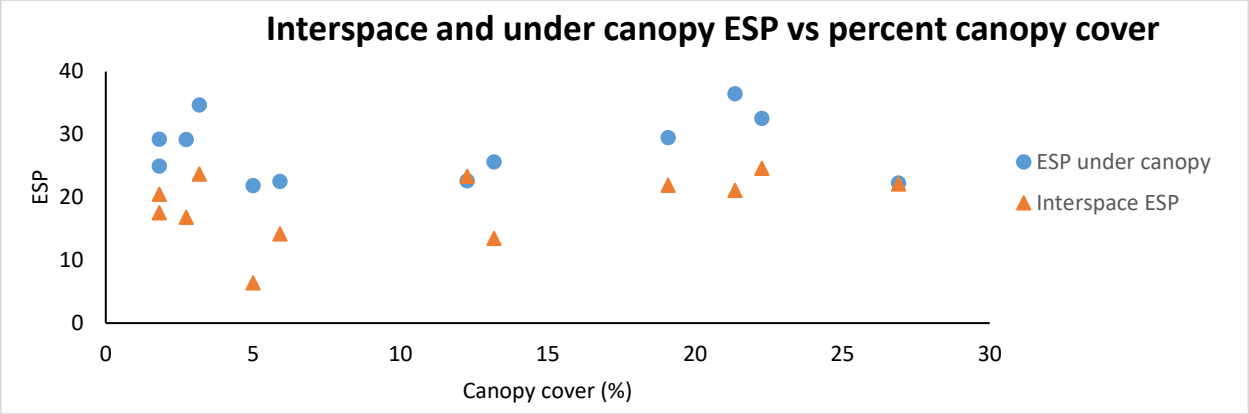

Figure 33. Interspace and under canopy ESP for different percent canopy covers in Dry X-II, 2015.

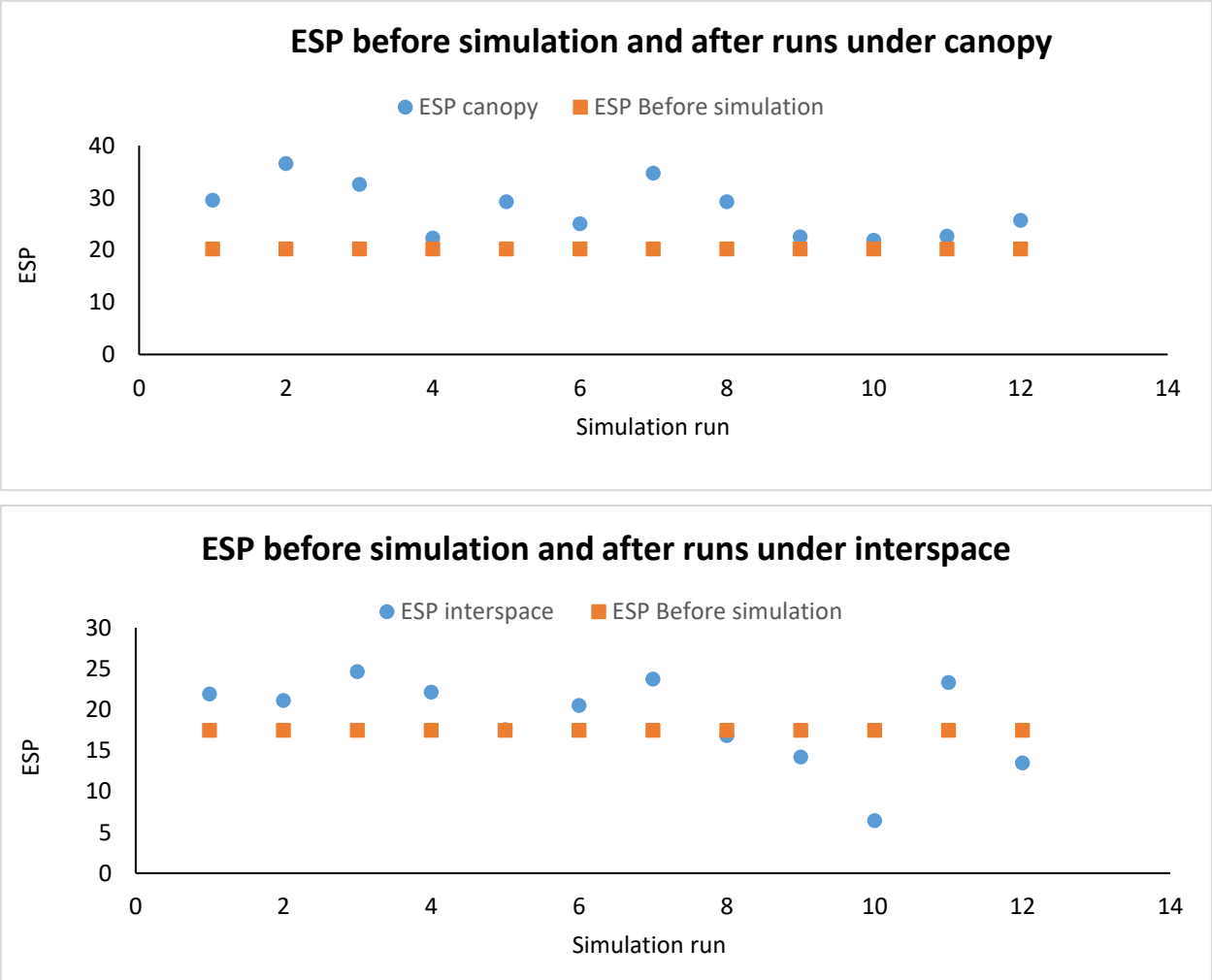

Figure 34. Changes in ESP under canopy and interspaces as a result of simulation for Dry X-II, 2015.

due to the dispersing effect of some cations on clay minerals (feedback mechanism). This information will be useful in the design of management and mitigation strategies. One possible course of action to reduce salt load in runoff is to promote deposition along runoff pathways. A better understanding of the kinetics of salt dissolution in runoff along the hillslope would allow for optimized placements of depositional areas along slopes of the watershed to minimize the transfer of salts into the Colorado River system. This indicates that a significant amount of the salts is bound to the soil aggregates and are not readily dissolved in the runoff water. However, if these soil aggregates do reach a perennial water source, then with time ionic dispersion will occur and additional salt will be released in the water column. The exact rate of this transformation is dependent on various factors such as water temperature and pH. More research is needed to understand the kinetics of salt dissolution in runoff during hillslope erosion and transport processes before we can fully predict salt loading from direct input and from this transformation process once the soil aggregates reach the Colorado River system through its tributaries.

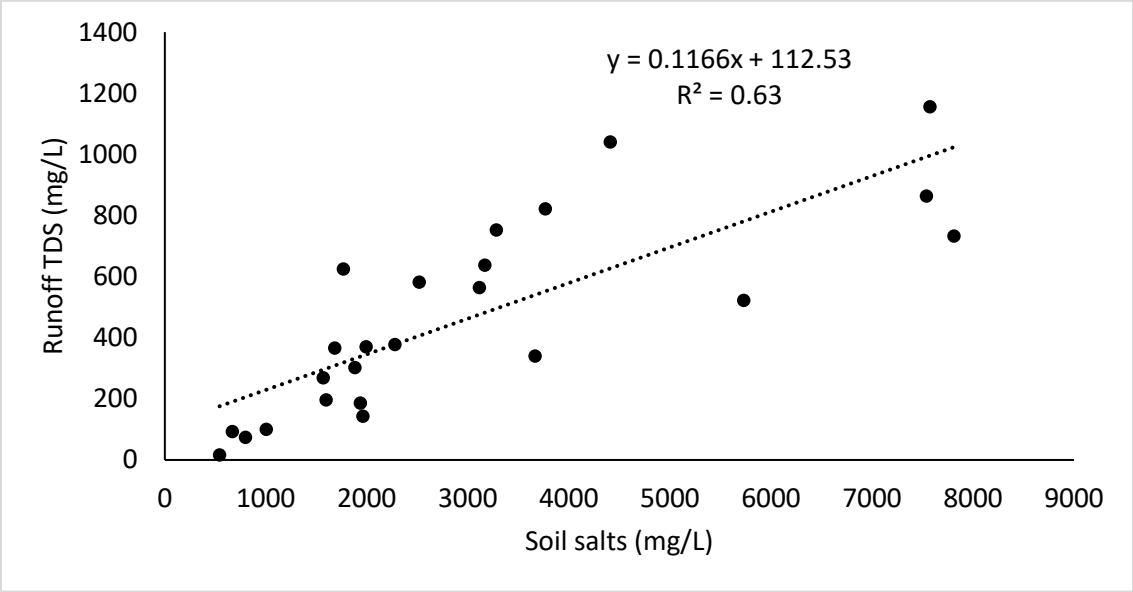

Figure 35 Runoff TDS as a function of Saturated Soil Water Extract EC in surface soil layer.

Saturated Soil Water Extract TDS is often not readily available information in standard soil pedon descriptions. Figure 36 shows that a good approximation of Saturated Soil Water Extract TDS can be made with the more readily available soil electrical conductivity (EC_e) that is available in the Natural Resources Conservation Service soil database. Soil EC_e can therefore be used as a factor to estimate the potential for salt production of a given site. This potential will be factored in the RHEM sediment and runoff output to estimate runoff TDS as the trigger for when to implement specific equations to estimate salt transport processes.

4.3. New parameter estimation equations to address saline conditions with the RHEM model

The data collected in the broader study at six experimental sites was used to develop new parameter estimation equations for the Rangeland Hydrology and Erosion Model (RHEM) to predict soil erosion, runoff quantity and quality on the saline / sodic soils of the UCRB. This work was the object of a journal publication (Nouwakpo et al. 2018) and has received the 2019 Superior Paper Award from the American Society of Agricultural and Biological Engineers (see appendix).

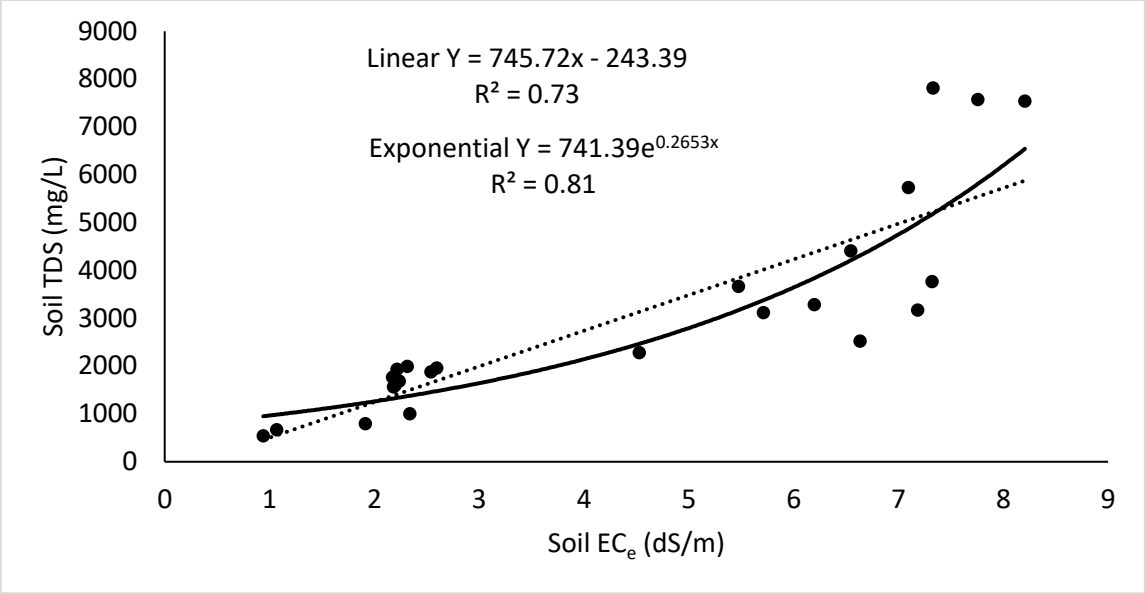

Figure 36. Saturated Soil Water Extract as a function of soil electrical conductivity (EC_e dS/m)

4.3.1. The RHEM model

RHEM is a process-based model developed by the United States Department of Agriculture – Agricultural Research Service to predict runoff and sediment yield on rangelands. The first generation of this model – RHEM v1.0 (Nearing et al. 2011a) was derived from the same scientific foundation as the Water Erosion Prediction Project – WEPP (Flanagan and Nearing 1995) but with cropland-specific equations replaced with new parameter-estimation functions specifically developed from rangeland data. Data from a total of 204 experimental plots at 49 rangeland sites distributed across 15 states of the western USA were used in this first iteration of RHEM (Nearing et al. 2011b). RHEM v1.0 uses vegetation characteristics, soil properties and topography to estimate hydraulic and hydrologic parameters which are combined with climate or hydrologic input to drive a kinematic wave model and solve for the sediment continuity equation. As in the WEPP model, RHEM v1.0 used the excess shear-stress concept to model concentrated flow erosion. Subsequent improvements and adjustments to the model have resulted in the second generation of RHEM (v2.0 and currently v2.3, used in this study) which substituted the shear-stress concept with the stream power model for concentrated flow erosion prediction (Al-Hamdan et al. 2015). Major new scientific developments incorporated in RHEM v2.0 and greater (Hernandez et al. 2017) include: 1) new equations to capture the effect of rangeland disturbance on soil erosion and infiltration processes, 2) a dynamic solution to the continuity equation to address the often observed decrease in soil erodibility with time after a disturbance, and 3) a framework to evaluate runoff and erosion risks and benefits associated with disturbances such as fire, climate change, and rangeland management practices.

4.3.2. Calibration procedure

Six plots were selected from each experimental site for a total of 36 plots to calibrate RHEM for saline sites, ensuring that each intensity simulated at the site was represented at least once in the calibration dataset. The calibration was performed in two steps to determine best parameter sets for (1) runoff prediction and (2) soil loss prediction. The numerical optimization was performed using a Markov Chain Monte Carlo (MCMC) implemented in SPOTPY (Houska et al. 2015), a model optimization tool written in the Python programming language.

To optimize runoff prediction, the RHEM parameters adjusted for each plot were: the soil saturation ratio (SAT), the effective hydraulic conductivity (Ke, mm/hr), the mean capillary drive (G, mm), variable (ALF) in the Smith-Parlange infiltration equation and the coefficient of variability of the hydraulic conductivity (CV). These parameters were estimated in a multi-objective optimization scheme in which errors in both total runoff SR (L) and 1-min-increment instantaneous discharges qt (mm/hr) were minimized throughout the rainfall event. Instantaneous discharges used as observations were interpolated from observed discharges that may not systematically occur at exactly 1 min time increments and were compared to predicted discharges at the same time increments. This multi-objective optimization procedure allowed the estimation of parameters that adequately predicted SR while matching as close as possible the detail hydrograph of a rainfall event.

For erosion prediction, the sheet and splash erodibility Kss was estimated using a separate multi-objective parameter optimization in which errors in total soil loss SL (Kg) and 1-min-increment instantaneous sediment discharge rates qst (g/s) were minimized. For both runoff and soil erosion parameter estimations, the final selection of parameters was done for each calibration plot by choosing the set of parameters that simultaneously minimized the error in cumulative runoff and total soil loss (SR and SL) and belonged to the 5% best performers in matching the detail hydrograph and sedograph. A total of 36 parameter sets were produced corresponding to the 36 calibration events.

4.3.3. Parameter estimation for saline sites

Parameter estimation equations have been developed for RHEM to translate soil biophysical characteristics into hydrology and hydraulics parameters. Currently, equations exist to estimate Ke, Kss and the Darcy Weisbach friction factor (F) from equations using ground and vegetation cover information as well as soil texture. For Ke and Kss, current RHEM equations are:

$$Ke = a\exp\left(b\left(basal + litter\right)\right) \quad (1)$$

$$Kss = 10^{\left(c + d\cdot GroundCover + f\cdot FoliarCover + g\cdot Slope\right)} \quad (2)$$

where coefficients a and b differ as a function of soil texture and vegetation community type (i.e. shrub, sod grass, bunch grass and forbs and annual grass) while coefficients c, d, f and g are functions of vegetation community type and ground cover. Basal, litter, ground cover, foliar cover are expressed as a real fraction. Basal cover represents the proportion of the soil surface that is in contact with the bases of plants. Litter cover is the proportion of the soil surface protected by detached vegetation residues. Ground cover is the sum of basal, litter, rock and cryptogam cover. Foliar cover is the fraction of the land surface that is occupied by the projection of plant leaves onto the soil surface. As cover decreases erosion will increase (Figure 37).

Parameters a, b, c, d, f and g were developed from a large dataset (more than 200 plots) of rainfall simulation experiment across the Western United States and represent a wide range of rangeland ecosystem types and conditions.

In this study, Ke and Kss values optimized using the MCMC routine (KeOpt and KssOpt) were compared to the values (KeRHEM, KssRHEM) predicted by the current version of RHEM for the calibration plots. Differences (ΔKe, ΔKss) and ratios (rKe, rKss) between optimized and RHEM-predicted values were calculated and related to soil biophysical characteristics and salinity. Linear regressions were performed between ΔKe, ΔKss, rKe and rKss and canopy cover, fraction of bare ground, sodium adsorption ratio (SAR), electrical conductivity (EC), silt content and slope. With a total of 36 calibration data points for this analysis, each explained variable was regressed against one explanatory variable at a time to prevent over-parameterization and maintain adequate statistical power.

From the linear regressions linking soil and vegetation attributes to Ke and Kss differences and ratios, factors accounting for the gap between RHEM-predicted and optimized Ke and Kss values were identified by selecting those exhibiting statistically significant effects on ΔKe, rKe, ΔKss and rKss. Factors with statistically significant effects were then evaluated against current terms used in RHEM parameter estimation equations (Eq. 1 and 2). Factors with statistically significant effects that were already presents in Eq. 1 and 2 suggest a modification of coefficients applied to these terms in these equations. Factors not previously accounted in Eq. 1 and 2 are introduced as new terms according to the nature of their relationships with RHEM-predicted parameters. In the case of statistical significance of a factor in the parameter differences ΔKe and ΔKss, the new parameter Kn is calculated as:

$$Kn = KnRHEM + (AX + B) \quad (3)$$

where X is one of the factors canopy cover, bare ground, SAR, EC, silt content and slope and A and B are significant coefficients of the linear regression where these factors have a significant effect.

Likewise, when the ratios rKe and rKss exhibit a significant effect of a given parameter, Kn is defined as:

$$Kn = KnRHEM\,(AX + B) \quad (4)$$

When more than one factor was found to have a statistically significant effect on a parameter Kn, the final correction equation retained was sequentially developed by first incorporating the factor with the highest R^2 and re-computing ΔKn or rKn values and relating these values to the subsequent factors to verify that any statistical significant effect remained. For example if bare ground has a statistically significant effect on ΔKe and EC has a significant effect on rKe with R^2 bare ground $> R^2$ EC, then Ke would be corrected for bare ground first Kebare = KeRHEM + (A×Bare+B) then rKe will be recalculated as KeOpt / Kebare and this new variable reevaluated against EC to see if the initial statistical significance remained.

4.3.4. Performance evaluation

The performance of the adjusted parameter estimation equations (Eq. 3 and 4) was assessed by comparing erosion and runoff predictions with the amended parameters Kn to those obtained with Eq. 1 and 2. Model performance metrics used for this comparison are the coefficient of determination R^2, the Nash- Sutcliffe Efficiency, NSE and the percent bias, pbias.

$$R^2 = 1 - \frac{\sum_{i=1}^{n}\left(Y_{lm,i} - Y_{o,i}\right)^2}{\sum_{i=1}^{n}\left(Y_{o,i} - \overline{Y_o}\right)^2} \quad (5)$$

$$NSE = 1 - \frac{\sum_{i=1}^{n}\left(Y_{p,i} - Y_{o,i}\right)^2}{\sum_{i=1}^{n}\left(Y_{o,i} - \overline{Y_o}\right)^2} \quad (6)$$

$$pbias = \left[\frac{\sum_{i=1}^{n} \left(Y_{p,i} - Y_{o,i} \right) \times 100}{\sum_{i=1}^{n} Y_{o,i}} \right] \quad (7)$$

where Y_o, Y_p, and Y_{lm} are respectively the observed, RHEM-predicted and linear model prediction between Y_o and Y_p for runoff or soil loss while $\bar{Y}_o$ is the average of all observations.

These performance metrics were calculated for the 36 calibration data points and the 36 validation data points. The linear model for salt load prediction was also evaluated with these performance metrics.

Figure 38 shows a flowchart diagram of the experimental data, describes its content and graphically illustrates how it was used to develop and test the new parameter-estimation equations. Additionally, the Welch's t-test was used to compare validation and calibration data to ensure equal means of input parameters between these two populations. Statistical analyses were conducted in R (R Core Team 2017) and a probability of 0.05 used as threshold of statistical significance.

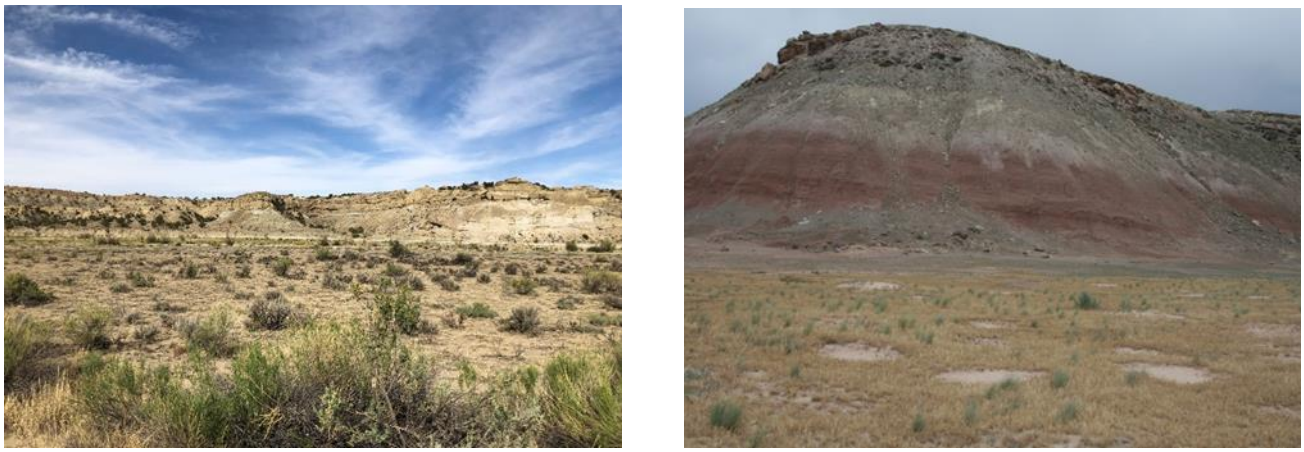

Figure 37. Research sites near Farmington, New Mexico (left) and Moab, Utah (right) showing naturally occurring erosive conditions due to geologic formation and parent materials, steep slopes, and minimal vegetation that facilitate high salt load transport capacities. No known vegetation management practices are available to reduce soil erosion and salt transport under these naturally occurring conditions. Salt loads can be exacerbated if sites are disturbed through off road activities such as from vehicles and bikes.

4.3.5. Results

Figures 40 and 41 show the results of the runoff and soil loss prediction on the 36 calibration data points using equations 1 and 2 to estimate Ke and Kss. NSE and R^2 for runoff were respectively 0.56 and 0.68, suggesting that relationships between soil biophysical properties and Ke represented in Eq. 1 were roughly consistent with observed patterns in runoff and infiltration at the experimental sites. Equation 1 under-predicted Ke, resulting in a

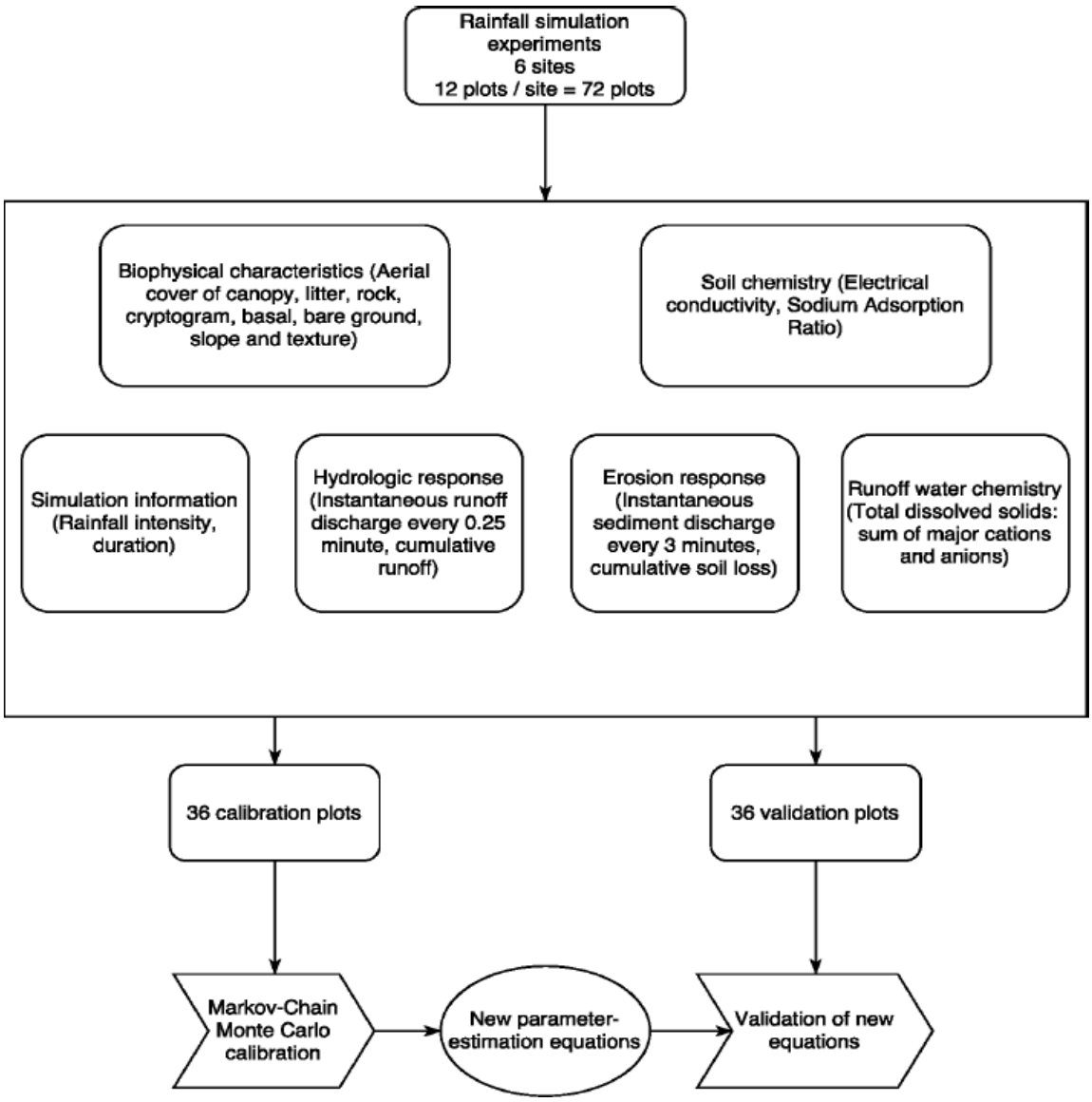

Figure 38. Flowchart diagram of the experimental data utilized for the development and validation of new parameter-estimation equations on saline sites.

positive bias in predicted cumulative runoff depths (predicted runoff > observed runoff, PBIAS = 32.03%). Soil loss was predicted with an NSE of 0.81 and a R^2 of 0.85 with a negative bias (PBIAS = -6.47%). This negative bias in soil loss prediction contrasts with the positive bias in runoff noted in Figure 39, which indicates an under-prediction of soil erodibility.

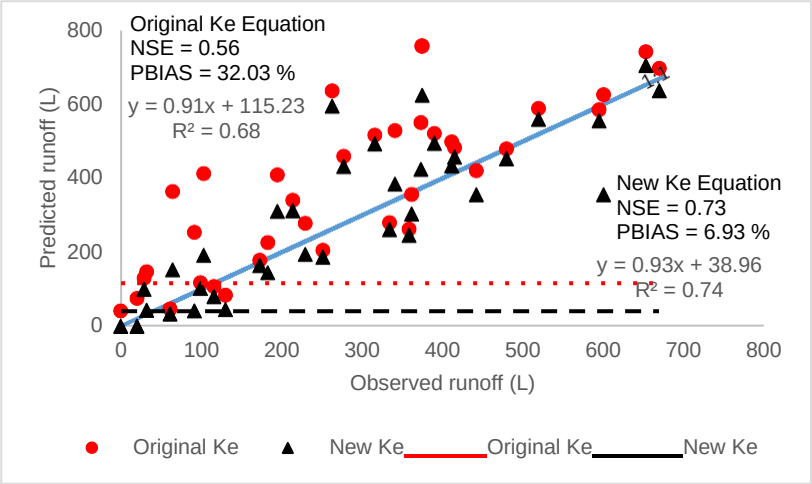

Figure 39. Observed vs. predicted runoff on 36 rainfall simulation calibration plots using current RHEM parameter estimation equations

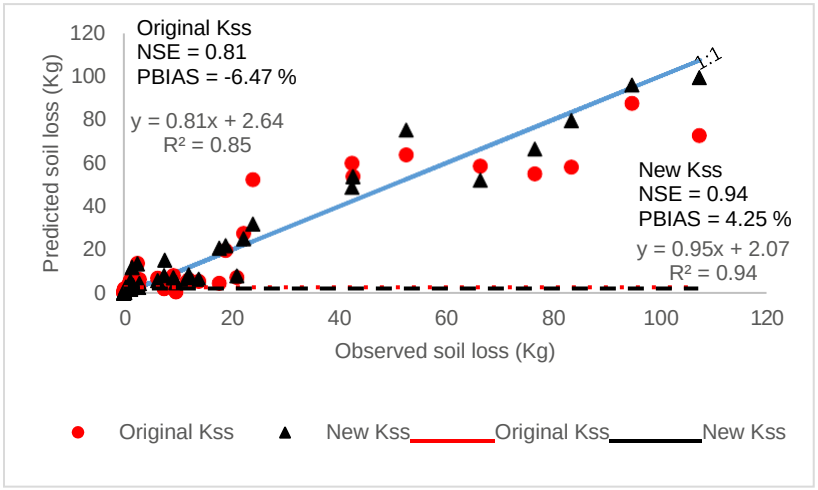

Figure 40. Observed vs. predicted soil loss on 36 rainfall simulation calibration plots using current RHEM parameter estimation equations.

The new equation for Ke developed from this dataset for saline sites was:

$$Ke = a\exp\left(1.554b\left(basal + litter\right)\right) \quad (8)$$

Performance of Eq. 8 on the calibration data was overall better than that of the additive correction model for bare ground with NSE = 0.73, PBIAS = 6.93% and $R^2 = 0.74$.

Differences and ratios between optimized and RHEM-predicted Kss values show significant effects of only SAR. ΔKss and SAR are related through a positive relationship ($R^2 = 0.26$, p = 0.002) while rKss relates to SAR with much less predictability ($R^2 = 0.13$, p = 0.042). Correcting RHEM Kss values for SAR with both additive (Eq. 3) and multiplicative (Eq. 4) models resulted in an improvement of NSE (0.94 and 0.89 vs 0.81) and R^2 (0.94 and 0.93 vs. 0.85) of soil loss prediction compared to current the RHEM Kss estimation equation. While the bias

achieved with the additive model (PBIAS = 4.25%) matched that achieved with Eq. 2, a greater bias was noted when the multiplicative model was used for the Kss correction (PBIAS = 17.18%). The additive model was then retained to adjust Kss for SAR.

Figures 41 and 42 show the result of the runoff and soil loss prediction with the new Ke and Kss equations on the 36 validation plots. Ke values estimated with Eq. 8 predicted runoff on the 36 validation plots with slightly improved NSE (0.88) and R^2 (0.89) over the original RHEM equation Eq. 1 (NSE = 0.83 and R^2 = 0.85). The runoff prediction bias was substantially improved on these validation plots dropping from PBIAS = 12.05% with Eq. 1 to PBIAS = 5.41% when the newly developed Eq. 8 was used.

The sheet and splash erodibility Kss were reasonably predicted on the validation data when SAR was added to the Kss prediction. Compared to the original Kss equation, the use of the SAR-adjusted Kss equation improved soil loss prediction from NSE = 0.38, R^2 = 0.6 and PBIAS = -24.25 to NSE = 0.69, R^2 = 0.73 and PBIAS = -3.82%. Nevertheless, validation NSE (0.69) and R^2 (0.73) declined compared to the calibration performance (NSE = 0.94 and R^2 = 0.94) due to increased error propagation from runoff prediction to soil loss estimates in the validation data. In effect, calibrated Ke values were used in the estimation of soil loss for evaluating Kss on the calibration data while for the validation data, estimates of Ke from Eq. 8 were used. The percent bias of the additive Kss model was maintained within the same order of magnitude across calibration and validation data (PBIAS = 4.25% for the calibration data and -3.82% for the validation).

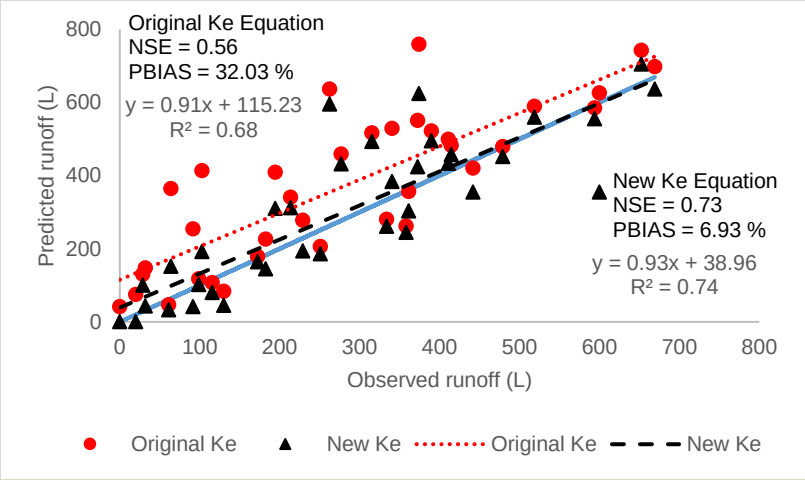

Figure 41. Observed vs. predicted runoff on the 36 validation data points using the current and the newly developed estimation equation for the hydraulic conductivity Ke

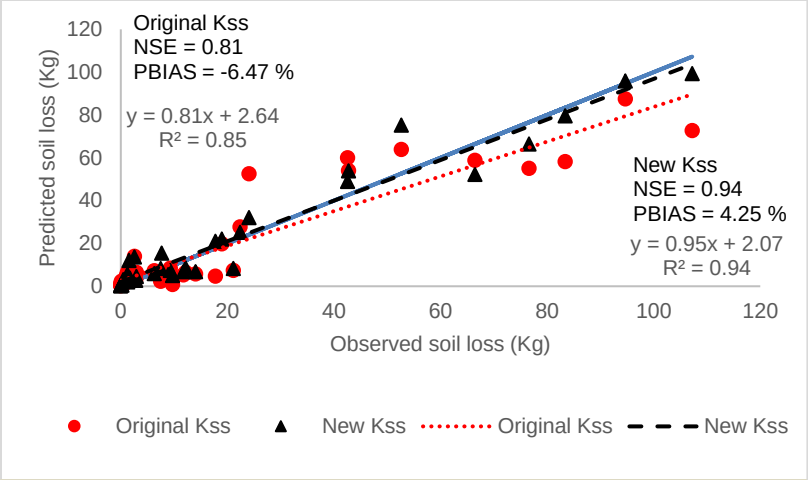

Figure 42. Observed vs. predicted soil loss on the 36 validation data points using the current and the newly developed estimation equation for the sheet and splash erodibility Kss

The relationship between soil loss and total dissolved solids is shown in Figure 43. The linear model was adequate to predict runoff chemistry from its sediment concentration ($R^2 = 0.94$). TDS was related to SL through a positive relationship. Based on the equation of the linear model in Figure 43, a 1 Kg change in total soil loss results in a 2.36 g change in TDS (p = 0.00). In other words, the average salt to sediment mass ratio of the runoff was 2.36 10^{-3} g/g or 0.24%. The non-zero intercept of the linear model was not statistically significant. The equation used for predicting TDS from soil loss was therefore:

$$TDS = 2.36 \times SL + 0.99 \qquad (9)$$

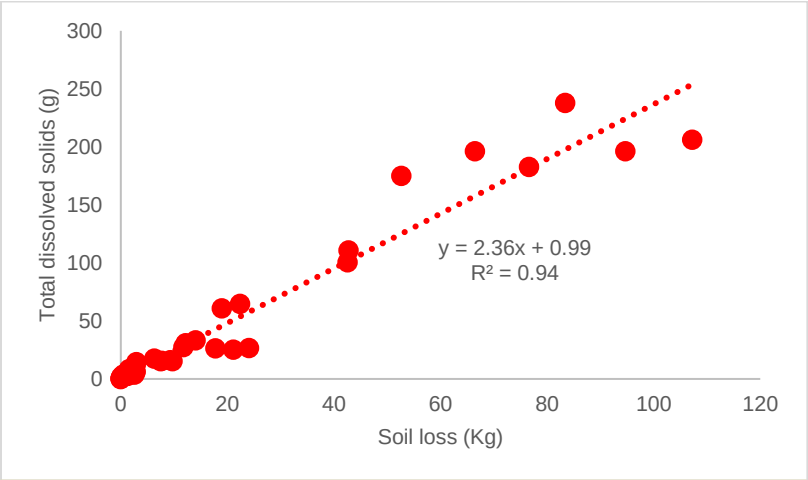

Figure 43. Relationship between cumulative soil loss and cumulative dissolved solids measured in runoff

Figure 43 shows that Eq. 9 performed well at predicting TDS when RHEM-predicted SL values were used on the calibration data (Fig. 44a) and the validation data (Fig. 44b). The improvement in soil loss prediction gained with the use of newly developed saline equations was reflected on TDS predictions as well. On the calibration data, NSE and R^2 improved from 0.75 and 0.83 with the original Ke and Kss equations to 0.90 and 0.91 with the saline

equations developed from this work (Figure 44). PBIAS on the calibration was overall low but showed a mild improvement from -6.34% to 4.16%. On the validation data, a more dramatic improvement was noted on the NSE which increased from 0.43 with the original Ke and Kss equations to 0.83 with the saline equations. R^2 improved from 0.51 to 0.61 while PBIAS degraded from - 6.29% to 23.18%. Soil loss predicted with the new Ke and Kss equations underestimated observed SL values especially in the high SL range. These findings contrast with the overestimation of TDS observed in Fig. 44b when the new Ke and Kss equations were used on the validation data, suggesting that this overprediction might be the result of the inherent variability in the runoff chemistry data.

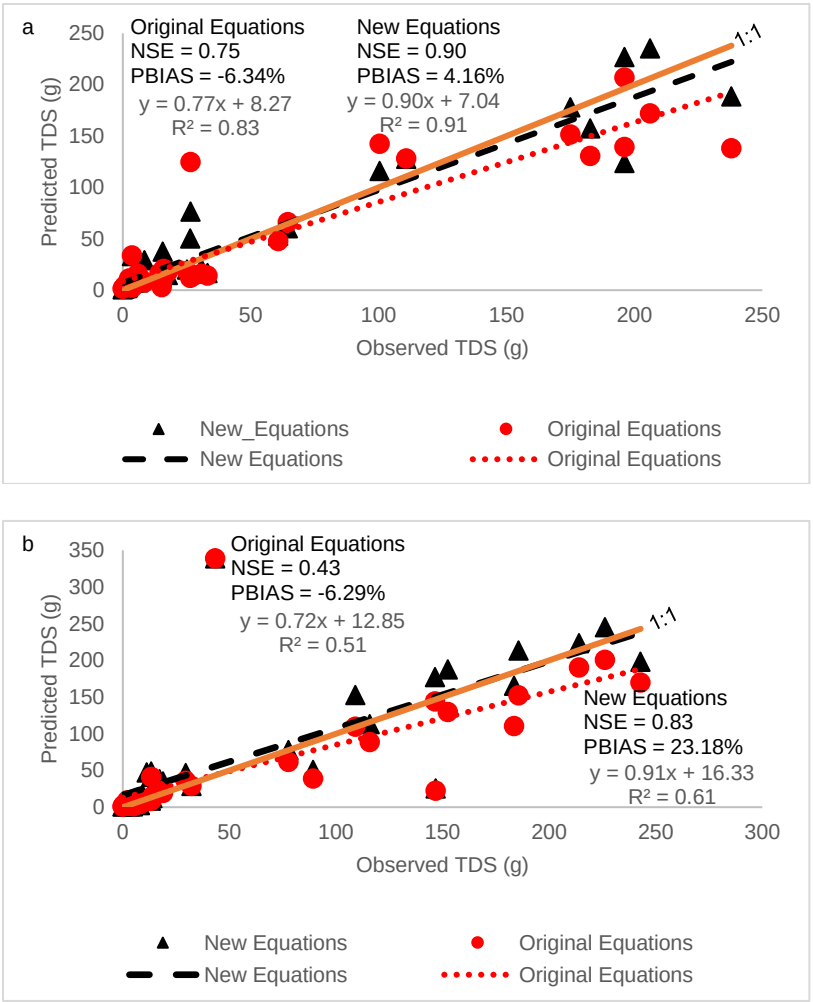

Figure 44. Observed vs. predicted total dissolved solids (TDS) on the 36 calibration (a) and 36 validation (b) data points using the current and the newly developed estimation equations for Ke and Kss.

5. Regional Hot Spot Analysis of Soil Erosion in the Upper Colorado River Basin

This analysis presents a method for mapping erosion potential across the Mancos Shale at a high spatial resolution using RHEM. RHEM acts at the hillslope scale to estimate localized erosion rates, so it requires less effort than models that compute flow and transport through the larger hydrologic network. This allows easy implementation across the discontinuous spatial extent of Mancos Shale outcrops because it does not consider the continuity of mass and energy balances or boundary conditions beyond the single cells of the grid of input data values. Here, RHEM is parameterized with existing geospatial datasets, satellite imagery, and field data from the National

Resource Inventory (NRI) dataset collected by the United States Department of Agriculture (USDA) National Resources Conservation Service (NRCS). This approach produces maps of erosion risk that can help land managers to define thresholds of accelerated soil loss, to assess the risk of crossing such a threshold, and to define hot spots where soil conservation can be applied to avert land and water degradation.

The study area was the extent of Mancos Shale outcrops that were compiled from maps of surface geology for Utah, Colorado, New Mexico, and Arizona (Figure 45). The region under consideration was limited to areas with low levels of agricultural or urban development and slopes less than 35%. These constraints reflect practical limitations for potential mitigation activities; also, the RHEM model is not well validated for very steep slopes. Data for developed land uses and slope were taken from the LANDFIRE vegetation map (USGS, 2019) and the United States Geological Survey (USGS) 1/3 arc second National Elevation Database (USGS, 2002). All map datasets for the study were raster grids that were projected to UTM Zone 12 with the NAD83 datum at a 30-meter spatial resolution.

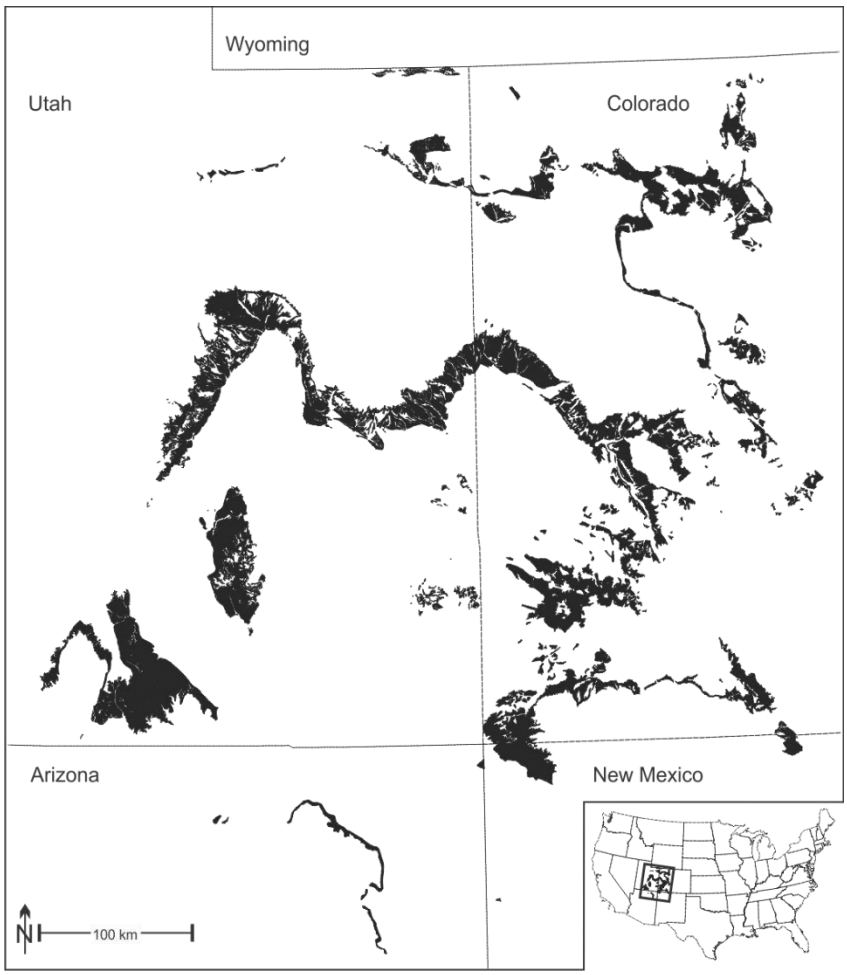

Figure 45: The Mancos Shale in Utah, Colorado, Arizona, and New Mexico.

For vegetation, RHEM requires estimates of percent cover by 1) annuals and forbs, 2) bunch grasses, 3) sod grasses, 4) shrubs, 5) litter (on ground), 6) basal area (rooted plant area), and 7) biological crusts. Given the arid to semi-arid climate of the study area, sod grasses were not considered. Also, data on the distribution of biological crusts throughout the region were not available and assumed to be zero. This assumption is revisited in the Discussion section. Remaining foliar and ground cover values were estimated on a per-pixel basis using a combination of field transect data from the NRI, satellite imagery, and the LANDFIRE vegetation map. Maps of

percent vegetation cover were created by developing a regression relationship between available field transect data and collocated values of the normalized difference vegetation index (NDVI; Rouse et al., 1974) from Landsat satellites. That relationship was then applied to Landsat NDVI data (30-meter spatial resolution) for areas that were mapped as Mancos Shale.

Plant foliar and ground cover data was obtained from the USDA-NRCS NRI non-federal rangeland on-site field study (NRCS, 1997). NRI data is collected as two 50m transects, oriented 45 degrees from north (NE-SW; NW-SE), with point-intercept samples every 0.9 m (Spaeth et al., 2003). These crossed transects are randomly located in ecosystems around the United States. Hernandez et al. (2013) found that NRI data were adequate to run RHEM and to effectively assess the influence of foliar cover, ground cover, plant life forms, soils, and topography on soil erosion rates in desert environments of the southwestern United States. The NRI data used here were from 134 crossed transects that were collected from 2004 to 2014 at locations that were within 1 km of the mapped distribution of the Mancos Shale. Total vegetation cover for each pixel was estimated by developing a regression between total cover at NRI locations and the corresponding median of Landsat NDVI collected during the growing season (April-September) of that year (Figure 46a). Pearson's correlation (r) between these two variables was 0.834. The analysis compensated for changes in Landsat bandwidths from the earlier Thematic Mapper sensor to the current Operational Land Imager (OLI) sensor using the method of Huntington et al. (2018). A Type II regression technique called reduced major axis (RMA) regression was used, since ordinary least squares regression would produce a deflated slope estimate due to measurement uncertainty in the independent variable (McGwire et al., 1993, Curran & Hay, 1986). The median of NDVI data derived from Landsat during the 2018 growing season was converted to 30-meter scale estimates of percent cover across the Mancos Shale (Figure 47a) for RHEM using the regression in Figure 46a.

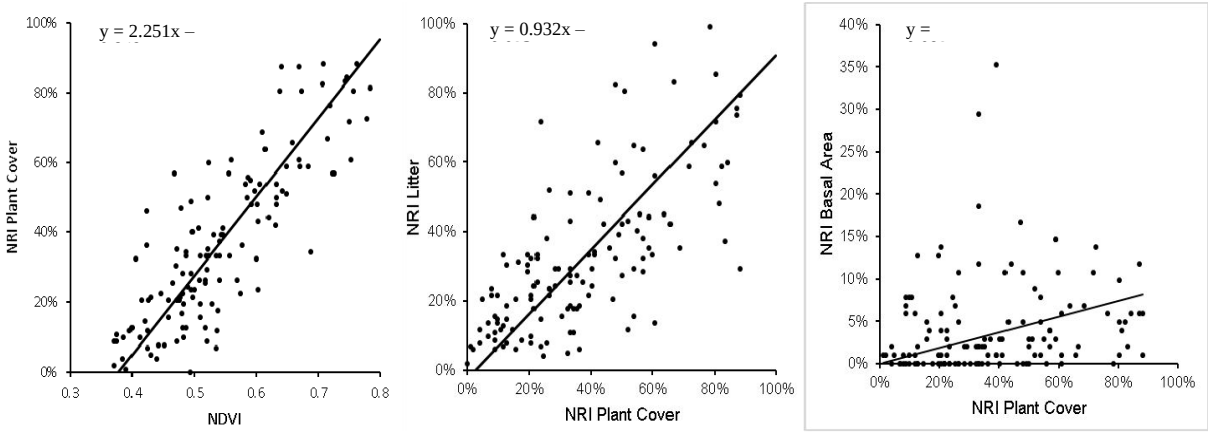

Figure 46: Regressions for estimating vegetation variables.

The proportion of shrub cover for each pixel (Figure 46b) was taken from the 140EVC attribute in version 1.4 of the LANDFIRE map which used an algorithm to estimate tree or shrub cover that was based on the example of Toney et al. (2009). Tree cover classes in the 140EVC attribute were treated as shrubs in the RHEM model. The shrub and tree cover attributes in LANDFIRE are reported at 10% intervals, so the midpoint of each interval was used (e.g. 10-20% = 15%). In the very rare case that the LANDFIRE shrub/tree cover class exceeded the Landsat regression estimate for total cover, the regression value was used for total cover and shrub cover since it was developed specifically from data for the local environs. For estimating proportions of annuals and forbs versus bunch grasses, NRI data in the vicinity of the Mancos Shale showed no predictive relationships to satellite data or percent vegetation cover that performed better than a simple area-wide mean. The mean proportion of the two categories was very similar in the NRI dataset, so Landsat-estimated cover that was in excess of the LANDFIRE shrub cover was split evenly between these two classes. The NRI dataset did demonstrate a useful relationship between litter and total plant cover (r = 0.709, Figure 46b), and this was applied using an RMA regression with

the Landsat estimate of plant cover. For basal area, a weak relationship to total plant cover (r = 0.13) was all that could be derived from the NRI dataset (Figure 46c). Attempts using NRI to predict basal areas based on life form (i.e. shrub, bunch grass, etc.) were no better than the single relationship in Figure 46c. Estimated values of foliar and ground cover were truncated if they exceeded the range of 0 – 100%.

Slope for the RHEM model (Figure 47c) was taken from the 1/3 arc second National Elevation Dataset which has spatial resolution of approximately 10 meters. Slope calculations are sensitive to interpolation artifacts in digital elevation models, often producing stepped changes in value. In order to minimize this effect, the 10-meter data were smoothed using a 9x9 Gaussian low-pass filter and then resampled to the 30-meter resolution of the other raster datasets prior to calculating slope. This smoothing would be expected to have a minimal effect on 30-meter slope estimates while ameliorating data artifacts. The RHEM model characterizes slope using sine of the slope angle, which at low slope values is similar to percent slope. In order to provide information on slope shape for RHEM, the longitudinal convexity of the smoothed 30-meter DEM was calculated using the topographic modeling function in the ENVI image processing software package (Version 5.5, Harris Geospatial). Using a visual interpretation of the slope and elevation datasets, a longitudinal convexity less than -0.25 was labeled convex, convexity up to 0.25 was labeled 'uniform', and values beyond 0.25 were concave.

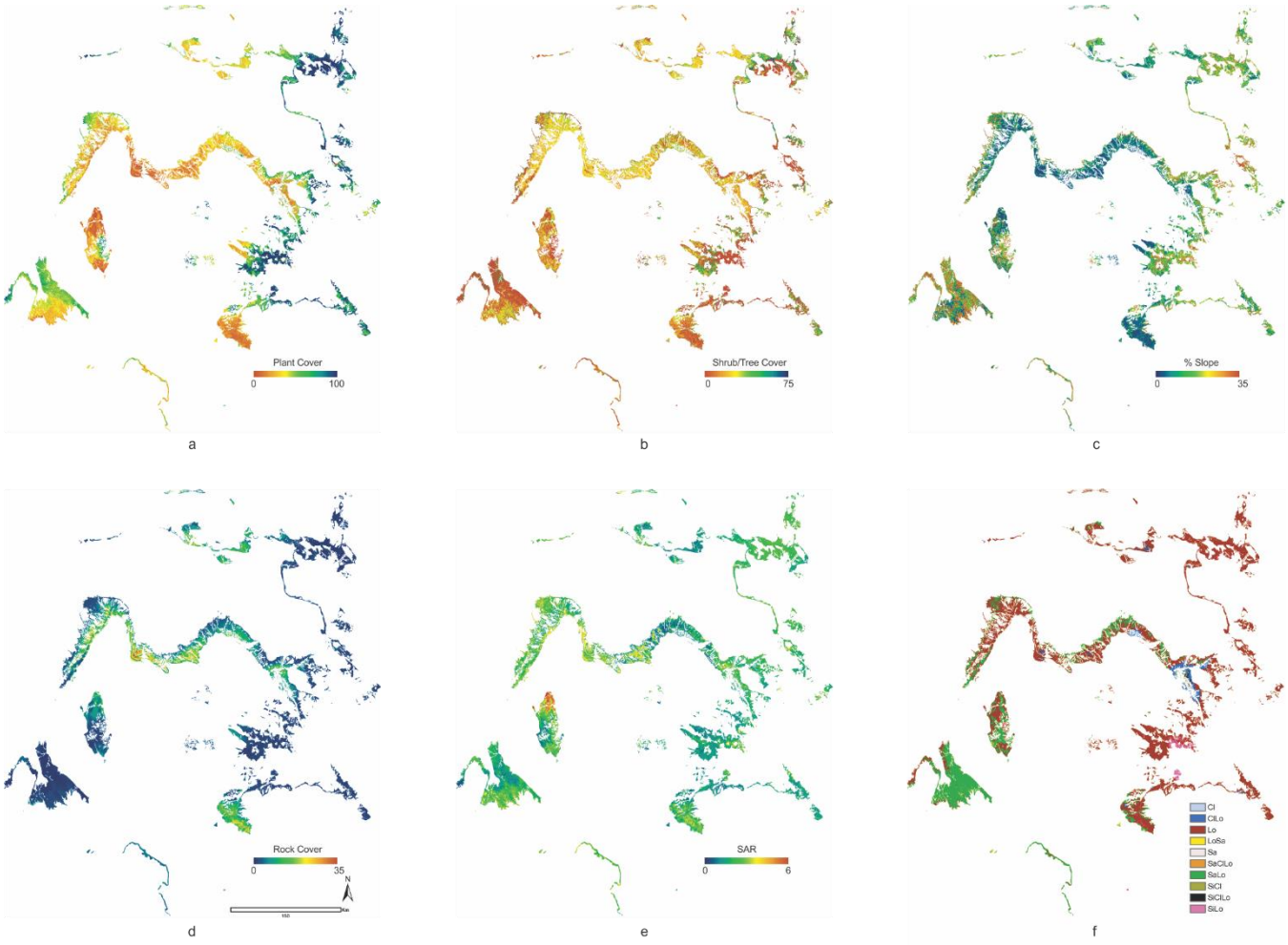

Figure 47: Geospatial variables: a) plant cover, b) shrub cover, c) slope, d) rock cover, e) SAR, and f) soil texture.

High-resolution SSURGO digital soils data from NRCS is not available for large portions of the Mancos Shale, and the lower resolution NRCS STATSGO soil maps are not sufficiently detailed for this scale of modeling. However, Nauman et al. (2019) used statistical models to develop uninterrupted estimates of soil parameters for the upper Colorado River basin at a 30-meter grid resolution. Percentages of sand, silt, and clay from Nauman et al. were converted to the twelve USDA soil texture classes for RHEM (Figure 48f) using the soil texture package (Moeys et al., 2018) that is available for the R statistical software package (R Core Team, 2018). Maps of statistically estimated rock fragment size, rock cover, and sodium adsorption ratio (SAR, Figure 47e) also were taken from Nauman et al. (2019). For RHEM, rock cover was set to 0% if the estimated fragment size was less than 5mm, and the estimated total rock cover was applied to the remaining areas (Figure 47d).

The precipitation rates used in this study were taken from the gridded datasets of Atlas 14 of the United States National Atmospheric and Oceanographic Administration (NOAA). The RHEM model was run using 30 and 60-minute duration storms associated with 10-year and 25-year return intervals (four simulations). The study area overlapped two different geographic regions of the Atlas 14 product, Midwest and Southwest, and there were noticeable discrepancies along the boundaries of these two regions. This issue is considered later in the interpretation of model outputs.

RHEM includes a term for canopy water storage that absorbs an initial quantity of rainfall. An accurate determination of this value is difficult, since interception and storage depend on canopy geometry, leaf angle distribution, type of foliage, and characteristics of precipitation and wind speed (Dunkerley, 2008; Owens et al., 2006; Pierson & Williams, 2016). However, this static storage term is generally small compared to the totals of larger rainfall events, such as those tested in this paper. The MCD15A3H product that is generated from NASA's MODIS sensor system on the Terra and Aqua satellites provides an estimate of leaf area index (LAI) that is based on general vegetation type and land surface reflectance. This LAI measure is the ratio of one-sided leaf area to ground area. The LAI product is produced at a 500 m spatial resolution and was resampled to 30 m using bilinear interpolation. Based loosely on Breuer et al. (2003), we assumed that the canopy stored 0.4*LAI mm of precipitation.

Per-pixel inputs and outputs of the RHEM model were managed using the IDL software package (version 8.7, Harris Geospatial). This study used version 2.3 of the RHEM model, with the addition of the sodium adsorption ratio parameter developed in Nouwakpo et al. (2018). The four modelled storm events were sampled with a 15 second time step, which was dynamically altered by RHEM as required for numerical stability. In order to reduce processing time for the more than 22 million Mancos Shale pixels, floating point input parameters were binned to discrete values, and the results for unique combinations of binned input values were stored for future use instead of re-running the model. This discretization balanced the expected sensitivity of model parameters with the relative precision of input data sources. Slope was binned to percent's (e.g. 0-1% = 0.5%). Total vegetation cover and shrub cover were binned by 5% intervals, and LAI to 0.25 intervals. Total rainfall was binned to 2.54 mm (0.1 in.) increments. SAR was binned to unit intervals (maximum SAR pixel value = 18).

Prior studies have performed rainfall experiments with the Walnut Gulch Rainfall Simulator (WGRS) at sites on the Mancos shale and nearby saline outcrops (Cadaret et al., 2016ab; Nouwakpo et al., 2018), and those data were used to assess the performance of this regional RHEM modeling approach. Specific GPS coordinates for each WGRS plot were not available, but map polygons indicating the spatial extent of each field site allowed average GIS parameters to be calculated. The field site names, and their geographic centroids are identified in Table 1. Multiple WGRS experiments were performed at each of these field sites, using a range of rainfall intensities from 50.8 to 139.7 mm/hr. The cumulative sediment yields after 20 minutes of WGRS rainfall were averaged for each intensity setting at each site and correlated with the 20-minute GIS-driven RHEM estimate for these locations and intensities.

5.1 Discussion

The time required to run RHEM for the entire Mancos Shale study area ranged from 29.4 hours to 49.4 hours on a PC with a 3.4 GHz I7-4770 processor, with the larger range of precipitation values in the 25-year 60-minute storm creating the greatest number of unique permutations of input parameters and time. Sediment yield estimates (t/ha) from the four storm simulations were highly correlated, so only the result for the 25-year 60-minute simulation is presented in Figure 49. The full output resolution could not be rendered directly, so the data in that figure were averaged to a 1 ha resolution. Table 2 lists the mean and maximum sediment yields associated with each storm simulation. There is an approximate doubling of mean estimated yields between the 10-year and 25-year storms, but more than fifteen-fold increase from 30-minute to 60-minute storms. This reflects the greater relative effect of canopy interception and initial infiltration on shorter storms.

Weltz et al. (2014) characterized erosion potential on non-federal rangelands across the western United States using field data from NRI and RHEM. However, using map data from the Protected Areas Database (USGS, 2018) and the U.S. Forest Service, Table 3 indicates that the majority of the Mancos Shale study area is managed

Table 1: WGRS site names, geological formations, and geographic centroids (UTM zone 12, NAD83)

Site Name	State	Formation	Easting	Northing
Delta	Colorado	Mancos Shale	758564	4298777
Ferron	Utah	Mancos Shale	489389	4313805
Ferron2H	Utah	Mancos Shale	489441	4313888
Ferron2L	Utah	Mancos Shale	489641	4313859
Ferron2M	Utah	Mancos Shale	489740	4314389
Farmington	New Mexico	Nacimiento	774513	4051428
Loma	Colorado	Mancos Shale	682411	4358501
Moab	Utah	Mancos Shale	598146	4295795
Moab2	Utah	Mancos Shale	595796	4295259
Price	Utah	Mancos Shale	533766	436822

by federal agencies. Note that areas of high urban or agricultural development or slopes greater than 35% were removed from the calculations in Table 3. Based on Weltz et al. (2014), RHEM output for the 25-year, 60-minute storm was categorized as low risk (< 2 t/ha), medium risk (2 – 4 t/ha) or high risk (> 4 t/ha), and the area in each category is presented in Table 3. The Bureau of Land Management manages the majority of rangelands on the Mancos Shale, and it also has the greatest area with erosion rates in excess of 4 t/ha. Private lands cover 27% of

Table 2: RHEM sediment yields (t/ha).

	10-yr 30-min	10-yr 60-min	25-yr 30-min	25-yr 60-min
Mean:	0.18	3.12	0.36	5.58
Maximum:	24.8	237.6	36.4	366.7

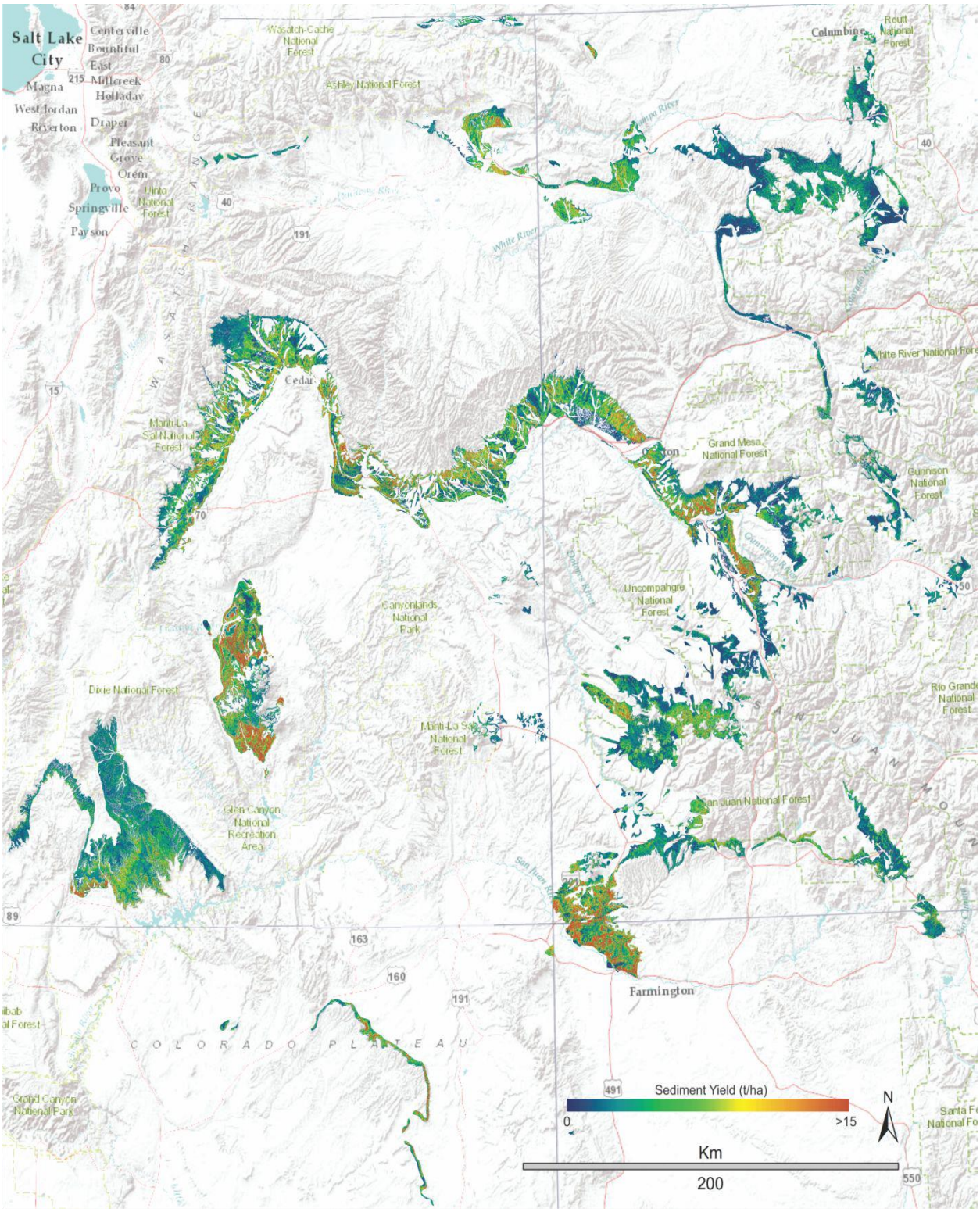

Figure 48: Sediment yield (t/ha) for 25-year, 60-minute storm (terrain reference: ESRI, HERE, Garmin, USGS, OpenStreetMap).

the Mancos Shale study area, but contained proportionately less area of high erosion risk, possibly reflecting the negative economic impacts of salinity and soil erosion on decision making regarding private land ownership. Given that developed areas were removed from this study, the actual area of private ownership on the entire Mancos Shale is larger than that reported in Table 3, and the percentage at high risk would actually be lower. Tribal lands cover only 8% of the total study area, but they generally have low levels of vegetation cover and the majority of their area was classified as high risk. Conversely, Forest Service lands tend to have high vegetation cover, and therefore have a lower percentage of land at high risk than the other public agencies with large land holdings.

The RHEM model provides a hillslope-scale estimate of soil erosion risk, so the risk map in Figure 48 does not account for streambank erosion, gullying, or transport and deposition at a broader scale. However, it does provide a useful representation of which areas would be expected to be most in need of soil conservation efforts. Figure 50 indicates that the area of greatest erosion risk is on steeper slopes with silt loam soils, despite the fact that these sites are generally well vegetated. However, these figures do not communicate the great difference in the spatial extent of different soil textures, and that only slopes less than 35% were considered. The mapped extent of silty loam was just 1.7% of the study area, while loam covered forty times more area. Thus, while other soils had areas with high values for yield, precipitation, slope, and cover, their overall statistical distribution trended lower than the small regions of silt loam in Figure 50.

In assessing the uncertainty of the model outputs, there are numerous issues of scale when attempting to relate the GIS-driven RHEM model (900 m^2 pixels) to the WGRS experiments (12 m^2 plots). Site selections for the prior

Table 3: Area of the Mancos Shale study area by land management category and erosion risk (low < 2 t/ha, medium 2 – 4 t/ha, high > 4 t/ha), sorted by area at high risk.

Management	Total (ha)	Low Risk (ha)	Medium Risk (ha)	High Risk (ha)	High Risk (%)
U.S. Bureau of Land Management	789463	218025	196825	374613	47.5%
Private	471659	274991	93242	103426	21.9%
Tribes	145886	30523	26611	88752	60.8%
U. S. Forest Service	229009	117957	47216	63836	27.9%
State Lands	112851	39795	27343	45713	40.5%
U.S. Bureau of Reclamation	831	229	219	383	46.1%
U.S. Fish and Wildlife Service	17	8	7	2	11.8%

WGRS studies were made to target localized types of slope and vegetation cover, rather than attempting to provide an unbiased representation of the wider environment. Conversely, generalization in the creation of map data means that plot-level heterogeneity could not be represented in RHEM. Also, each map input has some level of measurement or attribute error. The differences between RHEM and WGRS erosion estimates at the Ferron locations (Figure 51a) are primarily due to a map error. Cadaret et al. (2016b) report an extraordinarily high laboratory-measured SAR value of 35.2 for the Ferron location, while the statistically modeled map estimate from Nauman et al. (2019) predicted an average value of 1.24 for these sites. This is important, since a high SAR creates very dispersive and erodible soil. Substituting the SAR value reported by Cadaret et al. (2016b) for Ferron locations, Spearman's rank-order correlation between RHEM and the WGRS simulations increased to 0.926 (Figure 51c), indicating a very strong predictive relationship for mapping relative erosion risk with RHEM when the GIS inputs are accurate. The relative importance of the uncertainty in the SAR map may be lower if an area has high predicted sediment yield despite low SAR inputs, or vice versa. For example, the area of highest SAR values that is left of center in Figure 47e has relatively low sediment yield in Figure 48, due primarily to very low slopes (Figure 47c). In that case, we might presume that the uncertainty in those high SAR values is less an issue

than for an area of moderate or steep slopes where the predicted SAR and yield are both low. Also, one could identify discrepancies between the RHEM SAR input or predicted yield versus prior studies of stream chemistry like Tillman et al. (2018). Since we used datasets from Nauman et al. (2019), that source should not be considered entirely independent.

Another issue with the accuracy of RHEM inputs was apparent with discrepancies along the boundary between regional precipitation products from NOAA Atlas 14. Little of this boundary zone intersected the Mancos Shale, and the output from the RHEM model does not show a very dramatic visible difference. The average difference in precipitation across this boundary where the Mancos Shale was present was about 3 mm for the 25-year 60-minute data. The largest local discontinuity is north of Shiprock, New Mexico, but the effect on predicted yields appeared weak in a visual inspection of the RHEM output. There is potential for improving a future version of Atlas 14 by increasing the amount of overlap between regions during the interpolation, and by deriving interpolation parameters in a more localized manner. However, in this study the uncertainty in the SAR map product was likely much more of an issue than the precipitation.

While this study did not include biological soil crusts due to the lack of a known map data source, they are an important component of some ecosystems in the study area and can have important effects on soil erosion (Gao et al., 2002; Belnap, 2006). The greatest amount of biocrust at the WGRS field sites was an average of 53% cover at Delta. Even though the soil crust parameter was not used in RHEM, data points associated with the Delta site are not outliers in Figures 51b and 51c. Despite this, it will be important for decisionmakers to acknowledge the possible role of soil crusts when using this RHEM map to prioritize various sites for study or erosion control activities.

RHEM predictions of relatively high sediment yield for some areas with high vegetation cover (Figure 5c) are important for interpreting studies like Nauman et al. (2019) that limit expected sediment and salinity source areas to very bare soils. Indeed, as indicated in many studies (e.g., Pierson et al., 2010, 2013; Roundy et al., 2017; Williams et al., 2014), the encroachment of dense pinyon-juniper tree cover in the arid southwest can lead to greatly increased soil erosion as intervening herbaceous cover is suppressed and concentrated flow paths in the interspaces come to dominate surface flow.

Background soil color is known to affect satellite-based vegetation indices in areas with limited vegetation cover (Huete & Tucker, 1991). Kautz et al. (2019) also used a Landsat vegetation index to predict foliar cover for the RHEM model, obtaining a very high R^2 of 0.85 for predicting cover. However, that study was for a single, small watershed with fewer confounding effects than the broad scale of application performed here. Using 134 NRI points spread across the region, our regression between NDVI and foliar cover had a good, but lower, R^2 of 0.70. The strong relationship between RHEM and the WGRS experiments after correcting the known SAR error (Figure 51c) suggests that Landsat-based estimates of vegetation cover are a useful input for physically-based models of soil erosion at this scale of application, despite the influence of soil color.

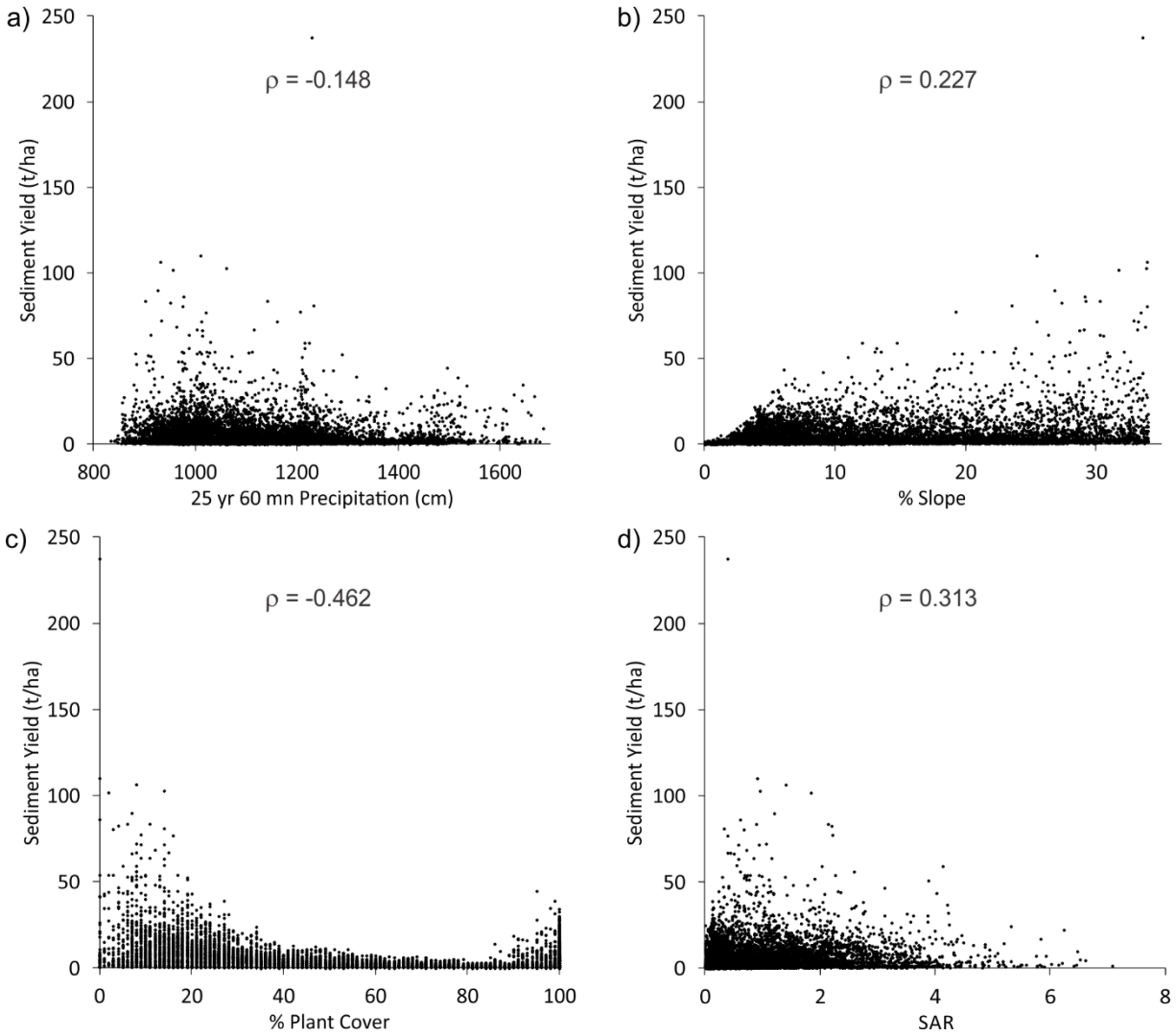

Figure 49: Sediment yield versus a) precipitation amount, b) percent slope, c) percent vegetation cover, and d) sodium adsorption ratio with Spearman's rho.

An issue not dealt with in this study is temporal variation in landscape characteristics. At a fine scale, the seasonal leafing-out of vegetation makes foliar cover and canopy storage parameters dependent on the date of a given storm. This concern is ameliorated to some degree by the circumstance that the most intense precipitation in the region is typically associated with late summer monsoonal events when much of the potential leaf area would have been developed. However, herbivory could reduce leaf area through a season, counteracting this assumption in our method. Also, making litter cover a simple function of total vegetation cover does not consider that the generation and removal of plant litter varies through a season, and it depends greatly on the types of vegetation and land management. Further, RHEM only predicts erosion from rainfall events, so contributions of sediment and salinity associated with snowmelt, seeps and springs are not considered in this analysis. At a coarser temporal scale, periodic wildfire or other dramatic disturbance events in the region would render the current RHEM inputs obsolete at those locations.

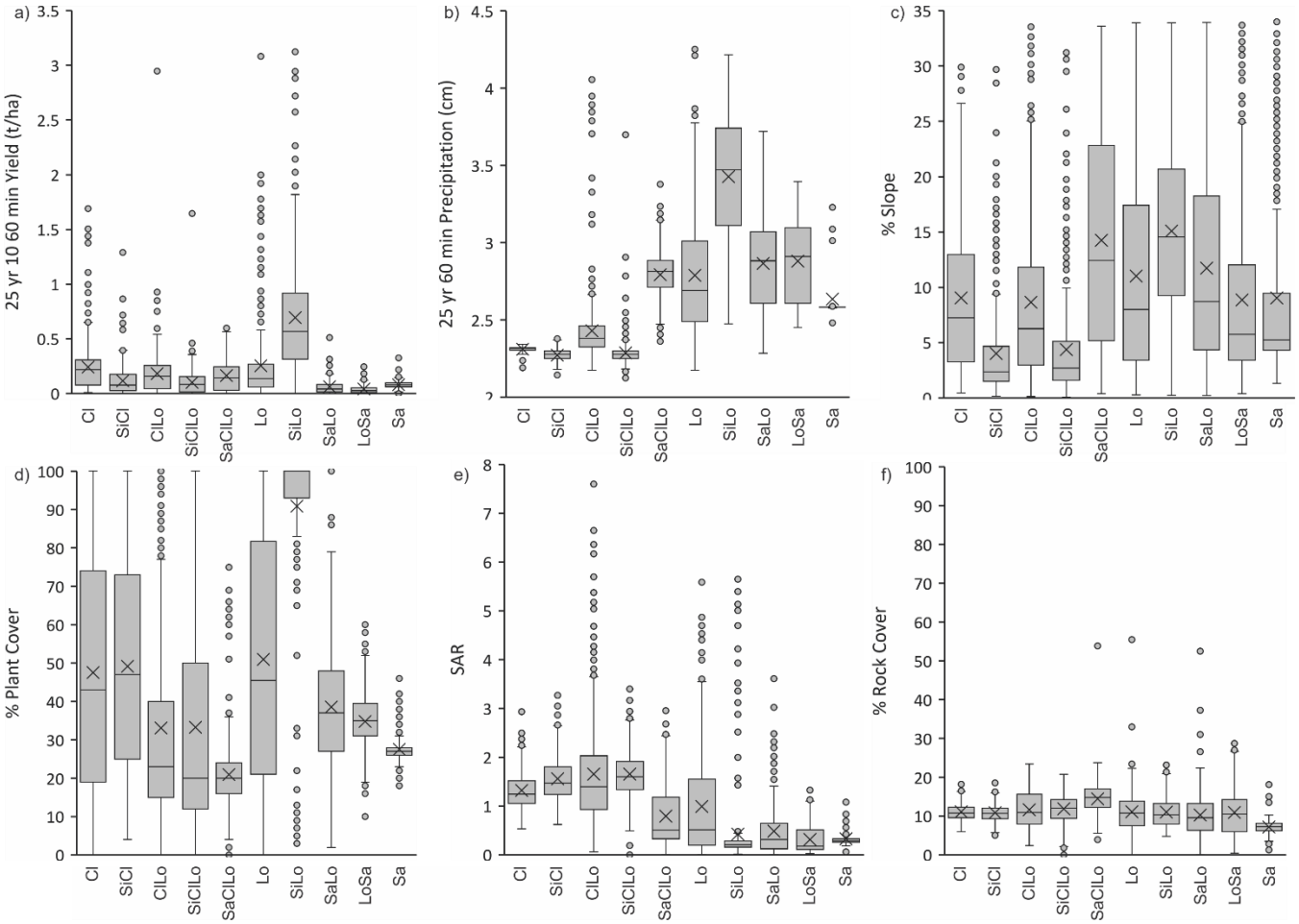

Figure 50: Relationship of soil texture to a) sediment yield, b) precipitation, c) percent slope, d) percent vegetation cover, e) percent rock cover, and d) sodium adsorption ratio.

Despite the many uncertainties in map inputs and the fact that the WGRS field experiments were not designed for the purpose of model validation, the high rank-order correlation between RHEM and WGRS simulations indicates that the RHEM product can provide useful insights for prioritization of locations where rangeland soil erosion is most likely to affect water quality. Given the nature of errors in various map inputs, field observations will be important for decision making that incorporates this RHEM product.

5.2 Results

This study demonstrated the ability to apply the physically-based RHEM model of soil erosion over a large geographic domain for the purpose of assessing relative levels of risk to water quality. In particular, the focus on saline soils of the Mancos Shale and previously documented correlations between sediment yield and salinity on these formations can provide insights into sources of salinity to the Colorado River. Given the uncertainties of map accuracy and differences of scale in comparing WGRS simulations to the GIS-driven RHEM model, the moderately strong Spearman's correlation of 0.76 between the RHEM model and independent field studies provides good confidence in using the results as a starting point for decision making. However, the example of incorrect specification for SAR at the Ferron sites highlights the importance of incorporating other available sources of information and expertise.

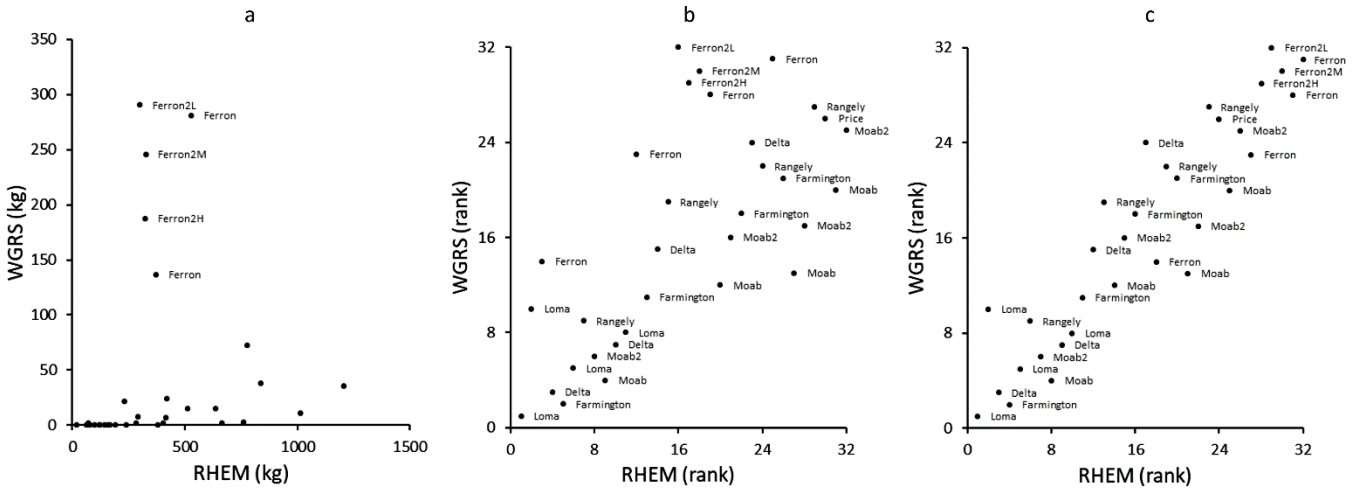

Figure 51: Erosion from RHEM versus WGRS rainfall experiments (a: sediment yield, b: rank order, c: rank order using field-measured SAR for Ferron sites).

Because they are based on physical properties of the soil and the specific growth forms of plant cover, physical models like RHEM are more defensible than USLE-based empirical methods when exploring the implications of alternative scenarios for rainfall regimes and changes in land cover or management. The application of RHEM at a per-pixel level is shown to provide a useful way to characterize hillslope-scale erosion over a very large region, identifying specific high-risk areas for mitigation methods like micro-catchments (Founds et al. 2019), or for localized implementation of more sophisticated, time-consuming models like WEPP (Flanagan et al, 2001) or KINEROS2 (Smith et al. 1995) that consider flow routing and deposition across a watershed. The erodible, saline soils of the Mancos Shale contain areas of high erosion risk across federal, state, and private lands, and this high-resolution map of predicted erosion can help those stakeholders to implement more effective soil conservation efforts for improving water quality of the Colorado River.

6. Conclusions

The experimental work led at the six sites in this project add to previously collected data at 3 BOR-funded sites to provide insight into the dynamic of soil erosion, salt transport, runoff quantity and quality as it relates to rainfall intensity, topography and soil surface biophysical properties on saline rangelands of the UCRB. Compared to non-saline and non-sodic rangelands, the studied sites tended to be highly vulnerable to erosion with soil loss values orders of magnitude higher than that expected from similarly vegetated rangelands not affected by salts. Runoff, sediment yield, and total dissolved solids in runoff were different as a function of site due to variability in controlling factors such as slope, vegetation cover, simulation intensity, and soil properties. Total dissolved solids were found to be significantly related to sediment concentration and new predictive equations were developed to estimate TDS from soil loss.

In this project, high-resolution spatial data collected in addition to traditional soil erosion and runoff measurement techniques helped provide insights into the interplay between the spatial distribution of plants and the connectivity of hillslope runoff and erosion production areas. Landscape pattern descriptions at one site have shown that when vegetation patches may control flow tortuosity and soil erosion in ways not adequately captured by process-based models such as RHEM. These results reinforce prior literature indicating that the spatial distribution of vegetation cover has an impact on infiltration and runoff, which may in turn drive soil erosion and salt transport processes (Johnson and Miller 2006). The research team will continue to explore how to use the collected remote sensing data to characterize patterns of vegetation and bare interspaces and inform the influence of patch dynamics on salt transport processes. The team will also continue to develop equations to improve estimation of rill formation that

incorporates tortuosity and sinuosity to improve estimation of sediment yield on saline and sodic rangeland hillslopes. The results of this study will help land managers to better select the practices that enhance soil properties and its production and reduce the deterioration of surface water reservoirs and ground water pollution.

The experimental data on runoff and soil loss was also used to test and calibrate the Rangeland Hydrology and Erosion Model as tool for soil erosion and runoff prediction on salt-affected rangelands. Parameter estimation equations have been developed to predict soil effective hydraulic conductivity Ke and sheet and splash erodibility Kss on saline / sodic rangelands. Effective hydraulic conductivity on these sites were under-estimated by the current RHEM Ke estimation which required a magnified ground cover effect in the Ke estimation equation to accurately predict runoff on saline rangelands. NSE, R^2 and PBIAS for runoff improved respectively from 0.56, 0.68 and 32.03% to 0.73, 0.74 and 6.93% on the 36 calibration data points when the current Ke estimation equation was replaced with the updated Ke equation. The improved performance of the newly developed Ke estimation equation over the current Ke equation was maintained on the 36 validation data points used in this study. For these validation points, NSE and R^2 were mildly improved (0.83 and 0.85 vs. 0.88 and 0.89) while PBIAS showed a more substantial improvement from 12.05% to 5.41%. Soil loss prediction was significantly affected by soil SAR. The current sheet and splash erodibility, Kss, estimation equation used in RHEM was inadequate at predicting soil loss especially on sodic sites (SAR > 15). Across all calibration data (sodic and non-sodic included), the original Kss equation yielded NSE, R^2 and PBIAS on soil loss prediction of 0.81, 0.85 and -6.47% while the SAR-adjusted Kss equation developed in this study yielded values of 0.94, 0.94 and 4.25% for these performance measures. Performance on the validation data improved from NSE = 0.38, R2 = 0.60 and PBIAS = -24.25% to NSE = 0.69, R2 = 0.73 and PBIAS = -3.82% when the original Kss estimation equation was replaced with the SAR-adjusted equation developed in this study. Performance improvement with the integration of SAR in the Kss estimation was dramatic on sodic soil but marginal on non-sodic soils. Conversely, the newly developed Ke estimation equation resulted in substantial runoff prediction improvements on non-sodic soils while sodic soils experienced only mild improvements. Salt load was related to soil loss through a strong linear model (R^2 = 0.94) which performed well to estimate runoff salt load from RHEM-predicted soil loss (NSE = 0.90, R^2 = 0.91 and PBIAS = 4.16% on the calibration data and NSE = 0.83, R^2 = 0.61 and PBIAS = 23.18% on the validation data). Sensitivity analyses on both Ke and Kss equation developed in this study revealed low sensitivity of runoff and soil prediction to input parameter prediction contrasting with the sizable improvement in prediction performance owed to these newly developed equations. The new Kss equation has been incorporated in the online RHEM tool and is available for land managers and interested stakeholders to predict soil erosion and salt load from salt-affected rangeland hillslopes. Techniques on how to use RHEM to assess regional vulnerability of salt loading in the UCRB has been explored and an effective approach has been developed to allow land managers to evaluate where land management practices might be effective in reducing salt loads to the Colorado river.

All the data collected has been included in a custom-designed database and is expected to be published as a data paper after deliver to BLM.

7. Potential Next Steps

The Automated Geospatial Watershed Assessment (AGWA) (http://www.tucson.ars.ag.gov/agwa/) tool was developed by USDA-ARS and it is a GIS-based hydrologic modeling tool that uses commonly available GIS data layers to fully parameterize, execute, and spatially visualize results for the RHEM, KINEROS2, KINEROS-OPUS, SWAT2000, and SWAT2005 watershed runoff and erosion models. Accommodating novice to expert GIS users, it is designed to be used by watershed, water resource, land use, and resource managers and scientists investigating the hydrologic impacts of land-cover/land-use change in small watershed to basin-scale studies.

To facilitate the selection of where a conservation practice may achieve optimal benefit the user may select an "Area of Interest" and AGWA will interactively locate the impacted watershed outlets and then uses the stream network and boundary polygons to cover the area with the fewest and smallest number of watersheds necessary to parameterize and simulate the area as one unit (i.e., pasture or grazing allotment) guided by the hot spot analysis discussed earlier. This option allows the user to determine if soil erosion and salt transport is initiated above the area of interest and is being routed through the area or if the soil erosion and salt transport is occurring within the area of interest. If salt transport is being initiated within the area of interest, then the user can evaluate if and where land management practices should be located to have optimal impact for the least cost. An example of this would be to evaluate the effectiveness of prescribed grazing or revegetation practices and the impact these practices would have on surface hydrologic processes and associated soil erosion and salt transport process and ultimately TDS in the river system. The AGWA model package allows managers to rapidly identify problem areas for further monitoring and management activities. Additional functionality can be derived from the AGWA decision tool by using it to generate alternative future land-use/cover scenarios and display differences between simulation outputs (potential change). This option is designed to provide decision support when combined with planning efforts to identify benefits and consequences of proposed management actions. AGWA is designed to provide qualitative estimates of runoff and erosion relative to landscape change as a function of either climate or management actions in ungauged river basins. If calibration data is not available, it can provide useful information on the relative difference between alternative management actions for estimating the potential impact on hydrologic and soil erosion processes. This information can then be used to guide the selection of appropriate conservation practices to deploy and where they should be deployed to optimize the cost-benefit ratios of large-scale restoration projects. The AGWA model package can provide reliable quantitative estimates of runoff, erosion, and salt transport if appropriate calibration datasets are available. To effectively reduce runoff, soil erosion, and salt transport, the most efficient approach would be to increase vegetation density and disrupt concentrated flow paths that directly transfer salts to the Colorado River from saline rangeland plants. A recent review of literature and a site visit to the Badia region of Jordan suggest that a mechanized water harvesting system can be used to successfully establish *Atriplex* spp. and *Salsola* spp. shrubs in desert environment where average annual rainfall is between 100 and 250 mm per year reducing runoff and sediment yield.

Gammoh and Oweis (2011) used a Vallerani plow (Figure 52) to create a U shape depression in the soil, effectively creating a small depression storage area to trap water, sediments, and salts. The Vallerani plow creates a divot and pushes up soil to form a berm (i.e., bund) that traps water from the uphill slope. This provides additional water to the shrubs transplanted into the depression that is necessary for their survival. Additionally, a ripping blade is part of the system that is pulled through the soil to a depth of 60 cm. This fractures the cemented petrocalcic subsoil and improves water storage capacity in the soil profile. If not treated, the cemented petrocalcic horizon impedes downward percolation of water and limits the volume of stored soil moisture to the upper 50 cm of the soil profile. This limits the ability of the soil to store the water derived from water harvesting that is critical for plant growth/survival in these dry areas.

The entrapment of nutrients along with sediments in these depressions creates areas of nutrient concentration where plants thrive in spaces alternated by bare or poorly vegetated zones of water and nutrient depletion, forming the premise of the "resource islands" or "vegetation island" concept. The use of the Vallerani plow mimics this natural process of VDSH and provides the necessary water for plant establishment and initiation of the restoration

process if properly located to prevent overtopping and breaching of the bunds. The Vallerani System has been successfully applied to nearly 100,000 ha of degraded rangeland in Morocco, Niger, Senegal, Sudan, Tunisia, Chad and Egypt (Malagnoux, 2008).

Figure 52. Vallerani plow

Haddad (2019) used the RHEM erosion tool to evaluate the effectiveness of the mico-catchments created with the Vallerani plow in the Badaia region of Jordan. She reported that RHEM depicted runoff and sediment yield with an average R^2 of 0.76 when comparing simulated with observed surface runoff. She concluded that the RHEM can be used within large-scale models to identify hot-spots for out-scaling of restoration taking into consideration the integrated watershed management approach. The model can be used by decision makers to develop ecological site descriptions that include the current eco-hydrological processes. It can be used to develop ecosystem transition status, thus to estimate the impact of several disturbances such as changes in land management and climate. The plant cover changes simulated by RHEM can be used as a reference to assess the livestock carrying capacities of the hillslopes areas, which provides essential information for sustainable livestock management in the Jordanian Badia (Figure 53).

Figure 53. Before and after images of a successful restoration effort of rangeland hillslopes in the Badia region of Jordan. The successful revegetation of a degraded watershed was implemented by using a Vallerani plot technique causing diversion of concentrated flow to support plant growth.

The key to success of watershed treatment in the Upper Colorado River Basin will be the establishment of vegetation in a spatial pattern that both reduces raindrop impact but increases tortuosity in the concentrated flow paths and thus reduction in slope length that will prevent rill formation through reduction in overland flow volume and velocity of surface runoff. An operational strategy to implement micro-catchments from use of the Vallerani plow at the hillslope scale should consider the statistical frequency and intensity of rainfall, slope angle, and soil properties that affect the stability and infiltration capacity for micro-catchment (Ziadat et. al., 2014). Micro catchments need to be sized and spaced adequately for optimal function and cost effectiveness (Akroush et al., 2014; Oweis et al., 2016). The sizing and distance both between micro-catchments and distance in rows down slope can be estimated with use of Guelph permeameter to determine ponded and unsaturated infiltration rates (Founds et al. 2019). The utilization of the Guelph permeameter would allow for accurate estimation of on-site

infiltration characteristics in areas where detailed soil maps are not available, as in much on the Upper Colorado River Basin, when considering potential sites for restoration and associated reductions in salt transport to the Colorado River.

The current design calls for the Vallerani plow to be pulled on the contour in the uplands with spacing of the bunds at approximately 3 to 4 meters. In the next row the bunds are offset and placed in the gaps created in the first row. This limits the net distance downslope water can travel before being captured in a bund. Anticipated row spacing is approximately 8 – 10 m. This design should minimize overland flow velocities and capture sediment and salts on the hillslope. A watershed restoration assessment of the cost-benefit of restoration efforts would be evaluated with the RHEM-KINEROS2-AGWA decision support system which can be utilized to optimize the design of the spacing of the bunds to address plant-water requirements but also soil erosion and salt transport concerns within the uplands based on slope length, steepness, shape, soil texture, presence and strength of physical soil crust, aspect, climate, and vegetation density and cover.

8. Cited references

Abrahams, A. D., and A. J. Parsons. 1991. Relation between infiltration and stone cover on a semiarid hillslope, southern Arizona. Journal of Hydrology **122**:49-59

Abrahams, A. D., A. J. Parsons, and S. H. Luk. 1991. The effect of spatial variability in overland flow on the downslope pattern of soil loss on a semiarid hillslope, southern Arizona. Catena **18**:255-270

Abrahams, A. D., and A. J. Parsons. 1994. Hydraulics of interrill overland flow on stone-covered desert surfaces. Catena **23**:111-140

Abrahams, A. D., A. J. Parsons, and J. Wainwright. 1995. Effects of vegetation change on interrill runoff and erosion, Walnut Gulch, southern Arizona. Geomorphology **13**:37-48

Akroush, S., Shideed, K., Bruggeman, A., 2014. Economic analysis and environmental impacts of water harvesting techniques in the low rainfall areas of Jordan. International Journal of Agricultural Resources, Governance and Ecology. https://doi.org/10.1504/ijarge.2014.061040

Al-Hamdan, O., F. Pierson, M. Nearing, C. Williams, M. Hernandez, K. Spaeth, J. Boll, and M. Weltz. 2015. Use of RHEM to assess runoff and erosion following disturbance on rangelands *in* Society for Range Management Meeting Abstracts.

Al-Hamdan, O. Z., F. B. Pierson, M. A. Nearing, J. J. Stone, C. J. Williams, C. A. Moffet, P. R. Kormos, J. Boll, and M. A. Weltz. 2012a. Characteristics of concentrated flow hydraulics for rangeland ecosystems: implications for hydrologic modeling. Earth Surface Processes and Landforms **37**:157-168.10.1002/esp.2227

Al-Hamdan, O. Z., F. B. Pierson, M. A. Nearing, C. J. Williams, J. J. Stone, P. R. Kormos, J. Boll, and M. A. Weltz. 2012b. Concentrated flow erodibility for physically based erosion models: Temporal variability in disturbed and undisturbed rangelands. Water Resources Research **48**.10.1029/2011wr011464

Al-Hamdan, O. Z., F. B. Pierson, M. A. Nearing, C. J. Williams, J. J. Stone, P. R. Kormos, J. Boll, and M. A. Weltz. 2013. Risk assessment of erosion from concentrated flow on rangelands using overland flow distribution and shear stress partitioning. Transactions of the Asabe **56**:539-548

Amrhein, C., and D. Suarez. 1990. Procedure for determining sodium-calcium selectivity in calcareous and gypsiferous soils. Soil Science Society of America Journal **54**:999-1007

Arslan, A., and G. Dutt. 1993. Solubility of gypsum and its prediction in aqueous solutions of mixed electrolytes. Soil Science **155**:37-47

Arslan, A. 1995. A computer program to express the properties of gypsiferous soils. Canadian Journal of Soil Science **75**:459-462

Barger, N. N., J. E. Herrick, J. Van Zee, and J. Belnap. 2006. Impacts of biological soil crust disturbance and composition on C and N loss from water erosion. Biogeochemistry **77**:247-263

Belnap, J., and D. A. Gillette. 1998. Vulnerability of desert biological soil crusts to wind erosion: the influences of crust development, soil texture, and disturbance. Journal of Arid Environments **39**:133-142

Belnap, J., J. R. Welter, N. B. Grimm, N. Barger, and J. A. Ludwig. 2005. Linkages between microbial and hydrologic processes in arid and semiarid watersheds. Ecology **86**:298-307.10.1890/03-0567

Belnap, J. 2006. The potential roles of biological soil crusts in dryland hydrologic cycles. Hydrological Processes **20**:3159-3178

Belnap, J., R. L. Reynolds, M. C. Reheis, S. L. Phillips, F. E. Urban, and H. L. Goldstein. 2009. Sediment losses and gains across a gradient of livestock grazing and plant invasion in a cool, semi-arid grassland, Colorado Plateau, USA. Aeolian Research **1**:27-43

Belnap, J., B. P. Wilcox, M. W. Van Scoyoc, and S. L. Phillips. 2013. Successional stage of biological soil crusts: an accurate indicator of ecohydrological condition. Ecohydrology **6**:474-482.10.1002/eco.1281

Bhark, E. W., and E. E. Small. 2003. Association between plant canopies and the spatial patterns of infiltration in shrubland and grassland of the Chihuahuan Desert, New Mexico. Ecosystems **6**:185-196.10.1007/s10021-002-0210-9

Bharmoria, P., H. Gupta, V. Mohandas, P. K. Ghosh, and A. Kumar. 2012. Temperature Invariance of NaCl Solubility in Water: Inferences from Salt–Water Cluster Behavior of NaCl, KCl, and NH4Cl. The Journal of Physical Chemistry B **116**:11712-11719

Blackburn, W., and C. Skau. 1974. Infiltration rates and sediment production of selected plant communities in Nevada. Journal of Range Management **27**: 476-480

Blackburn, W., F. Pierson, C. Hanson, T. Thurow, and A. Hanson. 1992. Spatial and temporal influence of vegetation on surface soil factors in semiarid rangelands. Transactions of the American Society of Agricultural Engineers **35**:479-486

Blackburn, W. H. 1975. Factors influencing infiltration rate and sediment production of semiarid rangelands in Nevada. Water Resources Research **11**:929-937

Bonnin, G. M., D. Martin, B. Lin, T. Parzybok, M. Yekta, and D. Riley. 2006. Precipitation-Frequency Atlas of the United States.*in* N. O. A. A. U. S. Department of Commerce, National Weather Service, editor. NOAA Atlas 14 Addendum: Precipitation-Frequency Atlas of the United States, Silver Spring, Maryland.

BoR (U.S. Bureau of Reclamation). 2013. Quality of water – Colorado River basin progress report no. 24. BoR Upper Colorado Region, Salt Lake City, UT.

Bowles, D. S., H. Nezafati, R. K. Bhasker, J. P. Riley, and R. J. Wagenet. 1982. Salt loading from efflorescence and suspended sediments in the Price River basin. Utah Water Research Laboratory, Utah State University, Logan, Utah.

Brakensiek, D., and W. Rawls. 1994. Soil containing rock fragments: effects on infiltration. Catena **23**:99-110

Branson, F. A., G. F. Gifford, K. G. Renard, and R. F. Hadley. 1981. Rangeland Hydrology. 2nd edition. Society for Range Management, Denver, Colorado.

Breuer, L., Eckhardt, K., & Frede, H.-G. (2003). Plant parameter values for models in temperate climates. Ecological Modelling, 169, 237–293. doi:10.1016/s0304-3800(03)00274-6

Brown, J. W., H. E. Hayward, A. Richards, L. Bernstein, J. T. Hatcher, R. C. Reeve, and L. A. Richards. 1954. Diagnosis and Improvement of Saline and Alkali Soils. U. S. Department of Agriculture, United States Salinity Laboratory.

Burt, R. 2011. Soil Survey Investigations Report, no. 45, version 2.0. Natural Resources Conservation Service

Cadaret, E.M., McGwire, K.C., Nouwakpo, S.K., Weltz, M.A., & Saito, L. (2016a). Vegetation canopy cover effects on sediment erosion processes in the Upper Colorado River Basin Mancos Shale formation, Price, Utah, USA. Catena, 147, 334-344. doi:10.1016/j.catena.2016.06.043

Cadaret, E.M., Nouwakpo, S.K., McGwire, K.C., Weltz, M.A., & Blank, R.R. (2016b). Experimental investigation of the effect of vegetation on soil, sediment erosion, and salt transport processes in the Upper Colorado River Basin Mancos Shale formation, Price, Utah, USA. Catena, 147, 650-662. doi:10.1016/j.catena.2016.08.024

Caldwell, T. G., M. H. Young, E. V. McDonald, and J. T. Zhu. 2012. Soil heterogeneity in Mojave Desert shrublands: Biotic and abiotic processes. Water Resources Research **48**:12.10.1029/2012wr011963

Cammeraat, L., and A. Imeson. 1998. Deriving indicators of soil degradation from soil aggregation studies in southeastern Spain and southern France. Geomorphology **23**:307-321

Carlyle-Moses, D. 2004. Throughfall, stemflow, and canopy interception loss fluxes in a semi-arid Sierra Madre Oriental matorral community. Journal of Arid Environments **58**:181-202

Cerdà, A. 2001. Effects of rock fragment cover on soil infiltration, interrill runoff and erosion. European Journal of Soil Science **52**:59-68

Costin, A., D. Wimbush, D. Kerr, and L. Day. 1959. Studies in catchment hydrology in the Australian Alps. 1. Trends in soils and vegetation. CSIRO Aust. Div. Plant Ind. Tech Pap. No. 13

Curran, P. & Hay, A. (1986). The importance of measurement error for certain procedures in remote sensing at optical wavelengths. Photogrammetric Engineering and Remote Sensing, 52, 299-241.

D'Odorico, P., K. Caylor, G. S. Okin, and T. M. Scanlon. 2007. On soil moisture–vegetation feedbacks and their possible effects on the dynamics of dryland ecosystems. Journal of Geophysical Research: Biogeosciences **112**

Davenport, D. W., D. D. Breshears, B. P. Wilcox, and C. D. Allen. 1998. Viewpoint: sustainability of piñon-juniper ecosystems--a unifying perspective of soil erosion thresholds. Journal of Range Management **51**:231-240

De Ploey, J. 1984. Stemflow and colluviation: Modeling and implications. Pedologie. XXXIV-2: 135-146

Devitt, D. A., and S. D. Smith. 2002. Root channel macropores enhance downward movement of water in a Mojave Desert ecosystem. Journal of Arid Environments **50**:99-108

Dunkerley, D. 2002. Infiltration rates and soil moisture in a groved mulga community near Alice Springs, arid central Australia: evidence for complex internal rainwater redistribution in a runoff–runon landscape. Journal of Arid Environments **51**:199-219

Dunkerley, D. 2008. Intra-storm evaporation as a component of canopy interception loss in dryland shrubs: observations from Fowlers Gap, Australia. Hydrological Processes **22**:1985-1995

Eldridge, D. 1993. Cryptogam cover and soil surface condition: effects on hydrology on a semiarid woodland soil. Arid Land Research and Management 7:203-217

Eldridge, D. J., and T. B. Koen. 1998. Cover and floristics of microphytic soil crusts in relation to indices of landscape health. Plant Ecology **137**:101-114.10.1023/A:1008036214140

Eldridge, D. J., and R. Rosentreter. 2004. Shrub mounds enhance water flow in a shrub-steppe community in southwestern Idaho, U.S.A. Pages 77-83 *in* Seed and Soil Dynamics in Shrubland Ecosystems: Proceedings RMRS-P-31. Dept. of Agriculture, Forest Service, Rocky Mountain Research Station, Laramie, WY.

Emmett, W. W. 1970. The hydraulics of overland flow on hillslopes. United States Geological Survey.

Evangelou, V. P. 1981. Chemical and mineralogical composition and behavior of the Mancos Shale as a diffuse source of salts in the upper Colorado River basin. California Univ., Davis. Water Resources Center., PANELIST02.

Flanagan, D., and M. Nearing. 1995. USDA-Water Erosion Prediction Project: Hillslope profile and watershed model documentation. USDA ARS National Soil Erosion Research Lab, W. Lafayette, IN.

Flanagan D.C., Ascough J.C., Nearing M.A., Laflen J.M. (2001) The Water Erosion Prediction Project (WEPP) Model. In: Harmon R.S., Doe W.W. (eds) Landscape Erosion and Evolution Modeling. Springer, Boston, MA. doi: 10.1007/978-1-4615-0575-4_7

Founds, M.J., K.C. McGwire, M.A. Weltz, S. K. Nouwakpo, and P. S.J. verburg. 2019. Predciting micro-catchment ponded infiltration dynamice. Catana. 190(2020) 104524 pg 11.

Gagnon, S. R., J. R. Sears, J. R. Makuch , C. G. Rossi, S. K. Nouwakpo, M. A. Weltz, and G. W. Frasier. 2014. Salinity mobilization and transport: Hydrologic and aeolian processes and remediation techniques for rangelands. A selected bibliography. USDA-ARS, Beltsville, Maryland.

Gao, L.Q.; Bowker, M.A., Sun, H., Zhao, J., & Zhao, Y.G. (2020). Linkages between biocrust development and water erosion and implications for erosion model implementation. Geoderma, 357, 113973. doi:10.1016/j.geoderma.2019.113973

Gammoh, I., and T. Oweis. 2011. Performance and Adaptation of the Vallerani Mechanized Water Harvesting System in Degraded Badia Rangelands. Journal of Environmental Science and Engineering **5**

Gassman, P.W., Reyes, M.R., Green, C.H., & Arnold, J.G. (2007). The Soil and Water Assessment Tool: historical development, applications, and future research directions. Trans. of the ASABE, 50, 1211–1250. doi:10.13031/2013.23637.

Gharaibeh, M. A. Eltaif, N. I. and Albalasmeh, A. A. 2011. Reclamation of highly calcareous saline sodic soil using atriplex halimus and by-product Gypsum. International Journal of Phytoremediation, 13:873–883.

Gifford, G. F. 1984. Vegetation allocation for meeting site requirements. Westview Press, Denver CO.

Giménez, R., and G. Govers. 2001. Interaction between bed roughness and flow hydraulics in eroding rills. Water Resources Research **37**:791-799

Govers, G., R. Gimenez, and K. Van Oost. 2007. Rill erosion: Exploring the relationship between experiments, modelling and field observations. Earth-Science Reviews **84**:87-102.10.1016/j.carscirev.2007.06.001

Haddad, M. 2019. Exploring Jordans rangeland transitions: Merging restoration experiment with modeling - A case study from Al Majdiyya vilage. M.S. Thesis. University of Jordan. pg

Hamilton, E. L., and P. B. Row. 1949. Rainfall interception by chaparral in California. California Dept of Natural Resources, Division of Forestry, in cooperation with the California Forest and Range Experiment Station, Sacramento, CA.

Hernandez, M., Nearing, M.A., Stone, J.J., Pierson, F.B., Wei, H., Spaeth, K.E., Heilman, P.H., Weltz, M.A, & Goodrich, D.C. (2013). Application of a rangeland soil erosion model using National Resources Inventory data in southeastern Arizona. Journal of Soil and Water Conservation, 68, 512-525. doi:10.2489/jswc.68.6.512

Hernandez, M., M. A. Nearing, O. Z. Al-Hamdan, F. B. Pierson, G. Armendariz, M. A. Weltz, K. E. Spaeth, C. J. Williams, S. K. Nouwakpo, and D. C. Goodrich. 2017. The Rangeland Hydrology and Erosion Model: A dynamic approach for predicting soil loss on rangelands. Water Resources Research **53**:9368-9391

Houska, T., P. Kraft, A. Chamorro-Chavez, and L. Breuer. 2015. SPOTting model parameters using a ready-made python package. Plos One **10**:e0145180

Huntington, J., McGwire, K., Morton, C., Snyder, K., Peterson, S., Erickson, T., Niswonger, R., Carroll, R., Smith, G., & Allen, R. (2016). Assessing the role of climate and resource management on groundwater dependent ecosystem changes in arid environments with the Landsat archive. Remote Sensing of Environment, 185, 186-197. doi:10.1016/j.rse.2016.07.004. doi:10.1016/j.rse.2016.07.004

Huete, A.R., & Tucker, C.J. (1991). Investigation of soil influences in AVHRR red and near-infrared vegetation index imagery. International Journal of Remote Sensing 12, 1223–1242. doi:10.1080/01431169108929723

Iorns, W.V., Hembree, C.H, & Oakland, G.L. (1965). Water resources of the Upper Colorado River Basin. Technical report: U.S. Geological Survey Professional Paper 441, 370 p.

Imeson, A., H. Lavee, A. Calvo, and A. Cerda. 1998. The erosional response of calcareous soils along a climatological gradient in Southeast Spain. Geomorphology **24**:3-16

Johnson, C., and N. Gordon. 1988. Runoff and erosion from rainfall simulator plots on sagebrush rangeland. Transactions of the ASAE **31**:421-427

Johnson, D. D., and R. F. Miller. 2006. Structure and development of expanding western juniper woodlands as influenced by two topographic variables. Forest Ecology and Management **229**:7-15

Jones, C.P., Grossl, P.R.. Amacher, M.C., Boettinger, J.L., Jacobson, A.R., and Lawley, J.R. 2017. Selenium and salt mobilization in wetland and arid upland soils of Pariette Draw, Utah (USA). Geoderma 305:363-373.

Kautz, M.A, Holifield-Collins, C.D., Guertin, D.P., Goodrich, D.C., van Leeuwen, & W.J., Williams, C.J. (2019). Hydrologic model parameterization using dynamic Landsat-based vegetative estimates within a semiarid grassland. Journal of Hydrology, 575, 1073-1086. doi:10.1016/j.jhydrol.2019.05.044.

Kinnell, P.I.A. (2005). Why the universal soil loss equation and the revised version of it do not predict event erosion well. Hydrol. Process, 19, 851–854. doi:10.1002/hyp.5816

Kenney, T. A., S. J. Gerner, S. G. Buto, and L. E. Spangler. 2009. Spatially referenced statistical assessment of dissolved-solids load sources and transport in streams of the Upper Colorado River Basin. U.S. Geological Survey, Reston, Virginia.

Khechai, S., and Y. Daoud. 2016. Characterization and Origin of Gypsum Rhizoliths of Ziban Oases Soil-Algeria. World Applied Sciences Journal **34**:948-955

Knight, R., W. Blackburn, and L. Merrill. 1984. Characteristics of oak mottes, Edwards Plateau, Texas. Journal of Range Management:534-537

Langbein, W. B., and S. Schumm. 1958. Yield of sediment in relation to mean annual precipitation. Transactions, American Geophysical Union **39**:1076-1084

Laronne, J. B., and H. W. Shen. 1982. The effect of erosion on solute pickup from Mancos Shale hillslopes, Colorado, USA. Journal of Hydrology **59**:189-207.10.1016/0022-1694(82)90011-7

Lebedev, A., and V. Kosorukov. 2017. Gypsum solubility in water at 25° C. Geochemistry International **55**:205-210

Lebron, I., M. Madsen, D. Chandler, D. Robinson, O. Wendroth, and J. Belnap. 2007. Ecohydrological controls on soil moisture and hydraulic conductivity within a pinyon-juniper woodland. Water Resources Research **43**

Leighton-Boyce, G., S. H. Doerr, R. Shakesby, and R. Walsh. 2007. Quantifying the impact of soil water repellency on overland flow generation and erosion: a new approach using rainfall simulation and wetting agent on in situ soil. Hydrological Processes **21**:2337-2345

Lesch, S. M. and Suarez, D. L. 2009. A short note on calculating the adjusted sar index. Transactions of the ASABE 52(2): 493-496.American Society of Agricultural and Biological Engineers ISSN 0001-2351

Li, J., C. Zhao, H. Zhu, Y. Li, and F. Wang. 2007. Effect of plant species on shrub fertile island at an oasis–desert ecotone in the South Junggar Basin, China. Journal of Arid Environments **71**:350-361

Li, J., G. S. Okin, J. E. Herrick, J. Belnap, M. E. Miller, K. Vest, and A. E. Draut. 2013. Evaluation of a new model of aeolian transport in the presence of vegetation. Journal of Geophysical Research: Earth Surface **118**:288-306

Li, X., X. Li, W. Song, Y. Gao, J. Zheng, and R. Jia. 2008. Effects of crust and shrub patches on runoff, sedimentation, and related nutrient (C, N) redistribution in the desertified steppe zone of the Tengger Desert, Northern China. Geomorphology **96**:221-232

Loope, W. L., and G. F. Gifford. 1972. Influence of a soil microfloral crust on select properties of soils under pinyon-juniper in southeastern Utah. Journal of Soil and Water Conservation **27**:164-167

Ludwig, J. A., B. P. Wilcox, D. D. Breshears, D. J. Tongway, and A. C. Imeson. 2005. Vegetation patches and runoff-erosion as interacting ecohydrological processes in semiarid landscapes. Ecology **86**:288-297.10.1890/03-0569

Malagnoux, M., 2008. Degraded Arid Land Restoration f 589 or Afforestation and Agro-Silvo-Pastoral Production through New Water Harvesting Mechanized Technology, in: The Futureof Drylands. https://doi.org/10.1007/978-1-4020-6970-3_30

Marshall, J. K. 1973. Drought, land use and soil erosion. Pages 55-77 *in* J. Lovett, editor. The Environmental, Economic and Social Significance of Drought. Angus and Robertson, Sydney.

Martinez-Meza, E., and W. G. Whitford. 1996. Stemflow, throughfall and channelization of stemflow by roots in three Chihuahuan desert shrubs. Journal of Arid Environments **32**:271-287.10.1006/jare.1996.0023

McGwire, K., Friedl, M., & Estes, J. (1993), Spatial structure, sampling design, and scale in remotely sensed imagery of a California savanna woodland. International Journal of Remote Sensing, 14, 2137-2164. doi:10.1080/01431169308954026

Meire, D., J. M. Kondziolka, and H. M. Nepf. 2014. Interaction between neighboring vegetation patches: Impact on flow and deposition. Water Resources Research **50**:3809-3825.10.1002/2013wr015070

Miller, M.P., Buto, S.G., Lambert, P.M., & Rumsey, C.A. (2017). Enhanced and updated spatially referenced statistical assessment of dissolved-solids load sources and transport in streams of the Upper Colorado River Basin. U.S. Geological Survey Scientific Investigations Report 2017–5009, 23 p., doi:10.3133/sir20175009.

Moore, E., E. Janes, F. Kinsinger, K. Pitney, and J. Sainsbury. 1979. Livestock Grazing Management and Water Quality Protection EPA 910/9-79-67, US Environmental Protection Agency and US DI Bureau of Land Management.

Moeys, J., Shangguan, W., Petzold, R., Minasny, B., Rosca, B., Jelinski, N., Zelazny, W., Souza, R.M.S., Safanelli, J.L., & ten Caten, A. (2018). Functions for Soil Texture Plot, Classification and Transformation (version 1.5.1). Accessed on 2/8/2019 from https://github.com/julienmoeys/soiltexture.

Mubarak, A., and R. Olsen. 1976. Immiscible displacement of the soil solution by centrifugation. Soil Science Society of America Journal

Nauman, T.W., Ely, C.P., Miller, M.P., & Duniway, M.C. (2019). Salinity yield modeling of the Upper Colorado River Basin using 30-meter resolution soil maps and random forests. Water Resources Research, 55, 4954-4973. doi:10.1029/2018WR024054

Navar, J., and R. Bryan. 1990. Interception loss and rainfall redistribution by three semi-arid growing shrubs in northeastern Mexico. Journal of Hydrology **115**:51-63

Nearing, M., L. Norton, D. Bulgakov, G. Larionov, L. West, and K. Dontsova. 1997. Hydraulics and erosion in eroding rills. Water Resources Research **33**:865-876

Nearing, M., H. Wei, J. Stone, F. Pierson, K. Spaeth, M. Weltz, D. Flanagan, and M. Hernandez. 2011a. A Rangeland Hydrology and Erosion Model. Transactions of the American Society of Agricultural and Biological Engineers **54**:901-908

Nearing, M. A., J. R. Simanton, L. D. Norton, S. J. Bulygin, and J. Stone. 1999. Soil erosion by surface water flow on a stony, semiarid hillslope. Earth Surface Processes and Landforms **24**:677-686.10.1002/(sici)1096-9837(199908)24:8<677::aid-esp981>3.3.co;2-t

Nearing, M. A., H. Wei, J. J. Stone, F. B. Pierson, K. E. Spaeth, M. A. Weltz, D. C. Flanagan, and M. Hernandez. 2011b. A rangeland hydrology and erosion model. Transactions of the Asabe **54**:901-908

Nouwakpo, S., M. Weltz, M. Hernandez, T. Champa, and J. Fisher. 2016. Performance of the Rangeland Hydrology and Erosion Model for runoff and erosion assessment on a semiarid reclaimed construction site. Journal of Soil and Water Conservation **71**:220-236

Nouwakpo, S. K., M. A. Weltz, K. C. McGwire, J. C. Williams, A. H. Osama, and C. H. Green. 2017. Insight into sediment transport processes on saline rangeland hillslopes using three-dimensional soil microtopography changes. Earth Surface Processes and Landforms **42**:681-696

Nouwakpo, S. K., M. A. Weltz, A. Arslan, C. H. Green, and O. Z. Al-Hamdan. 2018. Process-based Modeling of Infiltration, Soil Loss and Dissolved Solids on Saline and Sodic Soils. Transactions of the American Society of Agricultural and Biological Engineers **61**:1-16.https://doi.org/10.13031/trans.12705

NRCS (U.S. Department of Agriculture National Resource Conservation Service) (1997). National resources inventory. Natural Resources Conservation Service. Revised 2014.

NRCS (U.S. Department of Agriculture National Resource Conservation Service) (2018). 2018 National Resources Inventory Rangeland Resource Assessment. https://www.nrcs.usda.gov/wps/portal/nrcs/detail/national/technical/nra/nri/results/?cid=nrcseprd1343027

Nulsen, R. A., K. J. Bligh, I. N. Baxter, E. J. Solin, and D. H. Imrie. 1986. The fate of rainfall in a mallee and heath vegetated catchment in southern Western Australia. Australian Journal of Ecology **11**:361-371.10.1111/j.1442-9993.1986.tb01406.x

Okin, G. S., A. J. Parsons, J. Wainwright, J. E. Herrick, B. T. Bestelmeyer, D. C. Peters, and E. L. Fredrickson. 2009. Do changes in connectivity explain desertification? BioScience **59**:237-244

Orr, H. K. 1970. Runoff and erosion control by seeded and native vegetation on a forest burn: Black Hills, South Dakota. USDA Forest Service Rocky Mountain Forest and Range Experiment Station, Fort Collins CO.

Oweis, T.Y., 2016. Rainwater harvesting for restoring degraded dry agro-pastoral ecosystems: a conceptual review of opportunities and constraints in a changing climate. Environ. Rev. https://doi.org/10.1139/er-2016-0069

Owens, M. K., R. K. Lyons, and C. L. Alejandro. 2006. Rainfall partitioning within semiarid juniper communities: effects of event size and canopy cover. Hydrological Processes **20**:3179-3189

Packer, P. E. 1951. An approach to watershed protection criteria. Journal of Forestry **49**:639-644

Page, A., R. Miller, and D. Keeney. 1982. Methods of soil analysis. Part 2. Chemical and microbiological properties. American Society of Agronomy *in* Soil Science Society of America.

Paige, G. B., J. J. Stone, J. R. Smith, and J. R. Kennedy. 2004. The Walnut Gulch rainfall simulator: A computer-controlled variable intensity rainfall simulator. Applied Engineering in Agriculture **20**:25-31

Parsons, A. J., A. D. Abrahams, and J. Wainwright. 1996. Responses of interrill runoff and erosion rates to vegetation change in southern Arizona. Geomorphology **14**:311-317

Pierson, F., P. Robichaud, C. Moffet, K. Spaeth, C. Williams, S. Hardegree, and P. Clark. 2008a. Soil water repellency and infiltration in coarse-textured soils of burned and unburned sagebrush ecosystems. Catena **74**:98-108

Pierson, F. B., W. H. Blackburn, S. S. Van Vactor, and J. C. Wood. 1994a. Partitioning small scale spatial variability of runoff and erosion on sagebrush rangeland. Water Resources Bulletin **30**:1081-1089

Pierson, F. B., K. E. Spaeth, M. A. Weltz, and D. H. Carlson. 2002. Hydrologic response of diverse western rangelands. Journal of Range Management **55**:558-570.10.2307/4003999

Pierson, F. B., J. D. Bates, T. J. Svejcar, and S. P. Hardegree. 2007a. Runoff and erosion after cutting western juniper. Rangeland Ecology and Management **60**:285-292.10.2111/1551-5028(2007)60[285:raeacw]2.0.co;2

Pierson, F. B., W. H. Blackburn, and S. S. Van Vactor. 2007b. Hydrologic impacts of mechanical seeding treatments on sagebrush rangelands. Rangeland Ecology & Management **60**:666-674

Pierson, F. B., P. R. Robichaud, C. A. Moffet, K. E. Spaeth, S. P. Hardegree, P. E. Clark, and C. J. Williams. 2008b. Fire effects on rangeland hydrology and erosion in a steep sagebrush-dominated landscape. Hydrological Processes **22**:2916-2929.10.1002/hyp.6904

Pierson, F. B., C. A. Moffet, C. J. Williams, S. P. Hardegree, and P. E. Clark. 2009. Prescribed-fire effects on rill and interrill runoff and erosion in a mountainous sagebrush landscape. Earth Surface Processes and Landforms **34**:193-203.10.1002/esp.1703

Pierson, F. B., C. J. Williams, P. R. Kormos, S. P. Hardegree, P. E. Clark, and B. M. Rau. 2010. Hydrologic vulnerability of sagebrush steppe following pinyon and juniper encroachment. Rangeland Ecology and Management **63**:614-629

Pierson, F. B., C. J. Williams, S. P. Hardegree, M. A. Weltz, J. J. Stone, and P. E. Clark. 2011. Fire, plant invasions, and erosion events on western rangelands. Rangeland Ecology and Management **64**:439-449.10.2111/REM-D-09-00147.1

Pierson, F. B., C. J. Williams, S. P. Hardegree, P. E. Clark, P. R. Kormos, and O. Z. Al-Hamdan. 2013. Hydrologic and Erosion Responses of Sagebrush Steppe Following Juniper Encroachment, Wildfire, and Tree Cutting. Rangeland Ecology & Management **66**:274-289.10.2111/rem-d-12-00104.1

Pierson, F. B., C. J. Williams, P. R. Kormos, and O. Z. Al-Hamdan. 2014. Short-Term Effects of Tree Removal on Infiltration, Runoff, and Erosion in Woodland-Encroached Sagebrush Steppe. Rangeland Ecology & Management **67**:522-538.10.2111/rem-d-13-00033.1

Pierson, F. B., Jr., S. S. Van Vactor, W. H. Blackburn, and J. C. Wood. 1994b. Incorporating small scale spatial variability into predictions of hydrologic response on sagebrush rangelands. Pages 23-34 *in* W. H. Blackburn, F. B. Peirson, Jr., G. E. Schuman, and R. Zartman, editors. SSSA Special Publication; Variability in rangeland water erosion processes. Soil Science Society of America {a}, 677 South Segoe Road, Madison, Wisconsin 53711, USA.

Pierson, F.B., & Williams, C.J. (2016). Ecohydrologic impacts of rangeland fire on runoff and erosion: A literature synthesis. U. S. Dept of Agriculture, Forest Service, Rocky Mountain Research Station, Fort Collins.

Poesen, J., F. Ingelmo-Sanchez, and H. Mucher. 1990. The hydrological response of soil surfaces to rainfall as affected by cover and position of rock fragments in the top layer. Earth Surface Processes and Landforms **15**:653-671

Poesen, J., and F. Ingelmo-Sanchez. 1992. Runoff and sediment yield from topsoils with different porosity as affected by rock fragment cover and position. Catena **19**:451-474

Poesen, J., D. Torri, and K. Bunte. 1994. Effects of rock fragments on soil erosion by water at different spatial scales: a review. Catena **23**:141-166

Ponce, S. L. 1975. Examination of a non-point source loading function for the Mancos shale wildlands of the Price River Basin, Utah. Ph.D. Utah State University.

Puigdefabregas, J., A. Sole, L. Gutierrez, G. del Barrio, and M. Boer. 1999. Scales and processes of water and sediment redistribution in drylands: results from the Rambla Honda field site in Southeast Spain. Earth-Science Reviews **48**:39-70.10.1016/s0012-8252(99)00046-x

Puigdefabregas, J. 2005. The role of vegetation patterns in structuring runoff and sediment fluxes in drylands. Earth Surface Processes and Landforms **30**:133-147.10.1002/esp.1181

R Core Team (2018). R: A language and environment for statistical computing. R Foundation for Statistical Computing, Vienna, Austria. URL https://www.R-project.org/.

Reclamation, B. o. 2013. Quality of Water: Colorado River Basin Progress Report No. 24 United States Department of Interior, Bureau of Reclamation.

Rasely, R.C., Roberts, T.C., & Pyper, G.P. (1991). Upper Colorado River basin rangeland salinity control project: watershed resource condition evaluation phase II procedure. Colorado River Basin Salinity Forum.

Reid, K. D., B. P. Wilcox, D. D. Breshears, and L. MacDonald. 1999. Runoff and erosion in a piñon–juniper woodland influence of vegetation patches. Soil Science Society of America Journal **63**:1869-1879

Ridolfi, L., F. Laio, and P. D'Odorico. 2008. Fertility island formation and evolution in dryland ecosystems. Ecology and Society **13**

Rodrigues de Souza, Edivan, Maria Betânia Galvão dos Santos FreireB, Heitor Henrique Félix DuarteC and Fernando José Freire. 2010. Removal of salts by Atriplex nummularia depending on soil moisture. 19th World Congress of Soil Science, Soil Solutions for a Changing World 1 – 6 August 2010, Brisbane, Australia. Published on DVD.

Rominger, J. T., and H. M. Nepf. 2011. Flow adjustment and interior flow associated with a rectangular porous obstruction. Journal of Fluid Mechanics **680**:636-659.10.1017/jfm.2011.199

Roundy, B. A., W. Blackburn, and R. Eckert Jr. 1978. Influence of prescribed burning on infiltration and sediment production in the pinyon-juniper woodland, Nevada. Journal of Range Management:250-253

Roundy, B.A., Farmer, M., Olson, J., Petersen, S., Nelson, D.R., Davis, J., & Vernon, J. (2017). Runoff and sediment response to tree control and seeding on a high soil erosion potential site in Utah: evidence for reversal of an abiotic threshold. Ecohydrology, 10, e1775. doi:10.1002/eco.1775

Schlesinger, W. H., J. F. Reynolds, G. L. Cunningham, L. F. Huenneke, W. M. Jarrell, R. A. Virginia, and W. G. Whitford. 1990. Biological feedbacks in global desertification. Science **247**:1043-1048

Schlesinger, W. H., A. D. Abrahams, A. J. Parsons, and J. Wainwright. 1999. Nutrient losses in runoff from grassland and shrubland habitats in Southern New Mexico: I. Rainfall simulation experiments. Biogeochemistry **45**:21-34

Schlesinger, W. H., and J. A. Andrews. 2000. Soil respiration and the global carbon cycle. Biogeochemistry **48**:7-20

Shirnian-Orlando, A.A., & Uchrin, C.G. (2000). A method for determining salt sources in surface waters. Journal of the American Water Resources Association, 36, 749-757. doi:10.1111/j.1752-1688.2000.tb04303.

Skau, C. 1964. Interception, throughfall, and stemflow in Utah and alligator juniper cover types of northern Arizona. Forest Science **10**:283-287

Smith, R.E., Goodrich, D.C., & Quinton, J.N. (1995). Dynamic, distributed simulation of watershed erosion: The KINEROS2 and EUROSEM models. Journal of Soil and Water Conservation, 50, 517-520.

Spaeth, K.E., Pierson, F.B., Weltz, M.A., & Blackburn, W.H. (2003). Evaluation of USLE and RUSLE estimated soil loss on rangelands. J. Range Management, 56, 234-246. doi:10.2458/azu_jrm_v56i3_spaeth

Spaeth, K.E., Pierson, F.B., Herrick, J.E., Shaver, P.L., Pyke, D.A., Pellant, M., Thompson, D., & Dayton, B. (2003). New proposed national resources inventory protocols on nonfederal rangelands. Journal of Soil and Water Conservation, 58, 18A-21A.

Spaeth, K. E., M. A. Weltz, H. D. Fox, and F. B. Pierson. 1994. Spatial pattern analysis of sagebrush vegetation and potential influences on hydrology and erosion. Pages 35-50 *in* W. H. Blackburn, F. B. Pierson, G. E. Schuman, and R. Zartman, editors. Variability in Rangeland Water Erosion Processes. Soil Science Society of America, Madison, Wisconsin.

Spahr, N.E., Apodaca, L.E., Deacon, J.R., Bails, J.B., Bauch, N.J., Smith, M., & Driver, N.E. (2000). Water quality in the upper Colorado River basin, Colorado, 1996–98. U.S. Geological Survey Circular 1214. Denver, CO. doi:10.3133/cir1214

Sumner, M., and W. Miller. 1996. Cation exchange capacity and exchange coefficients. Methods of Soil Analysis Part 3—Chemical Methods:1201-1229

Taucer, P., C. Munster, B. Wilcox, M. Owens, and B. Mohanty. 2008. Large-scale rainfall simulation experiments on juniper rangelands. Transactions of the Asabe **51**:1951-1961

Team, R. C. 2017. R: A language and environment for statistical computing. R Foundation for Statistical Computing, Vienna, Austria.

Tillman, F.D., Anning, D.W., Heilman, J.A., Buto, S.G., & Miller, M.P. (2018). Managing salinity in upper Colorado River basin streams: selecting catchments for sediment control efforts using watershed characteristics and random forests models. Water, 10, 676. doi:10.3390/w10060676

Thurow, T., W. Blackburn, S. Warren, and C. Taylor Jr. 1987. Rainfall interception by midgrass, shortgrass, and live oak mottes. Journal of Range Management:455-460

Thurow, T. L., W. H. Blackburn, and C. A. Taylor Jr. 1986. Hydrologic characteristics of vegetation types as affected by livestock grazing systems, Edwards Plateau, Texas. Journal of Range Management **39**:505-509

Thurow, T. L., W. H. Blackburn, and C. A. Taylor Jr. 1988. Infiltration and interrill erosion responses to selected livestock grazing strategies, Edwards Plateau, Texas. Journal of Range Management **41**:296-302

Tiscareno-Lopez, M., V. Lopes, J. Stone, and L. Lane. 1993. Sensitivity analysis of the WEPP watershed model for rangeland applications I: Hillslope processes. Transactions of the ASAE **36**:1659-1672

Tongway, D. J., and B. Ludwig. 1997. The nature of landscape dysfunction in rangelands. Pages 49-61 *in* B. Ludwig, D. J. Tongway, D. Freudenberger, J. Noble, and K. C. Hodgkinson, editors. Landscape Ecology, Function and Management: Principles from Australia's Rangelands. CISRO Publishing, Melbourne, Australia.

Toney, C., Shaw, J.D., & Nelson, M.D. (2009). A stem-map model for predicting tree canopy cover of forest inventory and analysis (FIA) plots. Forest Inventory and Analysis (FIA) Symposium October 21-23, 2008, Proceedings RMRS-P-56, Rocky Mountain Research Station. Fort Collins, Co.

Tromble, J., K. Renard, and A. Thatcher. 1974. Infiltration for three rangeland soil-vegetation complexes. Journal of Range Management:318-321

Turnbull, L., J. Wainwright, R. E. Brazier, and R. Bol. 2010. Biotic and abiotic changes in ecosystem structure over a shrub-encroachment gradient in the Southwestern USA. Ecosystems **13**:1239-1255

Turnbull, L., B. P. Wilcox, J. Belnap, S. Ravi, P. D'odorico, D. Childers, W. Gwenzi, G. Okin, J. Wainwright, and K. Caylor. 2012. Understanding the role of ecohydrological feedbacks in ecosystem state change in drylands. Ecohydrology **5**:174-183

Tuttle, M.L., J.W. Fahy, J.G. Elliott, , R.I. Grauch, and L.L. Stillings. 2014. Contaminants from Cretaceous black shale: I. Natural weathering processes controlling contaminant cycling in Mancos Shale, southwestern United States, with emphasis on salinity and selenium. Applied Geochemistry. 46: 57–71.

USDA-NRCS. 2018. 2018 National Resources Inventory Rangeland Resource Assessment. https://www.nrcs.usda.gov/wps/portal/nrcs/detail/national/technical/nra/nri/results/?cid=nrcseprd1343027

Urgeghe, A. M., D. D. Breshears, S. N. Martens, and P. C. Beeson. 2010. Redistribution of runoff among vegetation patch types: On ecohydrological optimality of herbaceous capture of run-on. Rangeland Ecology and Management **63**:497-504.10.2111/rem-d-09-00185.1

USGS (U.S. Geological Survey) (2002). National elevation dataset, 1/3 arc second. http://ned.usgs.gov, accessed 10/19/2016.

USGS (U.S. Geological Survey) (2017). LANDFIRE 1.4.0. https://www.LANDFIRE.gov, accessed 6/13/2018.

USGS (U.S. Geological Survey) (2018). Protected Areas Database of the United States (PAD-US). https://usgs.gov/gapanalysis/PAD-US, accessed 12/17/2019.

Valentin, C. 1994. Surface sealing as affected by various rock fragment covers in West Africa. Catena **23**:87-97

VanAmburg, L., D. Booth, M. Weltz, and M. Trlica. 2005. A laser point frame to measure cover. Rangeland Ecology and Management **58**:557-560

Warner, J.W., Heimes, F.J., & Middelburg, R.F. (1985). Ground-water contribution to the salinity of the upper Colorado River basin. USGS Water-Resources Investigations Report, U.S. Geological Survey. pp. 113. doi:10.3133/wri844198

Wainwright, J., A. J. Parsons, and A. D. Abrahams. 2000. Plot-scale studies of vegetation, overland flow and erosion interactions: Case studies from Arizona and New Mexico. Hydrological Processes **14**:2921-2943

Weltz, M., S. K. Nouwakpo, C. Rossi, L. Jolley, and G. Frasier. 2014. Salinity mobilization and transport from rangelands: assessment, recommendations, and knowledge gaps. U.S. Department of Agriculture, Agricultural Research Service, Reno, Nevada.

Weltz, M.A., Kidwell, M.R., & Fox, D.H. (1998). Influence of abiotic and biotic factors in measuring and modeling soil erosion on rangelands: State of knowledge. J. of Range Management, 51, 482-495. doi:10.2307/4003363

West, N. E. 1983. Intermountain Salt-Desert Shrubland. Pages 375-397 *in* N. E. West, editor. Temperate Deserts and Semi-Deserts. Elsevier, The Netherlands.

West, N. E. 1991. Nutrient cycling in soils of semiarid and arid regions. Pages 295-332 *in* J. Skujins, editor. Semiarid Lands and Deserts: Soil Resource and Reclamation. Marcel Dekker, New York, NY.
Wilcox, B., D. Davenport, J. Pitlick, and C. Allen. 1996. Runoff and erosion from a rapidly eroding pinyon-juniper hillslope. Los Alamos National Lab., NM (United States).
Wilcox, B., M. Seyfried, and D. Breshears. 2003a. The water balance on rangelands. Encyclopedia of water science:791-794
Wilcox, B. P., and M. K. Wood. 1988. Hydrologic impacts of sheep grazing on steep slopes in semiarid rangelands. Journal of Range Management **41**:303-306
Wilcox, B. P., M. K. Wood, and J. M. Tromble. 1988. Factors influencing infiltrability of semiarid mountain slopes. Journal of Range Management **41**:197-206
Wilcox, B. P. 1994. Runoff and erosion in intercanopy zones of pinyon-juniper woodlands. Journal of Range Management **47**:285-295
Wilcox, B. P., and D. D. Breshears. 1994. Hydrology and ecology of piñon-juniper woodlands: conceptual framework and field studies. US Department of Agriculture, Rocky Mountain Forest and Range Experiment Station, Fort Collins, CO, Flagstaff AZ.
Wilcox, B. P., D. D. Breshears, and C. D. Allen. 2003b. Ecohydrology of a resource-conserving semiarid woodland: Effects of scale and disturbance. Ecological Monographs **73**:223-239.10.1890/0012-9615(2003)073[0223:eoarsw]2.0.co;2
Wilcox, B. P., D. D. Breshears, and H. J. Turin. 2003c. Hydraulic conductivity in a pinon-juniper woodland: Influence of vegetation. Soil Science Society of America Journal **67**:1243-1249
Williams, C. J., F. B. Pierson, O. Z. Al-Hamdan, P. R. Kormos, S. P. Hardegree, and P. E. Clark. 2014a. Can wildfire serve as an ecohydrologic threshold- reversal mechanism on juniper- encroached shrublands. Ecohydrology **7**:453-477.10.1002/eco.1364
Williams, C. J., F. B. Pierson, P. R. Robichaud, and J. Boll. 2014b. Hydrologic and erosion responses to wildfire along the rangeland-xeric forest continuum in the western US: a review and model of hydrologic vulnerability. International Journal of Wildland Fire **23**:155-172.10.1071/wf12161
Williams, C. J., F. B. Pierson, P. R. Robichaud, O. Z. Al-Hamdan, J. Boll, and E. K. Strand. 2015. Structural and functional connectivity as a driver of hillslope erosion following disturbance. International Journal of Wildland Fire **25**:306-321.http://dx.doi.org/10.1071/WF14114
Williams, C. J., F. B. Pierson, K. E. Spaeth, J. R. Brown, O. Z. Al-Hamdan, M. A. Weltz, M. A. Nearing, J. E. Herrick, J. Boll, and P. R. Robichaud. 2016. Incorporating Hydrologic Data and Ecohydrologic Relationships into Ecological Site Descriptions. Rangeland Ecology and Management **69**:4-19
Wischmeier, W.H., & Mannering, J.V. (1969). Relation of Soil Properties to its Erodibility. Soil Science Society of America Journal, 33, 131-137. doi:10.2136/sssaj1969.03615995003300010035x.
Wischmeier, W.H., & Smith, D.D. (1978). Predicting rainfall-erosion losses: a guide to conservation planning. Agriculture Handbook (AH) 537. U.S. Dept. of Agriculture, Washington, DC. USA.
Wood, M. K., W. H. Blackburn, J. Eckert, R.E., and F. F. Peterson. 1978. Interrelations of the physical properties of coppice dune and vesicular dune interspace soil with grass seedling emergence. Journal of Range Management **31**:189-192
Wood, M. K., and W. H. Blackburn. 1981. Grazing Systems: Their Influence on Infiltration Rates in the Rolling Plains of Texas. Journal of Range Management **34**:331-335
Ziadat, F. (Food and A.O. of the U.N., Mazahreh, S. (National A.R.C., Haddad, M. (International C. for A.R. in D.A., Benabdelouahab, T. (Institut N. de R.A. de R., Kandakji, T., Attaher, S., Oweis, T.Y., Karrou, M., 2014. Similarity and Suitability Analysis to Assist the Out-Scaling of Sustainable Water and Land Management Practices in West Asia and North Africa. Lebanon.

9. List of publications:

Cadaret, E.M., McGwire, K.C., Nouwakpo, S.K., Weltz, M.A. and Saito, L., 2016. Vegetation canopy cover effects on sediment erosion processes in the Upper Colorado River Basin Mancos Shale formation, Price, Utah, USA. Catena, 147, pp.334-344.

Cadaret, E.M., Nouwakpo, S.K., McGwire, K.C., Weltz, M.A. and Blank, R.R., 2016. Experimental investigation of the effect of vegetation on soil, sediment erosion, and salt transport processes in the Upper Colorado River Basin Mancos Shale formation, Price, Utah, USA. Catena, 147, pp.650-662.

Gagnon, S.R., Sears, J.R., Makuch, J.R., Rossi, C.G., Nouwakpo, S.K., Weltz, M.A. and Frasier, G.W., 2014. Salinity mobilization and transport: Hydrologic and aeolian processes and remediation techniques for rangelands. A selected bibliography. In: USDA-ARS, editor Special Reference Briefs Series. USDA-ARS, Beltsville, MD. p. 364.

Nouwakpo, S.K., Weltz, M.A., McGwire, K.C., Williams, J.C., Osama, A.H. and Green, C.H., 2017. Insight into sediment transport processes on saline rangeland hillslopes using three- dimensional soil microtopography changes. Earth Surface Processes and Landforms, 42(4), pp.681-696.

Nouwakpo, S.K., Weltz, M.A., Arslan, A., Green, C.H. and Al-Hamdan, O.Z., 2018. Process- based Modeling of Infiltration, Soil Loss and Dissolved Solids on Saline and Sodic Soils.

Weltz, M., Nouwakpo, S.K., Rossi, C., Jolley, L. and Frasier, G., 2014. Salinity mobilization and transport from rangelands: assessment, recommendations, and knowledge gaps. General Technical Report 1. Reno, Nevada. 61.

Founds, M.J., K.C. McGwire, M.A. Weltz, S. K. Nouwakpo, and P. S.J. verburg. 2019. Predciting micro-catchment ponded infiltration dynamice. Catana. IN Press.

Nouwakpo, S. K., Weltz, M. A., Arslan, A., Green, C. H., Al-Hamdan, O. Z. 2019. Process-based modeling of infiltration, soil loss, and dissolved solids on saline and sodic soils. Transactions of the ASABE . 61(3) 2018 American Society of Agricultural and Biological Engineers ISSN 2151-0032 https://doi.org/10.13031/trans.12705

10. Conference presentations:

Nouwakpo, K., Weltz, M., Arslan, A., Green, C., MaGwwire, K., 71st Annual Meeting, Technical Training and Trade Show, Academic, Conference, "Infiltration and soil loss modeling with the Rangeland Hydrology and Erosion Model on saline and sodic soils", Accepted, Society for Range Management. (February 1, 2018).

Yespolov, T., Strohmeier, S., Beksultanov, M., Haddad, M., Weltz, M, Nouwakpo, K. , Spaeth, K., Burns, S., Nesbit, J., Arslan, A., Tolido, D, Hayek, M, 71st Annual Meeting, Technical Training and Trade Show, Academic, Conference, "International Cooperative Development of Techniques for Sustainability when Managing and Restoring Degraded Rangelands", Accepted, Society for Range Management. (February 1, 2018).

Arslan, A., Nouwakpo, K., Weltz, M., Green,C. , McGwire, K., 71st Annual Meeting, Technical Training and Trade Show, Academic, Conference, "The fate of salt affected rangeland soils and surface water quality using rainfall simulation", Accepted, Society for Range Management 71st Annual Meeting. (February 1, 2018).

Nouwakpo, K., Weltz, M., McGwire, K., Williams, J., Al-Hamdan, O., Arslan, A. 2019. Clarifying the role of vegetation in sediment transport processes on sparsely-vegetated semi-arid landscapes with Structure from Motion. EGU General Assembly, Vienna | Austria | 7–12 April 2019 X2.27 | EGU2019-3569.

Arslan, A., Nouwakpo, S., Weltz, M., McGwire, K. 2019. Runoff water quality from rainfall simulation on different salinity-alkalinity levels of rangeland plots. Proceedings of papers of the 5th Federal Interagency Hydrologic Modeling Conference and the 10th Federal Interagency Sedimentation Conference. Reno, NV, April 19 – 23, 2019

Nouwakpo, K., Weltz, M., Arslan, A., McGwire, K. 2019. Process-based modeling of upland erosion and salt load in the upper colorado river basin. Proceedings of papers of the 5th Federal Interagency Hydrologic Modeling Conference and the 10th Federal Interagency Sedimentation Conference. Reno, NV, April 19 – 23, 2019

11. Appendix I: List of Acronyms

AGWA	Automated Geospatial Watershed Assessment
ALF	Smith-Parlange infiltration equation parameter (α)
ARS	Agricultural Research Service
CAD	Channel areal deposition
CAE	Channel areal erosion
CEC	Cation exchange capacity
CV	coefficient of variation
CVD	Channel volume deposition
CVE	Channel volume erosion
CVN	Channel volume net change (erosion - deposition
CVRN	volume-based ratio of net volume change in channels with respect to entire plot
CZD	Channel depth of deposition
CZE	Channel depth of erosion
DEM	Digital elevation model
EC	Electrical conductivity
ESP	Exchangeable sodium percentage
GIS	Geographic information systems
IC	Ion chromatography
KINEROS	Kinematic Runoff and Erosion Model
MCMC	Markov chain Monte Carlo
NRCS	Natural Resources Conservation Service (USDA)
QA	Quality assurance
QC	Quality control
RHEM	Rangeland Hydrology and Erosion Model
SAR	Sodium absorption ratio
SAT	soil saturation ratio
SL	Total soil loss
SR	Total runoff
SWAT	Soil and Water Assessment Tool
TAD	Total plot areal deposition
TAE	Total plot areal erosion
TDS	Total dissolved solids
TVD	Total plot volume deposition
TVE	Total plot volume erosion
TVN	Total plot volume net change (erosion - deposition)
TZD	Total plot depth of deposition
TZE	Total plot depth of erosion
UCRB	Upper Colorado River Basin
USDA	United States Department of Agriculture
VDSH	vegetation-drivel spatial heterogeneity
WGRS	Walnut Gulch Rainfall Simulator

12. APPENDIX II: Field Data Collection

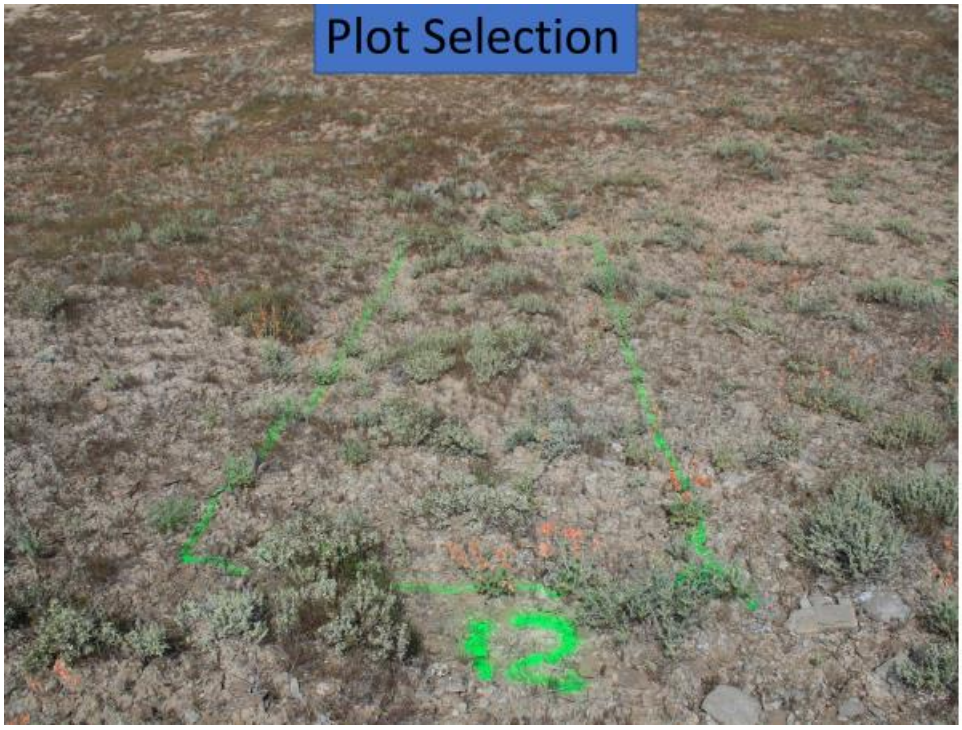


Plot Set Up

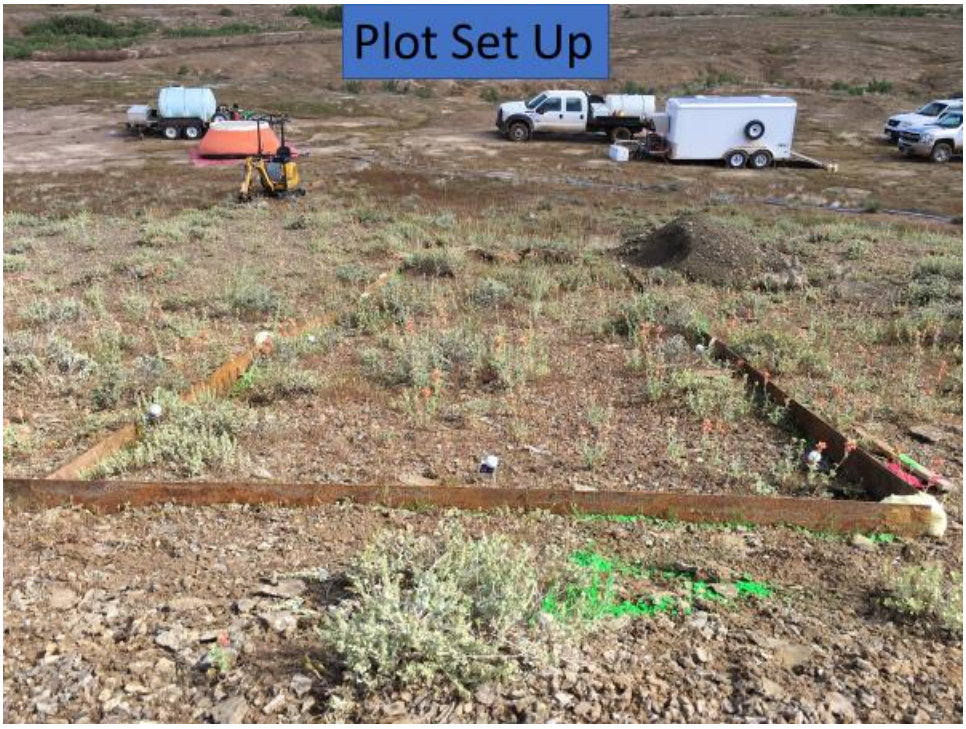
Plot Set Up


Plot Set Up

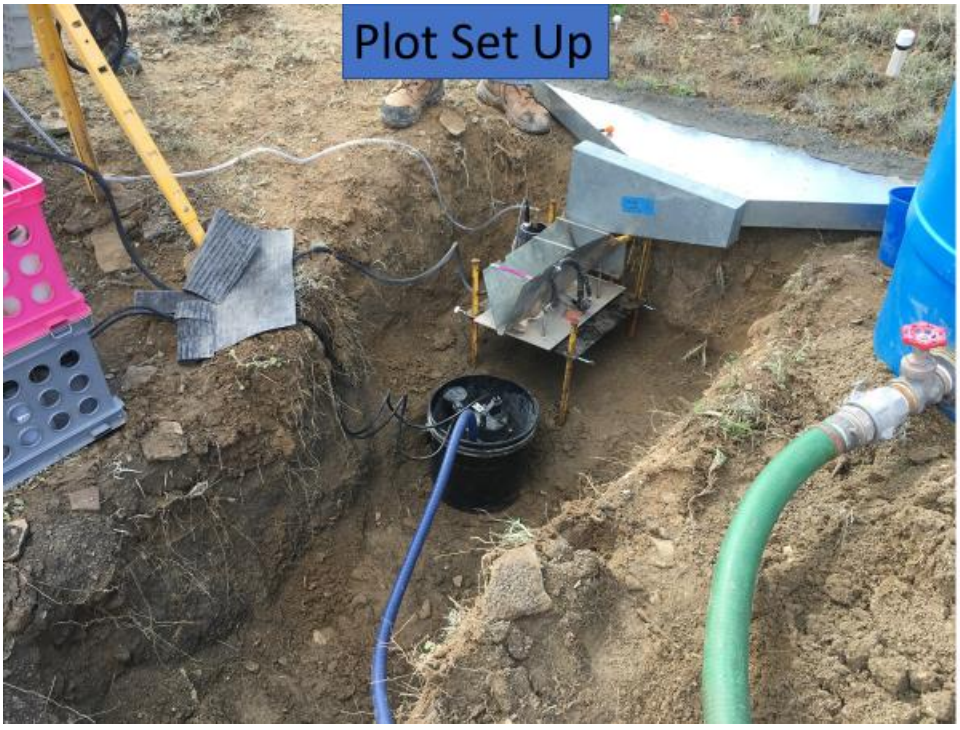
Plot Set Up

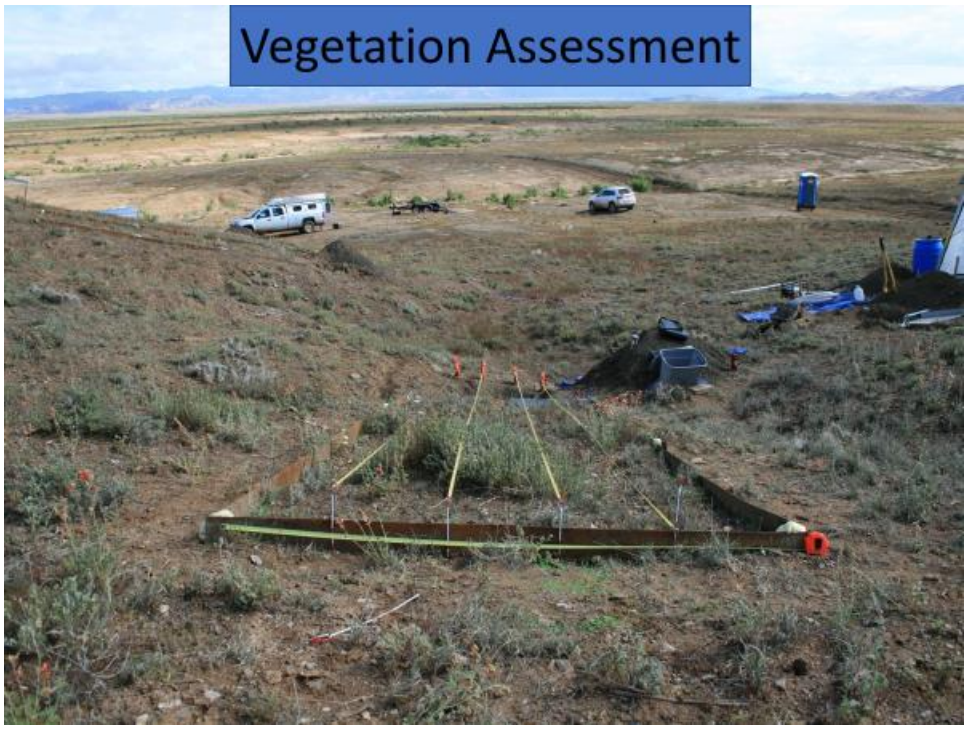
Vegetation Assessment


Soils Assessment


Installing Simulator

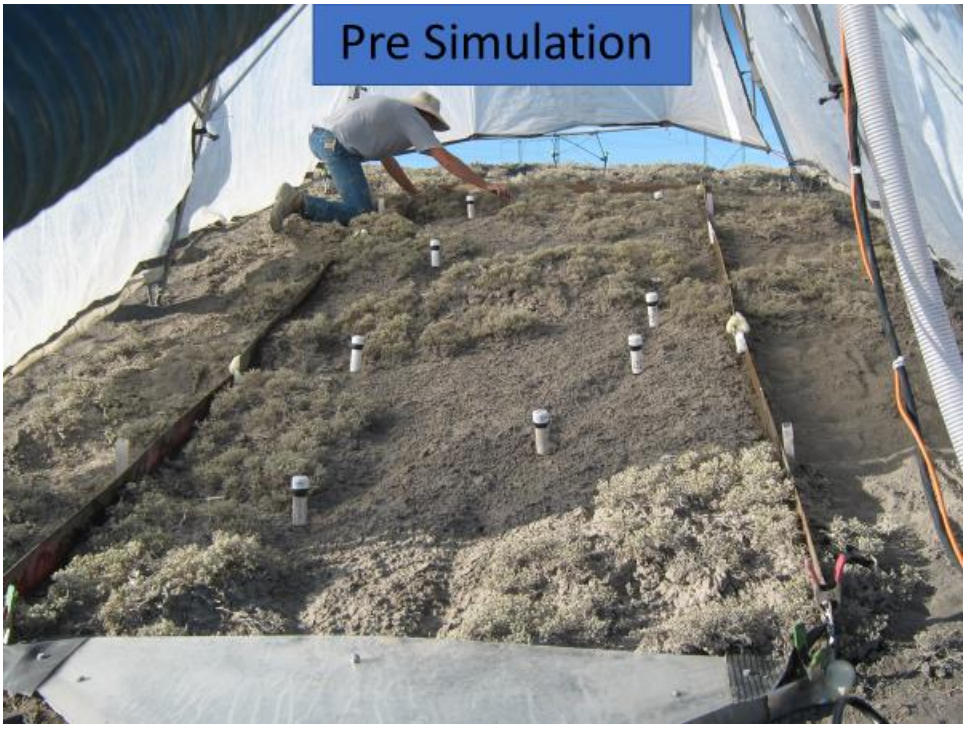
Pre Simulation


Simulation


Water Quality Sampling


Water Quality Sampling


Post Simulation: Rill Erosion


Rehabilitated Plots


Rehabilitated Plots